ELECTRON TRANSPORT COEFFICIENTS IN GAS MIXTURES.

RICHARD SKELDING.

A thesis submitted to the
University of Leicester
for the degree of
Doctor of Philosophy.

January 1984.

ProQuest LLC
789 East Eisenhower Parkway
P.O. Box 1346
Ann Arbor, MI 48106-1346


LEICESTER UNIVERSITY LIBRARY

Dedicated to the memory of
my father, Doug Skelding.
He encouraged and supported
all my interests, particularly
science, from my early years
until his death on 12 December
1982.
The strength of his friendship
and the extent of his support
are only matched by those of
my brave mother.

ACKNOWLEDGEMENTS.

I thank the Head of the Department of Physics for permitting this work to be carried out and the Science and Engineering Research Council for the award of a grant.

I am very grateful to my supervisor, Dr. E. Mathieson for his help and encouragement, both during the research and the last two years when teaching has diverted my energies most of the time.

The advice and work of Dr. T. J. Harris has been invaluable, thanks also to his staff in the Electronics Workshop.

My thanks are due to the staff in the Engineering Workshop, particularly Mr. R. Cox and Mr. C. Clarke who built most of the drift chamber and its parts and were very helpful at the design stage.

Finally my thanks to other members of the department in the X-ray Astronomy and Solid-State research groups for advice, use of equipment and facilities etc.

ELECTRON TRANSPORT COEFFICIENTS IN GAS MIXTURES.

RICHARD SKELDING.

ABSTRACT.

Experimental and theoretical approaches to the quantification of electron lateral and longitudinal diffusion coefficients and drift velocity in gases are reviewed.

The development and arrangement of the experiments to measure transport coefficients are discussed. The procedures used for measuring these in counter gases at low electric field strength to pressure ratios are given.

Lateral diffusion coefficient to mobility ratios were determined for electrons in the following gases; 100% methane, argon + methane mixtures (in the proportions 25% / 75%, 50% / 50% and 90% / 10%), 100% carbon dioxide, argon + carbon dioxide mixtures (in the proportions 50% / 50%, 75% / 25% and 90% / 10%), argon + 5% carbon dioxide + 3% acetylene, argon + 25% isobutane and neon + 10% methane.

Drift velocities and longitudinal diffusion coefficient to mobility ratios were determined in 100% methane, argon + 50% methane and argon + 10% methane.

The experimental results for the lateral diffusion coefficient to mobility ratio and the drift velocity are presented as functions of the ratio of the electric field strength to gas pressure and are compared with predictions made by solution of the Boltzmann equation and by Monte-Carlo simulation. Less reliable are the results for the longitudinal diffusion coefficient to mobility ratio, these are given as functions of the electric field strength to pressure ratio and compared with predictions made by Monte-Carlo simulation.

The inadequacy of the arrangement to measure longitudinal diffusion is considered together with its value for the determination of the other coefficients.

CONTENTS.

CHAPTER 1.

INTRODUCTION.

Interest in the transport of electrons in gases has a history going back as far as Roentgen's discovery of X-rays in 1895. The measurement of transport coefficients was begun by J.S.Townsend in the first decade of this century. Work in this field has involved J.J.Thomson, E.Rutherford, R.J.Van de Graaf and other pioneering scientists of this century. The growing involvement in atomic theory and radioactivity as well as experimental limitations drew attention away from electron transport in gases in the late 1920's.

In the last twenty years there has been much more dedication to this work, both experimentally and theoretically. As gas-filled counters have been developed, and more recently used in growing numbers of applications, work has accelerated in this field. Quantitative data on the drift velocity and diffusion of electrons in counter gases are required to obtain optimum performance of counters. Proportional counters are now used extensively in high-energy physics, astrophysics, medical physics, biological science and crystallography. For linearity of the space-time relationship of a drift chamber, electric field saturation of the drift velocity is essential. This avoids errors due to field irregularities near local imperfections. The effects of impurities in the gas must also be understood (Ezban and Morganti, 1974). In imaging and timing applications the primary limit to the resolution of a counter is the diffusion of a group of electrons into the gas as it drifts through the gas.

The transport of electrons in gases can be described in terms of the drift velocity and two diffusion coefficients. It was found in 1967 that diffusion is not isotropic. A lateral diffusion coefficient D and a longitud--inal diffusion coefficient D_L are necessary to describe the diffusion perpendicular and parallel to the direction of the drift respectively (Wagner et al, 1967).

The aim of this work has been to obtain experimentally transport coefficient data for certain useful counter gases, particularly mixtures of argon with ranges of proportions of methane or carbon dioxide. Some of this data had been published by several workers, including N.S.El-Hakeem (1978) at this laboratory. This data was mainly drift velocities and lateral diffusion coefficients. However it was incomplete and sometimes subject to large discrepancies as a result of instrumental limitations and other factors. Attempts were made in this work to quantify longitudinal diffusion as well as obtain drift velocity and lateral diffusion coefficient data with improved reliability and accuracy. Theoretical predictions of the transport coeffici--ents were also obtained from available collision cross-section data using the Boltzmann transport equation and by Monte-Carlo simulation. These were compared with the data obtained experimentally.

The experiments carried out involved low electric field to gas pressure ratios. The average electron energy in an electron swarm was sufficiently low to ensure that the macroscopic behaviour of the swarm could be attributed to only transformationless collisions, i.e. not events involving ionisation etc. The results of swarm experiments

under these conditions are useful to obtain information on electron scattering processes, i.e. collision cross-sections.

Two experiments were carried out using the same drift chamber, but with two methods of collecting the electrons. The first experiment used a Townsend concentrically divided plane anode. With this arrangement the lateral spread of the electrons, by diffusion, could be studied by comparing the currents arriving at the centre and on the annular outer portion of the anode. A continuous source of low energy electrons was used in this experiment. The second experiment used a counter, operated in the Geiger mode, in place of the plane collector. The electron source was pulsed. Arrival time spectra were obtained from the counter pulses. The position in time of the peak of a spectrum was used to calculate the electron drift velocity. The width of the spectrum was analysed to obtain the longitudinal spread of the electrons in the swarm.

The electrons were produced by photoemission at the cathode and drifted through a uniform electric field of variable length to the collector. The drift chamber had a continuous flow of counter gas through it to reduce contamin--ation. The gas pressure in the chamber was variable over a wide range. Counter purity gas which is commercially supplied was used throughout the experimental work.

Other experimental and theoretical work in the field is reviewed briefly here. Descriptions of the experiments carried out and the instruments used are presented here. The experimental results are shown in comparison with theoretical predictions obtained from collision cross-sections published by other workers in the field.

CHAPTER 2.

REVIEW OF TRANSPORT COEFFICIENT DETERMINATION BY EXPERIMENT.

2.1 LATERAL DIFFUSION COEFFICIENT TO MOBILITY RATIO.

A method of observing and quantifying the lateral diffusion of a stream of electrons moving in a gas under the action of an electric field was first described by Townsend (Townsend, 1908; Townsend and Tizard, 1913; Townsend, 1915). Figure 2.1 gives a schematic diagram of the apparatus.

Electrons were generated by photoemission from a metal cathode illuminated by ultra-violet light or gas atoms ionised by X-rays. The electrons enter the drift chamber through a small hole or a narrow slit, having drifted across a region under the action of an electric field of the same strength as the field in the main chamber, so that a steady state energy distribution is reached before the electrons enter the main drift region. After drifting the length of the chamber under the action of the electric field the electrons are collected by a flat metal plate. To measure the lateral spread of the electron stream the collector plate is divided into regions insulated from each other by narrow gaps. Two methods of dividing the collector used by Townsend are shown in figure 2.1, (a) was used with a circular source and (b) with a slit source. The ratio of the current collected by the central region to the total collected current is a measure of the spread of the electron stream perpendicular to the field, and is related to the ratio D/μ.

Townsend measured the quantity k_T, the Townsend energy ratio and Ne, the product of the molecular number

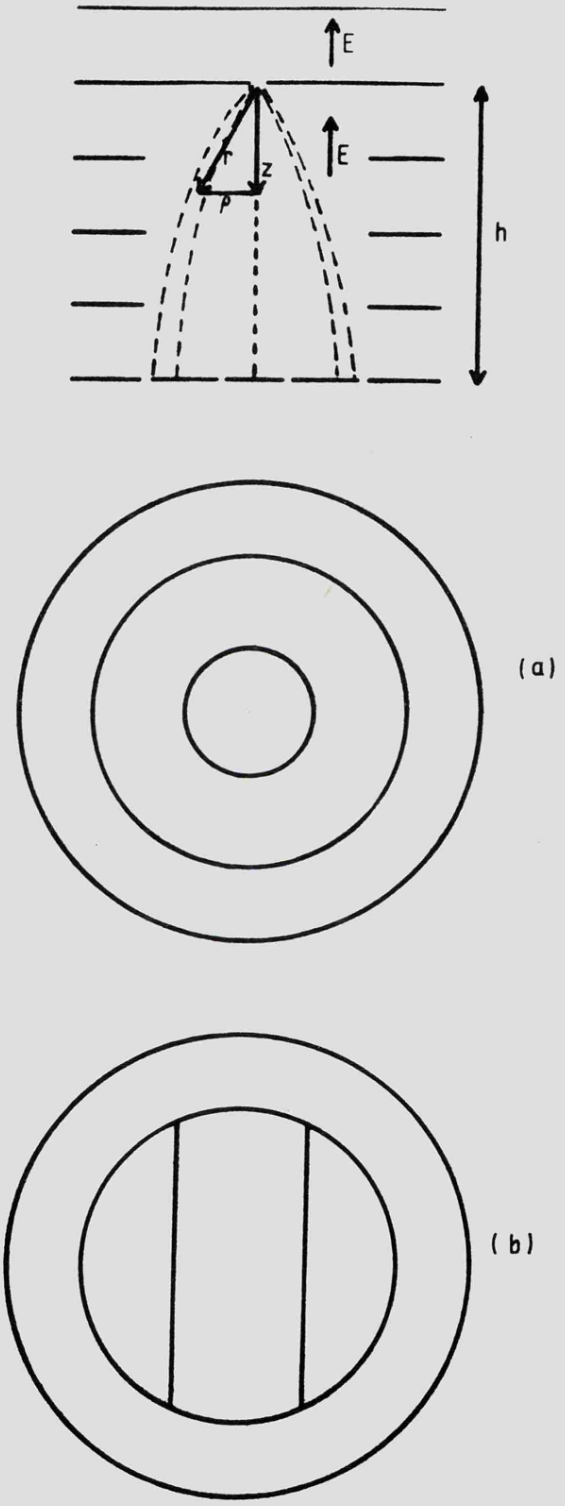

FIG 2·1

The Townsend Apparatus with two alternative methods of division of the collector (a) and (b).

and the electronic charge.

Townsend had previously obtained quantities related to D and to μ separately. The diffusion term by observing the fall in conductivity of a gas as it flows down a tube away from a region where ionisation has been caused (Townsend, 1899), this being due to diffusion of the charged particles to the wall of the tube. Values for drift velocity were obtained by Zeleny (1900) in a similar arrangement, by reducing the electric field strength the ions could be swept further by the gas flow as their drift velocities perpendicu-lar to the flow are reduced. Two collecting electrodes were placed at different distances along the flow, the field was varied to find its values for maximum collected current at each of these electrodes, from the two field values, the electrode separation and the gas flow Zeleny obtained values for the drift velocity W.

Calculations by Townsend (Townsend and Bailey, 1921) show the current ratio in the divided cathode arrange-ment to be a function of NeE/pk_T. Townsend and his co-workers published values for k_T and W, as functions of the ratio of the electric field strength to gas pressure, E/p, for air, nitrogen, hydrogen, oxygen, carbon dioxide, carbon monoxide, nitrous oxide and nitric oxide.

A mathematical analysis which could be easily applied to different dimensions and forms of apparatus was begun by Huxley (1940). The basic differential equation for the distribution of electrons in a stream moving in a uniform electric field E along a line Oz is

$$\nabla^2 n = 2\lambda \frac{dn}{dz}$$

where n = electron number density(cm^{-3})

$$\text{and } 2\lambda = \frac{W}{D}$$

Huxley obtained the solution

$$n = \frac{A}{r} \exp\ (-W(r-z)/2D)$$

for the distribution due to an isolated point source of electrons placed in a gas in a uniform field E, (r and z are shown in figure 2.1).

When the source is considered as a point hole in an electron absorbing plate, boundary conditions apply, $n = 0$ for $\rho \neq 0$ on the $z = 0$ plane and $n > 0$ for $z > 0$, these result in the solution

$$n = \frac{Az}{r^3}(1+\frac{Wr}{2D}) \exp(\ -W(r-z)/2D).$$

Also $n = 0$ at $z = h$, the collecting plate, an infinite series of terms representing image sources is built up. The solution produced an expression for the current ratio R which did not agree with experiment (Huxley, 1955). The following formula, obtained earlier by Huxley (1940), was justified on an empirical basis, and agreed well with experiment

$$R = 1 - \frac{h}{d} \exp(-\lambda(d-h)) \qquad (2.1)$$

Warren and Parker (1962) justified it mathematically. This solution does not have the condition $n = 0$ over the $z = 0$ plane except where $\rho = 0$, when the electron distribution equation is modified to account for this the expression for R is very different to 2.1 for long and short drift lengths and produces experimental values of D/μ which are pressure dependent for a given E/p. The solutions assume isotropic diffusion. Parker and Lowke (1969) demonstr--ated that electron diffusion is anisotropic, and so it is necessary to distinguish between D and D_L. The discrepancy

between the two solutions for R was resolved by assuming anisotropic diffusion (Lowke, 1973).

For anisotropic diffusion the equation for the distribution of electrons is

$$D\nabla^2 n + (D_L - D)\frac{d^2 n}{dz^2} - W\frac{dn}{dz} = 0$$

and the solution for R

$$R = 1 - (1 + (\tfrac{1}{2} - \frac{D_L}{D})(b/d)^2)\frac{h}{d}\exp(-\lambda(d-h))$$

and when $(b/d)^2$ is small (or $\frac{D_L}{D} \cong 0.5$) this reduces to the form derived empirically (Warren and Parker, 1962; Cottrell and Walker, 1967) from experiment and used extensively before the distinction between D and D_L was observed. For $\frac{b}{d} \sim 0.05$ the current ratio R is insensitive to the value of D/D_L (Gilardini, 1972; Huxley and Crompton, 1974).

In the present work b = 0.25 cm and drift lengths of 4 - 8 cm were normally used for the determination of D/μ, so $\frac{b}{d} \leq 0.05$. Having obtained the current ratio R for a set of drift lengths in a particular gas at a certain E/p at constant pressure D/μ was determined, see section 7.2.

2.2 DRIFT VELOCITY.

The drift velocity of electrons was of interest to Townsend in the determination of k_T, the Townsend energy ratio, this work and the measurements of drift velocity by Zeleny have been referred to in section 2.1. Townsend developed a more satisfactory method of measuring W using the divided collector arrangement, this method and subsequent others are described here.

2.2.1 The Townsend Method.

The method is used to find W as a function of E/p by deflecting a stream of electrons with a transverse magnetic field (Townsend and Tizard, 1912 and 1913; Townsend, 1915). The apparatus is shown in figure 2.2.

Ultra-violet light directed through the quartz window W releases electrons by photoemission from the metal plate A. The electrons move under the action of an electric field towards B, some electrons pass through a narrow slit in B into the chamber. The electric field strength is the same above and below B. The electrons continue to drift to the divided collector C_1, C_2, C_3. The rings R define and maintain the uniformity of the electric field in the region between B and C.

The two narrow gaps dividing the collector into a central strip C_2 and two equal segments C_1 and C_3 are parallel to the slit in B. The electron stream diffuses as it drifts towards the collector, some electrons are collected on C_1 and C_3, an equal number by each.

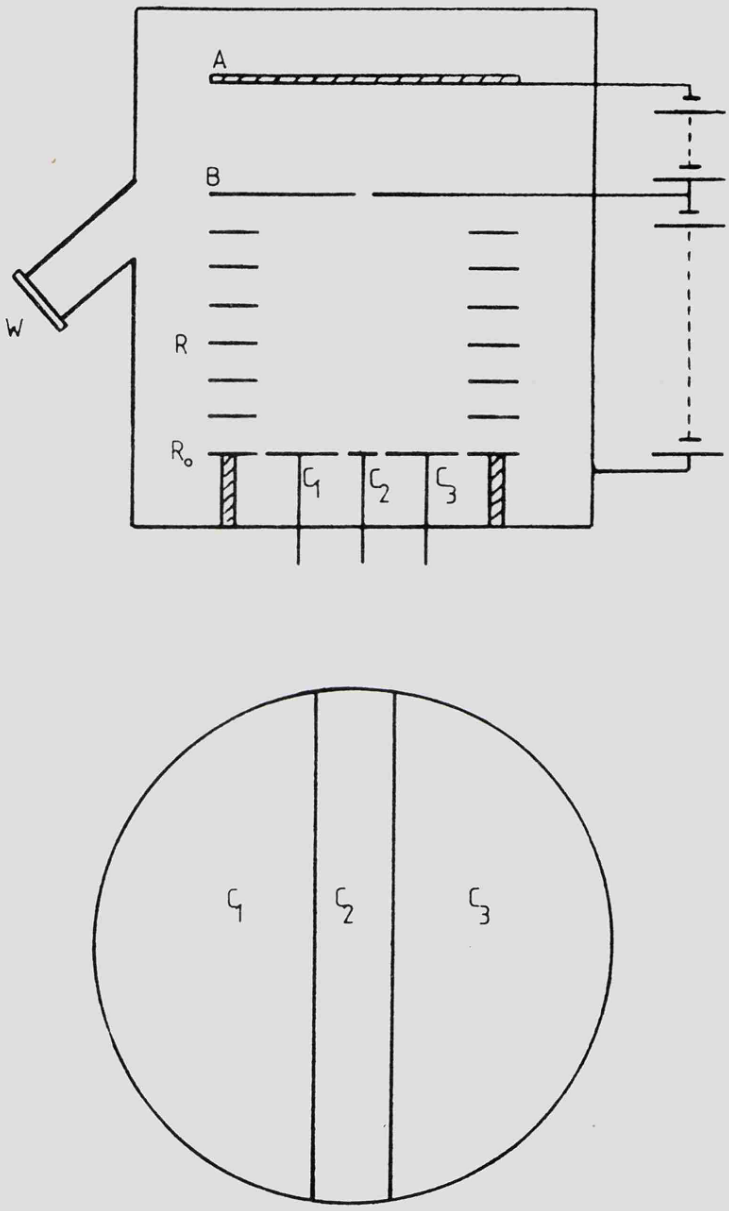

FIG 2·2 The Townsend Method for determining drift velocity.

A magnetic field of flux density B is applied parallel to the slit deflecting the electron stream, the flux is adjusted so that the charge collected by C_1 equals the charge collected by C_2 and C_3. Let the charge collected by each part of the collector be q_1, q_2, q_3, then when $q_1 = q_2 + q_3$ the centre of the electron stream has been deflected a distance a/2 where a is the width of C_2. Therefore the drift velocity of the electrons for a drift length l (≫ a) and an electric field E is given by

$$W = \frac{E}{B}\left(\frac{a}{2l}\right)$$

Recent methods have produced values for the drift velocity which differ from those obtained by Townsend by an amount far greater than the experimental error. Consider the arrangement as shown in figure 2.3. θ represents the direction of the axis of the stream when B is applied relative to the B = 0 direction, parallel to the z-axis.

$$\tan\theta = \frac{W_x}{W_z}, \text{ where } W_x \text{ and } W_z \text{ are components}$$

of W. The Townsend method assumes that $\tan\theta$ is equal to the ratio of the magnetic force to the electric force on the electron (Townsend, 1937), but these depend upon the magnetic drift velocity W_m, so

$$\tan\theta = \frac{BeW_m}{eE} = \frac{BW_m}{E} = \frac{a}{2l}$$

$$W_m = \frac{E}{B}\tan\theta$$

The true value of W is related to W_m (Huxley and Crompton, 1974). It has been shown (Daum, 1978) that the true drift velocity is dependent upon a magnetic field applied across the electric, generally it is inversely related to the magnetic flux density.

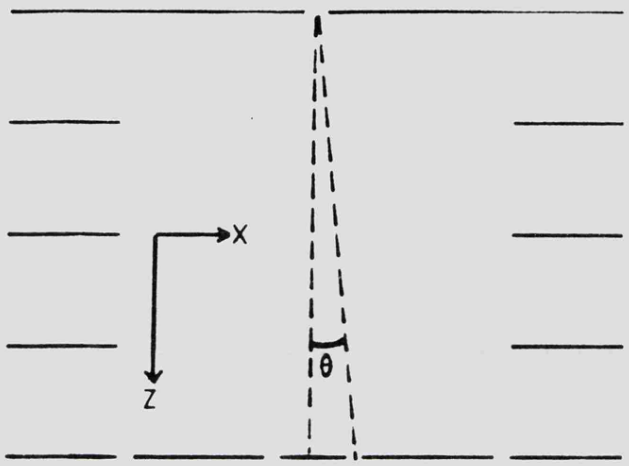

FIG 2·3 Analysis of the Townsend drift velocity experiment.

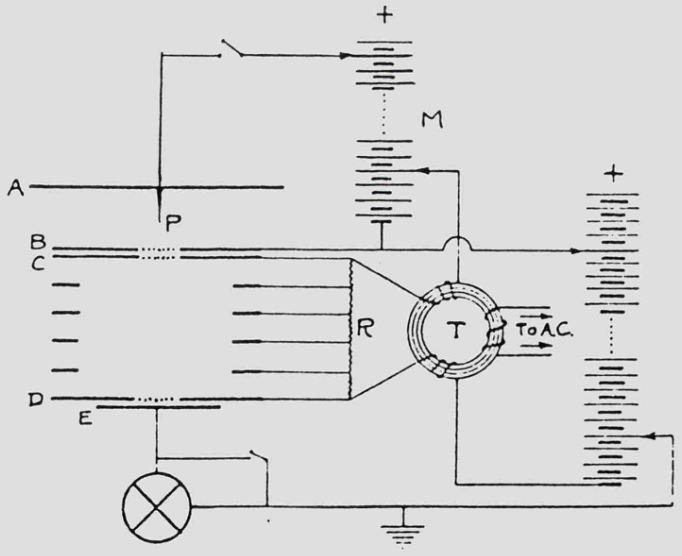

FIG 2·4 The Van de Graaf drift velocity experiment.

2.2.2 Electrical Shutter Methods.

A method of measuring electron drift velocity based upon Fizeau's determination of the velocity of light, was described by Van de Graaf (1928). The mean velocity of a group of electrons moving in a gas under the action of a steady, uniform electric field was found by measuring the time of flight of the electrons. Van de Graaf published his work a very short time before Tyndall described an identical method but a different apparatus (Tyndall, 1928). The description here is limited to the work of Van de Graaf.

Figure 2.4 is Van de Graaf's illustration of the experimental arrangement. An oscillating potential applied to the grids B,C, produces a shutter effect. The arrangement illustrated is for the determination of the drift velocity of positive ions, but requires only small modification to be used for electrons, namely a higher frequency oscillator and reversed fields. Ions are produced by a glow discharge at P. The collecting plate E is connected to an electrometer which measures the ion current. The regions BC and DE of the drift path have steady fields opposing the passage of positive ions. The region CD has a steady and uniform field acting upon the ions in the direction of D. Supplying an oscillating voltage to the transformer T, produces an equal change in potential at all points in the region CD, so that the field in this region is unaffected, but the regions BC and DE receive oscillating potentials superimposed upon their steady reverse biases, so for part of a half-cycle of the oscillating voltage these regions are forward biased. When the oscillating potential at C is at its negative maximum a group of positive ions passes

through the BC region, then through the uniform field region CD. The frequency of oscillation is adjusted so that the ions reach D when the potential at D is at its positive maximum and can pass through DE producing an electrometer reading. The ion current measured by the electrometer is maximised by adjusting the frequency of oscillation until an odd number of half-cycles is equal to the time of flight of the ions from C to D, then

$$W = \frac{d}{t} = \frac{2fd}{n}$$

where W = drift velocity

d = drift length

t = time of flight

f = frequency of oscillation

n = non-zero integer.

An electrical shutter method designed specifi--cally for the measurement of electron drift velocities, which are very large compared with those of ions, was described by Bradbury and Nielsen (1936). The method uses an electron shutter designed by Loeb and developed by other workers studying electron mobility (Cravath, 1929; Bradbury, 1933).

The electron shutter consists of a plane grid of parallel wires, alternate wires are connected together, this is shown schematically in end on view in figure 2.5. A steady flow of electrons emitted from an illuminated photocathode passes freely across the shutter when no voltage is applied between the two sets of wires in the grid. If a large voltage is applied the electron current is swept to one of the sets and collected.

Bradbury and Nielsen applied a high frequency alternating potential between the alternate wires of two

grids, one at each end of the uniform field drift region, figure 2.6. A series of electrons passes through the first grid corresponding to the alternating field passing through zero. The electrons drift to the second grid which has an alternating field of the same frequency, magnitude and phase as the first grid. If the drift velocity is such that the electrons reach the second grid when its field is near or at zero (i.e. an integral number of half-cycle periods after crossing the first grid) the electrons reach the collecting electrode. The frequency is adjusted to produce this situation, the time of flight and the drift velocity can then be determined from the frequency and the drift length.

Measurements of drift velocity by the Bradbury-Nielsen method can have an error of less that 1% (Crompton, 1970), assuming the drift length can be taken as the geometrical distance between the mid-planes of the shutter grids. Several end-effects have been pointed out which can cause the effective drift distance to differ from the geometrical distance (Elford and Robertson, 1973). These include contact potential differences between the shutters, diffusion effects, the change in mean energy as an electron swarm passes through a shutter, the variation of shutter transmission with electron energy and field distortion due to the large amplitude sinusoidal potential applied to the shutters.

The end-effects can be minimised by careful selection of the experimental conditions. For example, the contribution of contact potential differences becomes negligible if large applied voltages are used to generate the electric field, diffusion and mean energy change effects are reduced by using high gas pressures. Elford and Robertson

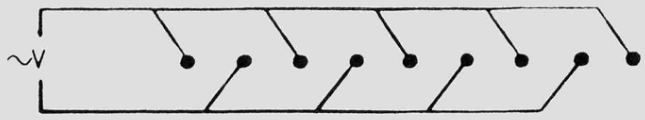

FIG 2·5 The Loeb electron shutter.

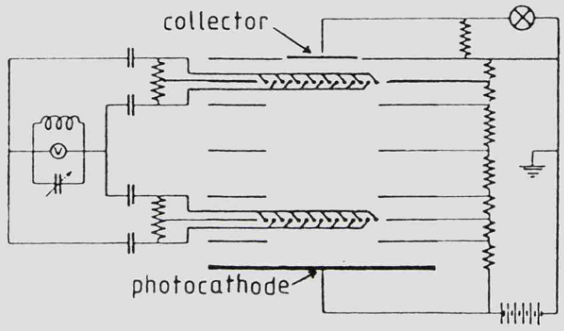

FIG 2·6 The Bradbury-Nielsen double shutter technique.

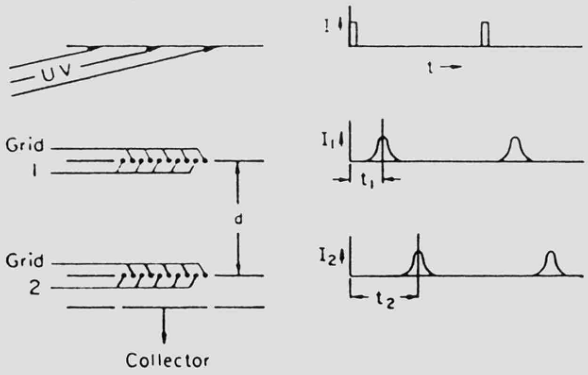

FIG 2·7 The Pack-Phelps double shutter technique.

obtained values for electron drift velocities in hydrogen and helium using drift lengths of 5, 10 and 50 cm for ranges of E/p and pressure. Agreement in hydrogen was within 0.1 %, in helium it was within 0.2 %. The conclusion being that careful choice of the experimental parameters to minimise end-effects can result in no significant difference between the effective and the geometrical lengths of the drift region and absolute errors of less that 1 % can be achieved.

The effect of diffusion, which increases at reduced pressure was examined by Lowke (1962; 1963). It was shown that the relationship used by Bradbury and Nielsen, i.e. $W = hf$, which is based upon the assumption that current maxima occur at alternating voltage frequencies which are an integral number of f/2, does not hold exactly. The time required for the centre of an undisturbed pulse of electrons to travel the distance h is 1/f, but the pulse is disturbed by several effects. Lowke obtained expressions for the errors due to the various factors which contribute to the total error in the electron drift velocity.

(1) relative error due to the back diffusion of electrons to the first shutter when it is closed displacing the centre of the pulse slightly forward, $2/h(W/D_L)$.

(2) the absorbing boundary presented by the second shutter before it opens produces a relative error of $1/h(W/D_L)$.

(3) the diffusion current has the effect of producing a discrepancy between the frequency corresponding to maximum electron current and the frequency corresponding to maximum electron density of an undisturbed pulse at the second shutter. This

introduces a relative error of $1/h(W/D_L)$.

(4) the variation of the number of electrons in each as the frequency is varied introduces a relative error of $-2/h(W/D_L)$.

(5) each pulse of electrons decays with time as it passes through the second shutter introducing asymmetry into the current-frequency relationship and an error of $1/h(W/D_L)$.

The total relative error, then, is of the order $3/h(W/D_L)$ or $3/V(\mu/D_L)$, this is reduced by using large applied voltages.

The double shutter technique was further developed and used for the measurement of electron drift velocities in helium at low values of E/p (Phelps et al,1960). Steady D.C. voltages were applied to both grids so that they were normally closed. The first grid was opened by applying short rectangular voltage pulses periodically, these reduced the field in the grid to zero. A similar pulse train was applied to the second grid but each pulse was slightly later than the corresponding pulse to the first grid. The delay between the two pulse trains was adjusted until the current to the collector reached its maximum, the delay then corresp--onded to the transit time of the electrons between the grids. An arrival time spectrum could be produced by plotting the collected current against the delay.

Although the field distortion in this develop--ment of the shutter method is minimised by using small amplitude pulses, end-effects were observed, i.e. at a particular E/p the drift velocity was slightly drift length dependent. This effect was eliminated by calculating the drift velocity from the ratio of the differences between two drift lengths and the corresponding drift times.

As a pulse train is used to operate the shutters the number of electrons per pulse is dependent upon the pulse width and not the repetition frequency, so this contribution to the total error is lost. However diffusion effects and so on are still present and the total relative error is of the order of $5/h(W/D_L)$ compared with $3/h(W/D_L)$ for the original Bradbury-Nielsen method.

The final refinement of the shutter technique to be discussed here is that of Pack and Phelps (1961). Measurements of electron drift velocity were made using the arrangement shown schematically in figure 2.7.

Photoelectrons were generated using a pulsed source of ultra-violet light, therefore a grid was not required to provide a time varying electron current. However two grids were involved in the experiment to determine the electron drift velocity, but they were used one at a time, the other remaining open. In this way the difference between the transit times to each grid could be used together with their separation to find the drift velocity, eliminating end-effects at the cathode and effects occurring equally at both grids.

Two modes of operation of the grids were used. Firstly the mode termed "conventional" by Pack and Phelps. The conventional mode involved the application of a voltage between the two halves of the first grid, this reduced the transmitted electron current to 5 % of the zero bias (open grid) current. The second grid was left open. The first grid was opened by applying a voltage pulse reducing the field between the alternate wires to zero. The transmitted current was maximised for some delay t_1 between the pulse to the grid and the light pulse. The collected current was plotted

against the delay time. Similarly the first grid was made passive (permanently open), and the second grid opened periodically by voltage pulses. This produced a second current against time plot which maximised at some delay t_2. For a given grid separation h the drift velocity is given by

$$W = \frac{h}{(t_2 - t_1)}$$

The second mode of operation used by Pack and Phelps was the "zero bias" or "rejection" mode. The intention of operating the apparatus in this mode was to reduce the effects of voltages applied to the grids, end-effects had appeared in the conventional mode when high bias voltages were applied. The end-effects produced a variation of (t_2-t_1) with bias voltage, when this was of the same order as the voltage producing the field in the drift space. This situation was unavoidable in the conventional mode for gases such as argon and neon and for low E/p values in other gases.

In the rejection mode the grids were held open by a zero bias, a pulsed voltage was used to reduce the transmission through one of the grids. The collector current would pass through a minimum when the delay time was such that the pulse was applied simultaneously with the arrival of the electrons at the operative grid.

The change in collector current was approxima--tely the same in both modes for equal pulse amplitudes, and the drift velocity values obtained were equal within the systematic error of the experiment.

This method is subject to the same diffusion effects as the Phelps double shutter technique. The number of electrons per pulse is independent of the delay between the light pulse and the grid pulse, it only depends upon the

duration of the ultra-violet light flash. So, again, the relative error in the transit time measurement is of the order $5/h(W/D_L)$. However this only applies to a very short duration flash (or very narrow pulses of electrons), this cannot be the case in the Pack and Phelps experiments, otherwise for some of the experimental conditions used the error would be extremely large, in excess of 25 % (Lowke,1962). Large errors did not appear in the results of Pack and Phelps as the diffusion errors were masked by the finite width of the initial pulse, and to a great extent, were cancelled by using the differencing method to calculate the drift velocities.

2.2.3 Electron Pulse Methods.

The electron pulse methods are distinct from the shutter methods as the electrons are produced, by whatever method, in pulses and no shutters are involved.

A pulsed UV light method was first introduced by Hornbeck to measure the drift velocity of electrons in helium (Hornbeck, 1951). A pulsed UV source operating at a repetition frequency of 60 Hz was used to produce 0.1 μs duration pulses of photoelectrons. The drift length was variable and currents of the order of 10^{-7}A were set up in the drift region. The method was adopted by several other workers for more accurate investigations in noble gases and nitrogen (Bowe, 1960).

The photoelectrons drift under the action of the uniform field from the cathode towards the anode, inducing a current in an external resistor in the collector circuit. The voltage developed across the resistor was amplified and displayed on an oscilloscope. The induced current rises from

zero when the electron pulse is released to a steady value, i while the electrons cross the drift region. i = NWe/h, where N is the total number of electrons and h is the drift length, neglecting diffusion and space-charge effects. The current drops to zero as the electrons are absorbed by the collector. The appearance of the current, as a function of time, is shown in figure 2.8.

The transit time of the pulse is assumed to be t_2-t_1 (Bowe, 1960). The use of t_2, for instance, was based upon the assumption that when half the electrons have been absorbed at the collector the centre of the pulse is at the collecting electrode. This is not accurate because the collec--tor is a plane conductor, so the electron concentration at its surface is always zero. The shape of the pulse becomes distorted, so the time at which half the electrons have been observed occurs slightly before the time at which the centre of the undisturbed pulse would have reached the collector. Therefore values of W obtained in this way are slightly high. The position of t_1 depends upon the rise in intensity of the UV light and also electron absorption due to back diffusion.

Lowke (1962) considered the error in the deter--mination of the time at which the centre of the electron pulse reaches the collector, and also the error due to back diffusion. The errors were found to be within the experimental error quoted by Bowe.

Electron drift velocities have also been found for electron pulses produced by ionisation of the gas by alpha particles, (English and Hanna, 1953; Klema and Allen, 1950; Bortner et al, 1957). Klema and Allen used a method similar to that of English and Hanna. A polonium source emitting about 50 alpha particles per second was evaporated onto a flat

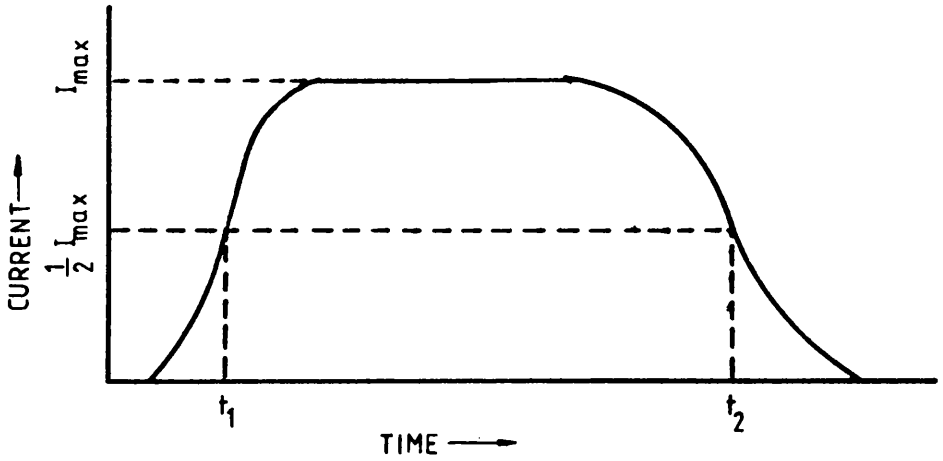

FIG 2·8 The induced current in the collector circuit of the Hornbeck drift velocity experiment.

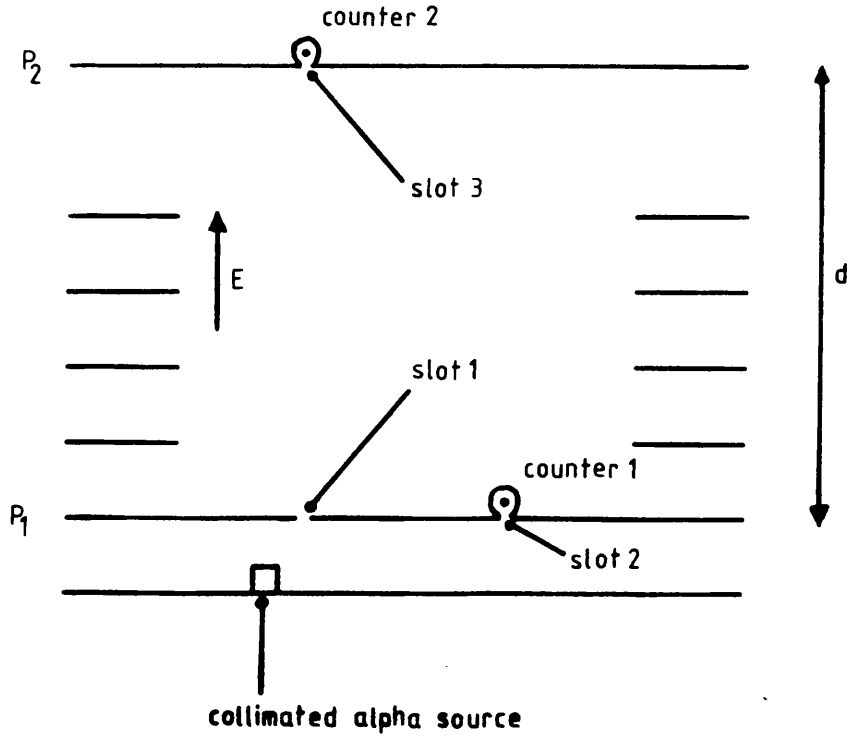

FIG 2·9 The Bortner drift velocity experiment.

electrode, forming the cathode of an ionisation chamber. The anode signal was amplified and two outputs taken, one to trigger the sweep circuit of an oscilloscope, and the second was delayed and displayed on the oscilloscope. The total rise time of the pulse from the chamber was measured, knowing the separation of the plates of the ionisation chamber the drift velocity could be calculated.

The procedure of Bortner et al was different, see figure 2.9. All the electrons were produced the same distance from the plate P1 by a collimated beam of alpha particles. The electric field acts on the electrons in the direction of plate P1 and are drawn simultaneously through slot 1 and into a proportional counter through slot 2. Counter 1 produces a pulse. The electrons drawn through slot 1 continue under the action of an electric field and finally pass through slot 3 into counter 2. The electrons detected by counter 2 have travelled an additional distance d. The delay between the pulses from the two counters is the time taken for the electrons to travel d, the drift velocity is then readily calculated.

Several factors will affect the accuracy of these techniques. A highly non-uniform electron density or the detection of electrons which have not reached the appropriate energy distribution could be significant.

An original method of observing a short pulse of electrons, drifting under the action of a uniform field from a source to a collector, was devised and tested in hydrogen by Breare and Von Engel (1964). An electron swarm was released from a pulsed discharge in the gas, it passed through the hydrogen filled chamber. The E/p was sufficiently high for the electrons to produce excitation and ionisation by collision with gas molecules. The UV photons from the

swarm were observed on two planes perpendicular to the direction of drift by collimated photomultiplier detectors. From the separation of the planes and the time interval between the signals from the detectors, for a given electron pulse the drift velocity was determined. The longitudinal diffusion coefficient was also determined, approximately, from the spread of light pulses with time from electron pulses which had drifted a certain distance.

The drift velocities of electrons in several argon+hydrocarbon mixtures were measured by Jean-Marie et al (1979). The method used a strontium-90 source to create secondary electrons, the electrons moved through the drift field and were ultimately detected by a proportional counter. Three sources were used at known distances from the counter, each could be blocked by a lead shield. After crossing the drift volume perpendicular to the field the beta particles were detected by a scintillator and photomultiplier. A scinti--llator was positioned opposite each source, a single photomultiplier viewed all three scintillators. The time between a photomultiplier signal and the corresponding proportional counter signal was measured for two of the sources. Knowing the separation of the sources, the drift velocity was found using the time difference.

The work of the Oak Ridge National Laboratory group on time-of-flight investigations of electron transport in gases is particularly important. This work revealed that electron diffusion is anisotropic with respect to the direction of the electric field (Wagner et al, 1967). A full review of this work from the point of view of longitudinal diffusion coefficient measurement is given in section 2.3. The principles behind drift velocity measurement by this method will be dealt

with briefly here.

The O.R.N.L. experimental arrangement used by Hurst et al (1963) consisted of a uniform field region bounded by a gold photocathode at one end and a Geiger-Mueller tube at the opposite end. Electrons were produced by illuminating the photocathode with UV light from a flash tube delivering 0.5 μs duration light pulses at the rate of 160 per second. The electrons then drifted 27 cm to a 1/16 inch diameter aperture and into the counter. A time-to-amplitude converter and a pulse-height analyser were used to measure the time-of-flight of the electrons. The timing was initiated by a signal from a photo-tube monitoring the UV flash tube. The Geiger counter provided the stop signal. The number of electrons arriving, as a function of time was recorded by the analyser over several minutes of operation. The time corresponding to the peak of this distribution determines the drift velocity. The experimental data was analysed by computer and fitted to the equation for the distribution determined from the solution of the differential equation for the electron density in time and space.

El-Hakeem and Mathieson (1978; 1979) success--fully measured the electron drift velocities in gas mixtures used in gas-filled detectors. The apparatus used was a time-of-flight arrangement based upon that of the O.R.N.L. group, but significantly different. The system was designed with measurements of longitudinal diffusion coefficients in mind and so will be discussed in section 2.3.

2.3 LONGITUDINAL DIFFUSION COEFFICIENT.

Until 1967 and the work of Wagner et al (1967) electron diffusion in gases in a uniform electric field was assumed to be isotropic. The analysis of the Townsend method of measuring D/μ was made using this assumption. It yielded a relationship between D/μ and the current ratio which did not agree with experimental results. The correct relationship, which was derived empirically, was finally justified theoreti-cally when diffusion was found to be anisotropic, see section 2.1.

The time-of-flight experiment has been referred to for the measurement of drift velocity. The drift velocity was obtained from the drift time of the centre of an electron pulse. This experiment is also capable of measuring D_L. D_L is obtained from the width of the electron pulse measured by plotting the arrival of electrons as a number against time distribution. The pulse width increases with drift distance.

Experimental observations by the O.R.N.L. group (Hurst and Parks, 1966; Wagner et al, 1967) show diffusion to be strongly anisotropic, i.e. the coefficient of diffusion perpendicular to the field obtained by the Townsend method is considerably different to the coefficient of diffusion parallel to the field obtained by the time-of-flight method.

The isotropic (lateral) diffusion coefficient is predicted using an electron energy distribution which is constant with position. The longitudinal diffusion coefficient is obtained by modifying the isotropic diffusion coefficient with an extra term accounting for the changes in the electron energy distribution due to the field acting upon the diffusion

current. In other words the assumption that diffusion was isotropic was based upon an assumed electron energy distribu--tion, this strictly would only apply to a situation where electron number density is uniform in space. Clearly such a distribution does not describe a system which involves diffusion. The real distribution only differs from the assumed distribution parallel to the field. The extent of the diffusion of electrons parallel to the field, therefore, is different to that predicted (Parker and Lowke, 1969).

The development of the time-of-flight technique used by the O.R.N.L. group is reviewed by Wagner et al (1967). A Geiger counter had been used as a single electron detector (Hurst et al, 1963; Hurst and Parks, 1966). This detector limited the gases in which electron diffusion could be investigated. Wagner et al described a new apparatus without this limitation by using an electron multiplier detector and a differential pumping system, this arrangement is shown in figure 2.10.

The apparatus consisted of a three-section chamber containing the drift region, the transition region and the detection region. The gas to be studied flowed through the drift region which was normally held at a pressure of up to 25 torr. The transition region and the detection region were differentially pumped and kept at pressures of the order of 10^{-3} torr and 10^{-6} torr respectively.

The drift region contained a 24.5 cm flight path for the electrons, this was bounded by the photocathode held at negative potential and the collecting plate at earth potential. A uniform electric field was established by four field rings between the cathode and the collector plate and connected to them by a potential divider.

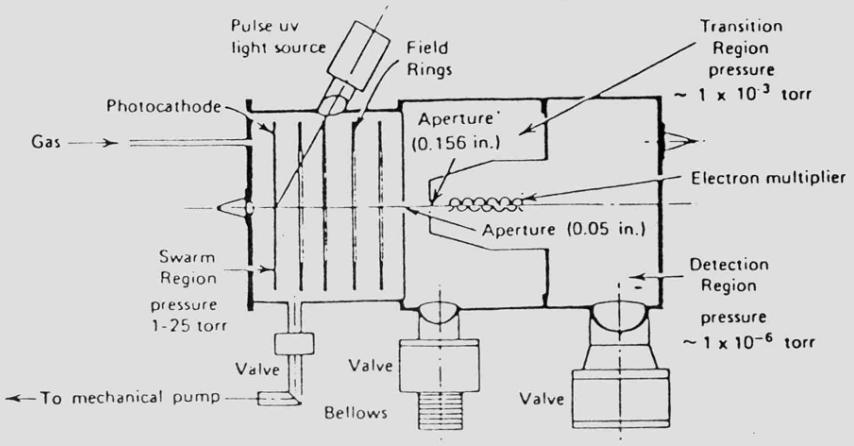

FIG 2·10 The Oak Ridge National Laboratory time-of-flight technique.

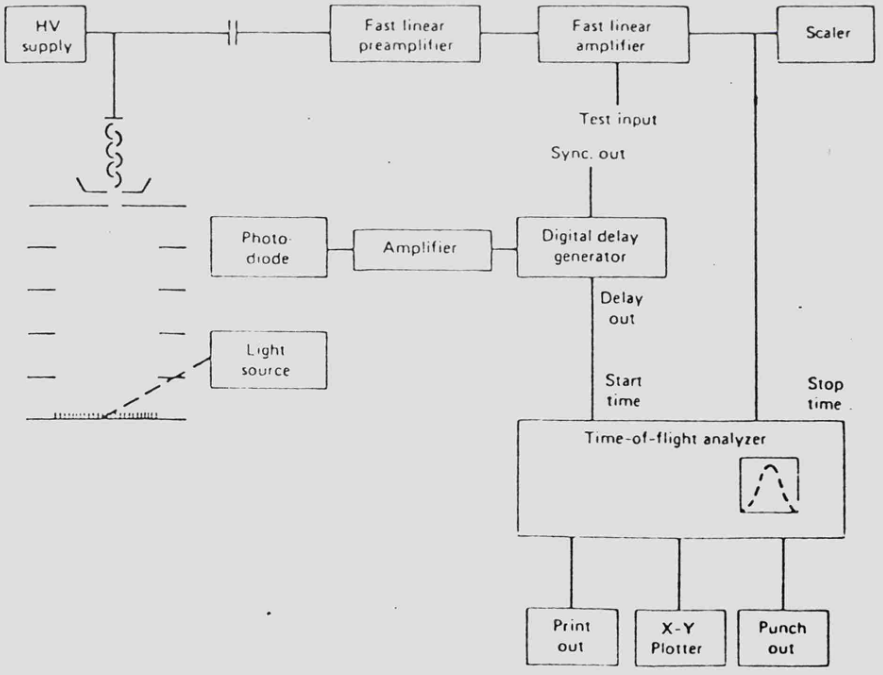

FIG 2·11 The electronics associated with O.R.N.L. experiment.

The three regions were connected by very small apertures through which the electrons passed. By using high speed pumps to evacuate the transition and detection regions, these regions could be maintained at pressures low enough for the operation of the electron multiplier, while the drift region, by careful control of the gas flow into it, could be held at pressures as high as 200 torr.

Electrons from the swarm region are drawn, through the 0.05 inch aperture in the collector plate and the 0.156 inch aperture, into the detection region by a 350 V potential difference applied across the transition region. The amplified electron multiplier pulses provided the stop signal for the time-of-flight analysis. The electron swarms were generated by pulses of UV light passing through a quartz window onto the photocathode. An E.G.&G. FX-6U xenon flash tube was used to produce UV pulses of 275 ns width at 1/e peak intensity and at a rate of 300 per second. The flash tube was monitored by an E.G.&G. SD-100 photodiode which provided the start signal for the time-of-flight analysis.

The electronics associated with this experiment are shown in figure 2.11. The amplification in the detector circuit gave a variable gain of up to 5 000 with an overall rise time below 10 ns. The time-of-flight analyser consisted of a time-to-amplitude converter and a pulse-height analyser. The pulse from each detected electron was recorded in the channel appropriate to its delay after the start pulse. The time interval per channel was variable from 31.25 ns to 64 μs. The experiment was allowed to run until a count against time spectrum with adequate statistics was built up in the analyser.

The theory of this method was described by Hurst and Parks (1966).

The differential equation describing the electron volume density n as a function of position x and time t for this geometry, ignoring ionisation and electron attachment is

$$\frac{dn(x,t)}{dt} = D_L \frac{d^2n(x,t)}{dx^2} - W\frac{dn(x,t)}{dx} \quad (2.2)$$

x = 0 defines the plane of the source

x = h defines the plane of the detector.

Ignoring the diffusion to the electrodes at x = 0 and x = h, the solution of equation 2.2 is

$$n(x,t) = N(4\pi D_L t)^{-\frac{1}{2}} \exp\left[\frac{-(x-Wt)^2}{4D_L t}\right] \quad (2.3)$$

N = area density of electrons when x = 0 at t = 0

n(x,t) = electron density at any point where $0 \leq x \leq h$ as a function of time.

Let the area of the aperture to the detector be A, then the number of electrons $\varepsilon(t)$ entering the detector between the times t and $t+\Delta t$ is given by

$$\varepsilon(t) = n(h,t)AW\Delta t$$

$$\text{or} \quad E(t)\Delta t = n(h,t)AW\Delta t \quad (2.4)$$

$$\text{so} \quad E(t) = NAW(4\pi D_L t)^{-\frac{1}{2}} \exp\left[\frac{-(h-Wt)^2}{4D_L t}\right] \quad (2.5)$$

Hurst et al (1963) showed that by measuring E(t) the parameters D_L and W could be approximated from the time t_m which maximises E(t) and δt, the half-width at 1/e of the maximum $E(t_m)$.

$$W = \frac{h}{t_m} \quad (2.6)$$

to a first approximation when $D_L/hW \ll 1$, the more exact equation is

$$W = \frac{h}{t_m} (1+\beta^2-....)^{-1}$$

where $\beta = \frac{\delta t}{2t_m}$ (Wagner et al, 1967).

$$\delta t = |t_1 - t_m| \qquad (2.7)$$

where $E(t_1) = \frac{1}{e} E(t_m)$

giving $D_L = \frac{h^2(\delta t)^2}{4t_m^3}$ (2.8)

to a first approximation when $2(D_L/hW)^{\frac{1}{2}} \ll 1$

More exactly (Wagner et al, 1967)

$$D_L = \frac{h^2}{t_m} \delta t^2 (1+2\beta^2+....)^{-1}$$

where $\beta = \frac{\delta t}{2t_m} \cong (D_L/Wh)^{\frac{1}{2}}$

Equation 2.5 assumes that the pulse width at the cathode is negligible compared with the width when it is sampled at the detector, that the electronic noise in the system has a negligible effect upon the distribution, and that no distortion is caused by the dead-time of the detection system.

Hurst and Parks (1963) considered the distortion due to dead-times of the order of several hundred microseconds in a Geiger counter detector. The electron arrival time distributions had widths of a few microseconds or less, because of long dead-times only the first electron arriving in the detector from a particular pulse would be analysed. To introduce random sampling of the range of arrival times the number of electrons per pulse which enter the detector should be one or less.

E(t) is determined from measurements on F swarms of electrons released from the photocathode with n_i electrons

per unit area.

N in equation 2.5 is replaced by

$$N = \sum_{i=1}^{F} n_i \tag{2.9}$$

If An_i is kept small so that the counting efficiency C/F is much less than 1, then the probability that an electron from a given swarm has of entering the detector and being counted will be small. The probability will infact be C/F, where C is the number of electrons detected out of F swarms. If $C/F \ll 1$ the probability of two or more electrons from the same swarm entering the detector (and the first being detected) is small compared with C/F. Hurst and Parks then set about determining a value for C/F which would not produce distortion of the measured distribution, shifting the peak towards short arrival times, and therefore producing measured drift velocities higher than the true values.

The proportion of the electrons arriving at the detector aperture between the times t and $t+\Delta t$, which are detected, is given by

$$P_s(t) = \frac{E''(t)\Delta t}{E(t)\Delta t} \tag{2.10}$$

$P_s(t)$ is the probability of the detector being sensitive at time t.

When the dead-time $t_D \gg \delta t$, the detector only counts one electron of a given swarm, then $P_s(t) = P_o(t)$ the probability that the detector had made no counts at time t, so

$$E''(t) = E(t).P_o(t) \tag{2.11}$$

$$= E(t) \exp\left[-\int_o^t \bar{n}_c.\frac{E(t)}{NA}.dt\right] \tag{2.12}$$

$$\text{where } \bar{n}_c = \frac{A}{F} \sum_{i=1}^{F} n_i \tag{2.13}$$

$\bar{n}_c$ is the average number of electrons entering the detector aperture from one swarm.

$$\frac{C}{F} = 1 - e^{-\bar{n}_c} \qquad (2.14)$$

From equation 2.12 it can be seen that for $\bar{n}_c \ll 1$, $E''(t) = E(t)$, Poisson distortion (as termed by Hurst and Parks) occurs when $E''(t) \neq E(t)$.

Figure 2.12 (Hurst and Parks, 1966) shows the distortion of the arrival time spectrum for values of $\bar{n}_c$ between 100 and 0. For $\bar{n}_c < 0.1$ the effects upon W and D by Poisson distortion are insignificant, so if $\frac{C}{F} \leq 0.1$ no distortion results.

The factors affecting the width of the distrib--ution, apart from diffusion, must also be considered. These are the UV light pulse width, and therefore the electron pulse width and the electronic noise. The flash duration at 1/3 peak amplitude of the E.G.&G. flash tube used by Wagner et al (1967) is quoted as 500 ns to 15 μs by the manufacturers (E.G.&G. Inc., Electro-Optics Division Data Sheet F1005D - 3, 1976), the actual duration being dependent upon the discharge capacitance. Wagner et al claimed a 1/e peak amplitude flash duration of 275 ns. A correction factor for D_L to remove the effects of light pulse width and electronic noise was used by Wagner et al. An error function $T_o(t)$ was obtained in a vacuum, this amounts to an arrival time spectrum for electrons when only non-diffusion effects are producing the spread of the arrival times.

The error function produces a smeared function $E'(\tau)$ for the distribution actually measured, where

$$E'(\tau) = \int_0^{\tau} E(t)T_o(\tau - t).dt \qquad (2.15)$$

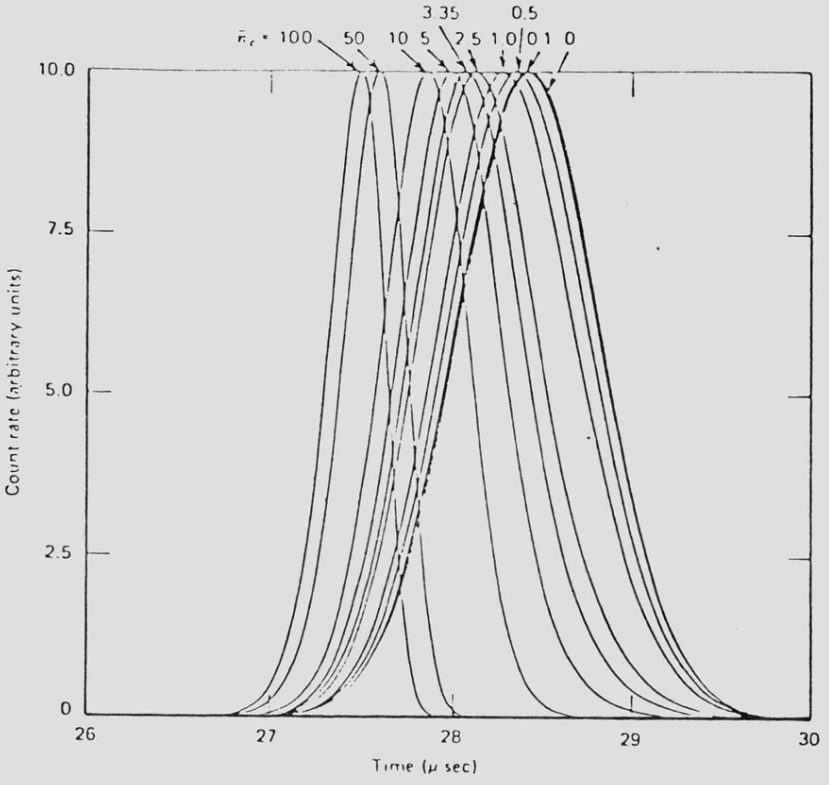

FIG 2·12 Arrival time spectrum distortion for a range of values of $\bar{n}_c$, (shown above the peaks).

and the real distribution is E(t).

The diffusion coefficient obtained from E'(τ) is D_L', the actual value which would be found from E(t) is D_L.

$$D_L' = \frac{h^2(\delta t')^2}{4\ t_m^3} \qquad (2.16)$$

$$\text{and } D_L = \frac{h^2(\delta t)^2}{4\ t_m^3} \qquad (2.17)$$

from equation 2.8. The correction factor f is given by

$$f = \frac{D_L}{D_L'} = \left(\frac{\delta t}{\delta t'}\right)^2 \qquad (2.18)$$

For an arbitrary δt, D_L is calculated from equation 2.8. The value for D_L obtained is used to generate E(t) by substitution into equation 2.5. E'(τ) can be found using equation 2.15 and the values for $T_o(t)$. Wagner et al plotted f as a function of $(2\delta t')^{-1}$ for their experimental arrangement.

The work on electron drift velocity and longit--udinal diffusion in counter gases of El-Hakeem and Mathieson has been referred to in section 2.2. The methods used will be described here as a substantial effort was made to measure D_L, although only drift velocity data was considered consistent enough for publication (El-Hakeem and Mathieson, 1978; 1979).

The experimental arrangement was based upon that of the O.R.N.L. group, (Hurst et al, 1963; Hurst and Parks, 1966; Wagner et al, 1967), but with significant differences. The O.R.N.L. method measured electron drift times, and their spread, over a fixed drift length. The method of El-Hakeem and Mathieson introduced a variable drift length and different analysis techniques. A proportional counter was used as the single electron detector, this was possible as only counter gases were studied (El-Hakeem, 1978).

The method eliminated first-order end-effects in drift velocity measurements, two drift lengths separated by a distance Δh were used resulting in two drift times with a difference $t_{m_1} - t_{m_2} = \Delta t$, then

$$W = \Delta h / \Delta t \qquad (2.19).$$

Generally time-of-flight distributions were obtained for up to five drift lengths with all the other variables fixed. The peak channel of each was obtained by computer analysis. At each E/p value the drift velocity was determined from the gradient of the peak channel as a function of drift time line obtained by a least-squares best fit program operating on up to five points. C/F values between 0.1 and 0.2 were used to minimise Poisson distortion.

The maximum drift length of the arrangement was 5 cm, and fairly high pressures were used because of poor gas control at lower pressures. Consequently the amount of diffusion was small and masked by the contribution of UV light pulse width. Longitudinal diffusion was observed by using a narrow electrical pulse to control the injection of electrons into the drift region. However the amount of diffusion was small and no consistent drift length dependence was found.

A similar arrangement has been used in this work, and some results for D_L obtained.

CHAPTER 3.

REVIEW OF TRANSPORT COEFFICIENT PREDICTION BY SOLUTION OF THE TRANSPORT EQUATION.

3.1 INTRODUCTION.

The dependence of the electron number density n upon the transport coefficients W, D and D_L is used in the analysis of the experiments carried out in this work. This aspect of the theory of electron motion is reviewed in section 3.2.

The predictions obtained for D by the solution of the transport equation, and for D_L and W by Monte - Carlo simulation used collision cross-section data obtained by other workers. The theory of the dependence of W, D and D_L on cross-sections is reviewed in section 3.3.

Under the action of a uniform electric field, drifting electrons quickly reach a state of steady motion. The mean kinetic energy of the electrons is then the same at all points in the field. This mean energy increases with the field strength. The lower limit to this energy is that due to thermal agitation, but for a finite field strength the electrons have a mean energy greater than that of the gas molecules. In this work only field strengths so low that the electrons have mean energies considerably less than the ionisation potentials of the gases have been used.

In a collision with a gas molecule an electron can lose insignificant energy compared with its total energy, in which case the collision is elastic. If the electron does lose significant energy, as a proportion of its total energy

then the collision is inelastic. When the mean energy of the electrons is greater than that of the gas molecules there is a mean energy loss by the electrons in each collision with a molecule. In the steady state this energy loss equals the energy gain due to acceleration by the electric field. There will of course be a distribution of energies about the mean and therefore of velocities about the mean velocity.

In the experiments discussed in this work the electron density has been kept very small compared with the molecule number density, collisions between electrons can therefore be ignored and the velocity and energy distributions are determined by collisions between electrons and gas molecules.

3.2 THE DEPENDENCE OF ELECTRON NUMBER DENSITY UPON THE TRANSPORT COEFFICIENTS.

The diffusion process depends upon the velocity of agitation of the electrons in a gas and is a tendency to produce a uniform distribution of electrons through the gas.

The electron number density n in a gas, in the absence of an electric field, varies continuously as a function of position defined by the coordinates x, y, z. The rate at which they move in a given direction, e.g. through the yz plane is proportional to $-\frac{dn}{dx}$ and is represented by $-D\frac{dn}{dx}$ where D is the diffusion coefficient.

Townsend (1913; 1915; 1947) considered electrons moving with velocity components u, v, w in the directions x, y, z and obtained expressions for the rate at which electrons moved across unit area planes in the three directions. An equation of number continuity was obtained

$$\frac{\delta n}{\delta t} = D\nabla^2 n \qquad (3.1)$$

this represents the rate at which the number of electrons in an elementary volume dxdydz increases as a result of diffusion.

Clearly D was assumed to be the same for each direction and is termed the isotropic diffusion coefficient.

Solutions of this equation of continuity depend upon conditions at t = 0 and on boundary conditions. For example if n_o particles are at r = 0 at t = 0 then a suitable solution is

$$n = \frac{n_o}{(4\pi Dt)^{3/2}} e^{-r^2/4Dt} \qquad (3.2)$$

(Huxley and Crompton, 1974) from which the mean square radius of the group of particles after some time t is given by

$$\overline{r^2} = 6Dt$$

In the presence of an electric field a drift is imposed on the electrons. Let the drift velocity $\underline{W}$ be in the direction z. The electron flux $\underline{J} = \underline{J}_D + \underline{J}_d$ where $\underline{J}_D$ is due to diffusion and is the same as $\underline{J}$ in the no field case, $\underline{J}_d$ is due to drift, $\underline{J}$ is now given by

$$\underline{J} = -D \text{ grad } n + n\underline{W} \tag{3.3}$$

The equation of continuity becomes

$$\frac{\partial n}{\partial t} = \text{div } \underline{J} = D\nabla^2 n - n \text{ div } \underline{W} - \underline{W} \text{ grad } n$$

If $\underline{W}$ is independent of the position coordinates div $\underline{W} = 0$, then

$$\frac{\partial n}{\partial t} = D\nabla^2 n - \underline{W} \text{ grad } n$$

$$= D\nabla^2 n - \underline{W} \frac{dn}{dz} \tag{3.4}$$

It is now known that diffusion is anisotropic due to the influence of density gradients upon the energy distribution (Wagner et al, 1967; Parker and Lowke, 1969; Skullerud, 1969). The longitudinal diffusion coefficient D_L for the z direction is introduced. The continuity equation is further modified as follows

$$\frac{\partial n}{\partial t} = D\nabla^2 n + (D_L - D)\frac{\partial^2 n}{\partial z^2} - \underline{W} \frac{\partial n}{\partial z} \tag{3.5}$$

The solution of this equation for an isolated group of n_o electrons uninfluenced by cathode or anode planes is

$$n = \frac{n_o}{(4\pi Dt)(4\pi D_L t)^{\frac{1}{2}}} e^{-(x^2+y^2)/4Dt} . e^{-(z-Wt)^2/4D_L t} \tag{3.6}$$

(Huxley and Crompton, 1974) from which $\overline{x^2} = 2Dt$ and $\overline{y^2} = 2Dt$ so that the mean square radius in the xy plane,

$$\overline{r^2} = \overline{x^2} + \overline{y^2} = 4Dt$$

and $$\overline{z^2} = 2D_L t + \bar{z}^2 = 2D_L t + (Wt)^2.$$

If $\frac{dn}{dx} = \frac{dn}{dy} = 0$ then

$$\frac{\partial n}{\partial t} = D_L \frac{d^2 n}{dz^2} - W \frac{dn}{dz} \qquad (3.7)$$

The solution to this is given by

$$n(z,t) = \frac{n_o}{(4\pi D_L t)^{\frac{1}{2}}} e^{-(z-Wt)^2/4D_L t} \qquad (3.8)$$

This is the solution relevant to D_L and W measurement. These quantities are found experimentally by time-of-flight measure--ments.

If t_m is the time at which the flux of electrons crossing the plane h from the cathode plane reaches its maximum value, then

$$W \cong \frac{h}{t_m}(1-\beta)$$

$$\text{where } \beta = \frac{D_L}{Wh} = \frac{D_L/\mu}{V}$$

and where V = Eh = potential drop in the drift region, and $\mu = W/E$ = electron mobility.

A more complete analysis, taking into account the flux of electrons due to diffusion and back-diffusion to the cathode shows that

$$W = \frac{h}{t_m}(1 - 5\beta) \qquad (3.9)$$

(Lowke, 1962; 1963 and section 2.2.2, Huxley and Crompton, 1974).

In principle D_L can be determined from the arrival time spectrum. The electron flux at the anode plane is given by Wn(h,t). At time $t' > t_m$ the flux is 1/e of its peak value, then

$$D_L \cong \frac{h^2}{4t_m^3}(t' - t_m)^2$$

(Wagner et al, 1967). Further analysis shows a more accurate result is

$$D_L \cong \frac{h^2}{4t_m^3}(t' - t_m)^2(1 - 2\beta) \qquad (3.10)$$

For D measurement the continuity equation 3.5 is used. For a continuous stream of electrons at a steady state $\frac{\partial n}{\partial t} = 0$, so equation 3.5 becomes

$$D\nabla^2 n + (D_L - D)\frac{d^2 n}{dz^2} - W\frac{dn}{dz} = 0 \qquad (3.11)$$

The solution must show the lateral diffusion of the electron swarm from a point, at z = 0, the cathode, i.e. n = 0 at the cathode except at x = y = z = 0. It can be shown that a suitable solution is, to a good approximation

$$n = \text{constant.}\ e^{\lambda_L z}(r')^{-\frac{1}{2}}K_{3/2}(\lambda_L r')\frac{z}{r'} \qquad (3.12)$$

where $\lambda_L = \frac{W}{2D_L}$, $r' = (x'^2 + y'^2 + z^2)^{\frac{1}{2}}$,

and $x' = \left(\frac{D_L}{D}\right)^{\frac{1}{2}}x$, $y' = \left(\frac{D_L}{D}\right)^{\frac{1}{2}}y$

$K_{3/2}$ is the modified Bessel function of the second kind of order 3/2. This is termed the dipole solution, corresponding to the term for k = 1 in the following fuller expression for n at distances large compared with the source aperture size. The term for k = 0 is the pole solution and in terms for k > 1 the coefficients diminish to such an extent that they are assumed to make the terms negligible

$$n = e^{\lambda_L z}\sum_{k=0}^{\infty} A_{2k+1}r'^{-\frac{1}{2}}K_{2k+3/2}(\lambda_L r')P_{2k+1}\left(\frac{z}{r'}\right)$$

P_{2k+1} is a Legendre polynomial with order 2k+1. (Huxley and Crompton, 1974).

The properties of the Bessel function show the dipole distribution 3.12 to be equivalent to

$$n = \text{constant.}(z/r')\left(1 + \frac{1}{\lambda_L r'}\right)\frac{e^{-\lambda_L(r'-z)}}{r'}$$

$$= \text{constant.}\, e^{\lambda_L z}\frac{\partial}{\partial z}(e^{-\lambda_L r'}/r')$$

The electron swarm is collected on a metal anode with a circular division, so that at $z = h$, n must be zero. The complete solution obtained by Huxley and Crompton is

$$n = -\text{constant}.e^{\lambda_L z} \frac{\partial}{\partial z}\left(\frac{e^{-\lambda_L r'}}{r'} + \frac{e^{-\lambda_L r''}}{r''}\right)$$

where $r'' = \rho^2 + (z-2h)^2$, $\rho = (D_L/D)^{\frac{1}{2}}\rho$

and $\rho^2 = x^2 + y^2$

The current density then has a z-component J_z at any plane between the cathode and the anode given by

$$J_z = e(nW - D_L\frac{\partial n}{\partial z}) = eD_L(2\lambda_L n - \frac{\partial n}{\partial z})$$

With considerable mathematical manipulation the current ratio at the divided anode with a central collector radius b can be calculated to a high degree of accuracy,

$$R = \frac{\text{current to central collector}}{\text{total current to the anode}} = 1-(1+(\tfrac{1}{2}- D_L/D)(b/d^2)\frac{he^{-\lambda(d-h)}}{d}$$

where $\lambda = W/2D$ and $d^2 = h^2 + b^2$.

In most experiments $b \ll h$ so that this expression reduces to

$$R = 1 - \frac{h}{d}(e^{-\lambda(d-h)}) \cong 1 - e^{-Wb^2/4Dh}.$$

3.3 THE DEPENDENCE OF THE TRANSPORT COEFFICIENTS UPON COLLISION CROSS-SECTIONS.

3.3.1 Introduction.

This topic, the establishment and solution of the Maxwell-Boltzmann equation, is of course the central theoretical problem in the study of electron drift and diffusion. A detailed treatment is however far beyond the scope of this thesis. Several definitive accounts have already been given (Huxley and Crompton, 1974 and Lowke et al, 1977 etc), and the topic is indeed still an important theoretical research area. Instead a very brief summary of the main arguments and equations relevant to the present measurements will be given. This summary will demonstrate how the standard theory has been correctly adapted to describe gas mixtures. It will point out the main approximations of the standard theory and discuss very briefly its inability to describe anisotropic diffusion.

The main source of reference for this section is Huxley and Crompton (1974). Where possible their nomencla-ture will also be employed here.

3.3.2 The Two-term Approximation.

The electron spatial and velocity distribution may be represented by the function $n(\underline{r},t)f(\underline{r},\underline{c},t)$ where n is the number density at vector position $\underline{r}$ at time t and f is the relative density in velocity space at vector velocity $\underline{c}$. That is $\int_0^\infty f(\underline{c})c^2 d\omega dc = 1$ where $d\omega$ is an infinitesimal solid angle in velocity space.

In order to make progress in the standard theory it is necessary to assume the relatively simple two-term form for $f(\underline{c})$,

$$f(\underline{c}) = f_0(c) + f_1(c)\cos\theta \qquad (3.13)$$

where θ is the polar angle in velocity space. Higher terms in the expansion are assumed to have negligible importance. The validity of this assumption has received considerable question--ing (Milloy and Watts, 1977; Francey and Stewart, 1972; Jacob et al, 1979).

Monte-Carlo simulation and Boltzmann theory predictions for drift velocity in various gas mixtures are presented in chapter 8, these show fairly good agreement, seeming to justify the assumption, even in cases where the ratio f_1/f_0 is not small compared with unity. As will be seen however the results for diffusion coefficient do not agree so favourably. There have been major changes in the theoretical approach to the solution of the Maxwell-Boltzmann equation recently which obviate the necessity of the expansion above (Kleban and Davis, 1977; Ferrari, 1978; Lin et al, 1979). A useful discussion of this quite different approach is not possible in the limited space available here.

3.3.3 The Scalar Equation.

By considering the conservation of electron number one can arrive at the following differential equation involving f_0 and $\underline{f}_1$ (where the direction of the vector $\underline{f}_1$ is the axis $\theta = 0$).

$$\frac{\partial}{\partial t}(nf_0) + \frac{c}{3}\,\mathrm{div}(n\underline{f}_1) + \frac{1}{4\pi c^2}\frac{\partial}{\partial c}(\sigma_E - \sigma_{coll}) = 0 \qquad (3.14)$$

where $\sigma_E = \frac{4\pi c^2}{3} \frac{e\underline{E}}{m} . n\underline{f}_1$

$$\sigma_{coll} = \sigma_{coll\ el} + \sigma_{coll\ inel}$$

$$\sigma_{coll\ el} = 4\pi nc^2 \frac{\nu_{el}}{M} \left(mcf_0 + kT \frac{\partial f_0}{\partial c}\right)$$

$$\nu_{el} = Ncq_{m\ el}$$

$$\sigma_{coll\ inel} = 4\pi nN \int_c^{c_1} f_0(x) x^3 q_{0inel} dx$$

$$c_1^2 = c^2 + c_{in}^2$$

In these expressions N is the gas molecule number density, M the molecular weight, $q_{m\ el}$ the momentum transfer cross-section for elastic collisions, q_{0inel} the total cross-section for inelastic collisions, c_{in} the threshold velocity for inelastic collisions and E the applied electric field. Clearly $q_{0inel}(x)$ is zero for $x < c_{in}$.

$\sigma_E(c)$ represents the net rate at which electrons, in unit volume drift through the surface of a sphere in velocity space of radius c, due to the application of the field E.

$\sigma_{coll}(c)$ represents the net rate of loss from the sphere due to collisions with gas molecules. In the expression for $\sigma_{coll\ inel}$, superelastic collisions (collisions of the second kind) have been ignored.

ν_{el} is the collision frequency for elastic collisions.

3.3.4. The Vector Equation.

By considering the conservation of momentum, Huxley and Crompton (1974), after a lengthy and detailed argument, were able to establish a second differential equation

in f_0 and $\underline{f}_1$.

$$n\underline{f}_1 = \frac{-e\underline{E}}{m\nu}\frac{\partial}{\partial c}(nf_0) - \frac{c}{\nu}\,\mathrm{grad}(nf_0) \qquad (3.15)$$

where $\nu(c) \cong \nu_{el}(c) + \nu_{0inel}$

$$\nu_{0inel} = Ncq_{0inel}$$

Here ν is the effective collision frequency, and the approx--imation sign indicates that isotropic inelastic scattering has been assumed. The effective collision cross-section for momentum transfer is $q_m(c) = \nu(c)/Nc$, that is

$$q_m = q_{m\ el} + \sum_k q_{0kinel} \qquad (3.16)$$

The summation shows the case when several inelastic scattering levels are present.

3.3.5 The 'Uniform Steady Stream' Approximation.

This procedure allows us to obtain integral expressions for the transport coefficients in terms of the distribution function f_0, but leads (incorrectly) to isotropic diffusion.

The scalar equation is multiplied throughout by $4\pi c^2 dc$ and integrated from 0 to ∞. Then, since $\sigma_E = \sigma_{coll} = 0$ at both $c = 0$ and $c = \infty$, and since $\int_0^\infty 4\pi c^2 f_0 . dc = 1$,

$$\frac{\partial n}{\partial t} + \mathrm{div}\left\{\int_0^\infty \frac{c}{3}\, n\underline{f}_1 4\pi c^2 dc\right\} = 0$$

Substituting for $n\underline{f}_1$ from the vector equation yields the expression

$$\frac{\partial n}{\partial t} - \mathrm{div}\,\mathrm{grad}\left\{\frac{4\pi}{3} n\int_0^\infty c^4 \frac{f_0}{\nu}\, dc\right\} - \mathrm{div}\left\{\frac{4\pi}{3}\, n\,\frac{e\underline{E}}{m}\int_0^\infty \frac{c^3}{\nu}\frac{\partial f_0}{\partial c} dc\right\}$$

$$= 0 \qquad (3.17)$$

The essentially incorrect assumption

is now made in this simple treatment, that f_0 is a function only of c and not of position $\underline{r}$. (This was the error made unknowingly in all early analyses). With this simplification equation 3.17 becomes

$$\frac{\partial n}{\partial t} - D \text{ div grad } n + W.\text{grad } n = 0 \qquad (3.18)$$

where $D = \frac{4\pi}{3}\int_0^\infty \frac{c^4 f_0}{\nu}\, dc$ and $W = \frac{-4\pi eE}{3m}\int_0^\infty \frac{c^3 df_0}{\nu\, dc}\, dc$

Hence D and W can be identified as the isotropic diffusion coefficient and the drift velocity respectively. These integral expressions allow D and W to be evaluated once the function f_0 has been calculated.

A much lengthier treatment is necessary if the dependence of f_0 on $\underline{r}$ is taken into account. This leads however to the correct explanation of anisotropic diffusion phenomena. A very brief indication of longitudinal diffusion theory is given in Appendix A of this chapter.

3.3.6 Integro-Differential Equation for f_0.

The final stage in this simplified standard theory of drift and diffusion is to obtain an equation for f_0. In general this equation can only be solved numerically, and then further numerical integration leads to values for D and W (and also mean electron energy).

In the 'uniform steady-stream' approximation $\text{div}(nf_1) = 0$ and $\frac{\partial n}{\partial t} = 0$ so that the scalar equation, equation 3.14 reduces to

$$\sigma_E = \sigma_{coll}$$

That is, since $\text{grad}(nf_0) = 0$ also,

$$\frac{-4\pi c^2 eE}{3}\cdot\frac{eE}{m}\cdot\frac{df_0}{m\nu\, dc} = 4\pi c^2 \nu_{M_{el}}(mcf_0 + kT\frac{df_0}{dc}) + 4\pi N\int_{c_2}^{c_1} f_0(x)x^3 q_{0_{inel}}(x)dx$$

which can be arranged in the form

$$c^2\frac{df_0}{dc}\left\{\frac{(eE/m)^2 l}{3\nu N}+\frac{kT\,\nu_{el}}{NM}\right\}+\frac{c^3 m\,\nu_{el}}{N\,M}f_0+\int_c^{c_1} f_0(x)x^3 q_{0\,inel}(x)dx = 0 \qquad (3.19)$$

It is usually more convenient to express quantities in terms of energy $\varepsilon = mc^2/2$ rather than velocity c. Further it is helpful simplification in nomenclature to introduce the symbol $z = \varepsilon/kT$. Then in terms of this normalised energy z, equation 3.19 may be written

$$z\,\frac{df_0}{dz}\left\{\frac{\alpha}{\theta'}+\theta z\right\}+z^2\theta f_0+\int_z^{z+z_i} f_0\,\eta\,z'dz' = 0 \qquad (3.20)$$

where $\alpha = \left(\frac{eE}{NkTq_0}\right)^2\frac{M_0}{6m}$, $\theta' = \frac{q_m}{q_0}$, $\theta = \frac{q_{m\,el}/q_0}{M/M_0}$, $\eta = \frac{M_0\,q_{0\,inel}}{2m\,q_0}$

Here M_0 is a convenient mass unit (e.g. hydrogen atomic mass) and q_0 is a convenient cross-sectional area (e.g. $10^{-15}cm^2$). Equation 3.20 was first obtained by Frost and Phelps (1962).

3.3.7 Expressions for D, W and $\bar{\varepsilon}$.

The energy distribution function f_0 in equation 3.20 may be replaced by f_0' where

$$f_0' = 4\pi\sqrt{2}(kT/m)^{\frac{3}{2}} f_0$$

f_0' is of course also a solution of equation 3.20. Then since $\int_0^\infty f_0 . 4\pi c^2 dc = 1$ it follows that $\int_0^\infty f_0'\, z^{\frac{1}{2}}dz = 1$.

In terms of f_0' and z the expressions for D and W from equation 3.18 can be written

$$D = \frac{1}{p}\left(\frac{2(kT)^3}{q_m q_0^2}\right)^{\frac{1}{2}}\int_0^\infty \frac{z f_0'}{\theta'}\,dz \qquad (3.21)$$

$$W = -\frac{E}{p}\left(\frac{2e^2kT}{q_m q_0^2}\right)^{\frac{1}{2}}\int_0^\infty \frac{z}{\theta'}\frac{df_0'}{dz}\,dz \qquad (3.22)$$

The mean electron energy $\bar{\varepsilon}$ may be obtained from

$$\bar{\varepsilon} = kT\int_0^\infty f_0' z^{3/2} dz \qquad (3.23)$$

3.3.8 Modification of the treatment for gas mixtures.

The present simple theory may be relatively easily modified to accommodate gas mixtures in a correct manner. The individual terms leading to equation 3.19 need to be considered.

In the elastic collision contribution to σ_{coll} (see section 3.3.3) there is the multiplying factor

$\frac{\nu_{el}}{M} = \frac{c}{kT}\frac{pq_{m\ el}}{M}$, where $p = NkT$ is the gas pressure. If several gas components are present, the j^{th} having partial pressure $f_j p$, then this multiplying factor clearly becomes

$$\frac{cp}{kT}\sum_j f_j \frac{q_{m\ el\ j}}{M_j}$$

where M_j is the molecular weight of the j^{th} component.

The inelastic contribution to σ_{coll} is proport--ional to the gas number density $N = p/kT$. Hence in the case of gas components this contribution becomes

$$\frac{p}{kT}\sum_j f_j \int_c^{c_{1j}} f_0(x) x^3 q_{0\ inel\ j} dx,$$

where $c_{1j}^2 = c^2 + c_{in\,j}^2$

It is also generally necessary to sum this contribution over several excitation levels for each gas component.

Finally, the term σ_E is determined by the effective collision frequency $\nu = Ncq_m = cpq_m/kT$. Thus in a gas mixture the total effective collision frequency becomes

$$\nu = \frac{cp}{kT} \sum_j f_j (q_{m\,el\,j} + q_{0\,inel\,j})$$

Again, the second term is itself generally a summation over several excitation levels.

With these modified terms in the equation preceding 3.19 a modified version of equation 3.19 is easily produced. Again this may be expressed in terms of the normal-ised energy term $z = \varepsilon/kT$. Thus

$$z\frac{df_0'}{dz}\left\{\frac{\alpha}{\theta'} + \theta z\right\} + z^2\theta f_0' + \sum_j \int_z^{z+z_{ij}} f_0' \eta_j z' dz' = 0 \qquad (3.24)$$

where $\alpha = (eE/pq_0)^2 M_0/6m$, $\theta' = \sum_j f_j (q_{m\,el\,j} + q_{0\,inel\,j})/q_0$,

and $\theta = \sum_j f_j \frac{q_{m\,el}/q_0}{M_j/M_0}$, $\eta_j = f_j \frac{M_0}{2m} \frac{q_{0\,inel\,j}}{q_0}$

If the various cross-sections are known as functions of z then an attempt may be made to evaluate the distribution function f_0' by solving, numerically, the integro-differential equation 3.24. If this can be achieved then D, W and $\bar{\varepsilon}$ can be found from equations 3.21, 3.22 and 3.23.

Equation 3.24 can be arranged in the form

$$-\frac{1}{f_0}\frac{df_0}{dz} = \frac{1 + S(z,f_0)/z^2\theta f_0}{1 + \alpha/z\theta\theta'} = G(z) \qquad (3.25)$$

In this expression $S(z,f_0)$ replaces the double summation and integral (inelastic scattering term) in equation 3.24, now

$$f_0(z) = A \exp\left(-\int_0^z G(z')dz'\right) \qquad (3.26)$$

where A is determined by the normalisation condition

$$\int_0^\infty z^{\frac{1}{2}} f_0(z) dz = 1.$$

The equation (3.25) has been solved numerically by a self-consistent, iterative method of the type first used

by Lucas (1969). An initial trial distribution $f_0(z)$ is used to compute $S(z,f_0)$ and then find the function $G(z)$ from equation 3.25. This function is then used, in equation 3.26, to find a new distribution $f_0(z)$, and so on. Iteration proceeds until f_0 remains stable. An upper energy limit ε_L of a few eV was chosen and the range divided into 2^n equal intervals for the purpose of integration and to define the functions f_0, S and G, n was increased by unit steps from 7 to 11. At each value of n iteration was allowed to proceed until the mean energy $\bar{\varepsilon}$ had stabilised to within 0.05 %. Depending upon the particular situation the number of iterations required at n = 7 varied between 7 and 32. At each increase in n, twice as many values are required to define the new trial function f_0. These new values were found by linear interpolation between the f_0 values for the previous n value. A Maxwellian distribution was chosen for the initial trial function (the case if the electric field is zero), for n = 7, it was established that the final function was independent of initial choice. The change in the calculated values for W, D and $\bar{\varepsilon}$ between n = 10 and n = 11 was always acceptably small, less than 0.2 % for W and D and less than 0.1 % for $\bar{\varepsilon}$.

The function $S(z,f_0)$ was evaluated in practice from the expression

$$S(z,f_0) = \sum_i \sum_j \int_z^{z_L} f_0(z')z' n_{ij}(z')dz' - \sum_i \sum_j \int_{z+z_{ij}}^{z_L} f_0(z')z' \times n_{ij}(z')dz'$$

where $z_L = \varepsilon_L/kT$. At each value of E/p it was established that the calculated results were independent of the choice of the upper energy limit ε_L. (Mathieson and El-Hakeem, 1979).

APPENDIX A

A BRIEF ACCOUNT OF THE THEORY OF LONGITUDINAL DIFFUSION.

A1 Introduction.

The outline given below is based closely on the treatment of Huxley and Crompton (1974), Chapter 4. However the final equations obtained differ in detail from those of Huxley and Crompton. The discussion below is meant only to provide 'sign-posts' for those interested in further study of the problem.

A2 Average and Local Distribution Functions.

It is useful to consider the behaviour of an isolated travelling group of electrons that have reached equilibrium with the gas and the applied field. Average velocity distribution functions for the group may be defined. Thus, integrating over all the space occupied by the group,

$$f_0^*(c) = \frac{1}{n_0} \int f_0(c,\underline{r},t)n(\underline{r},t)d\underline{r}$$

and $$f_1^*(c) = \frac{1}{n_0} \int f_1(c,\underline{r},t)n(\underline{r},t)d\underline{r}$$

where f_0 and f_1 are the local velocity distribution functions and are, in general, functions of position $\underline{r}$ and time t. The local density function is $n(\underline{r},t)$ and the total number of elect--rons in the group is n_0. It should be noted that

$$\int_0^\infty 4\pi f_0 c^2 dc = 1 \qquad \text{and} \qquad \int_0^\infty 4\pi f_0^* c^2 dc = 1.$$

It may be established (after considerable analysis and argument) that the average distribution function

for the group f_0^* is the same as that for the 'uniform steady stream' (that is as given by equation 3.19).

It may also be shown that the velocity W of the centroid of the group is given by

$$W = \frac{4\pi}{3}\int_0^\infty c^3 f_1^* dc = -\frac{4\pi}{3}\frac{eE}{m}\int_0^\infty \frac{c^3}{\nu}\frac{df_0^*}{dc}dc$$

A3 Fundamental Equation for nf_0.

By substituting for nf_1 from equation 3.15 into the 'scalar' equation 3.14, a complete integro-differen-tial equation for nf_0 is obtained. Choosing the electric field to be in the direction of the z-axis, this equation may be written as follows

$$-\frac{\partial}{\partial t}(nf_0) + \frac{cV'}{3}\frac{\partial}{\partial z}\frac{\partial}{\partial c}(nf_0) + \frac{c^2}{3\nu}\nabla^2(nf_0)$$
$$+\frac{1}{c^2}\frac{\partial}{\partial c}\left\{c^2\left[\frac{cV'}{3}\frac{\partial}{\partial z}(nf_0) + \frac{\nu_{el}}{3}(VV'+\frac{3kT}{M})\frac{\partial}{\partial c}(nf_0)\right.\right.$$
$$\left.\left.+\frac{mc}{M}\nu_{el}nf_0 + \frac{N}{c^2}nI(f_0)\right]\right\} = 0 \qquad (A.1)$$

where $I(f_0) = \int_c^{c_1} f_0(x) q_{0\ inel} x^3 dx$ as given in equation 3.14,

$V' = eE/m\nu$ and $V = eE/m\nu_{el}$

Equation A.1 is equivalent to equation 4.9 of Huxley and Crompton but includes the effect of inelastic scattering.

A4 Expansion of f_0.

The basic reason why diffusion is in general anisotropic is the positional dependence of the local velocity distribution function f_0 (see section 3.3). This dependence can be expressed as an expansion in terms proportional to the

spatial derivatives of $n(\underline{r})$. As pointed out by Huxley and Crompton, in most experimental situations large relative density gradients are not encountered so that the number of terms required is small.

For simplicity consider motion in one direction only. That is the density function q is given by

$$q(z,t) = \iint_{-\infty}^{\infty} n \, dx \, dy$$

By integrating each term in equation A.1 over all x and y, the same equation is obtained with q replacing n and $\frac{\partial^2}{\partial z}$ replacing ∇^2.

Now consider the following expression for $f_0(c,z,t)$

$$f_0 q = f_0^* \sum_{k=0}^{\infty} b_k(c) \frac{\partial^k}{\partial z^k} q$$

If consideration is restricted to the first two terms only

$$f_0 q = f_0^*(q + b_1 \frac{\partial q}{\partial z}) \text{ where } b_0 = 1 \qquad (A.2)$$

For simplicity the subscript on $b_1(c)$ will be dropped.

This expansion of $f_0 q$ will allow equation A.1 to be separated into equations which, in principle, allow the functions f_0^* and b to be determined.

A5 Mathematical Development.

It is convenient to introduce the longitudinal diffusion coefficient D_L by referring equation A.1 to a set of axes moving along the z-axis with the velocity W of the group centroid. That is $x' = x$, $y' = y$ and $z' = z - Wt$. It follows that

$$\frac{d}{dt} = W \frac{\partial}{\partial z'} + \frac{\partial}{\partial t} \quad \text{and} \quad \frac{\partial}{\partial z} = \frac{\partial}{\partial z'},$$

An observer moving in the dashed coordinate system would describe the time and position behaviour in the density q by means of the equation

$$\frac{dq}{dt} = D_L \frac{\partial^2 q}{\partial z'^2}$$

Thus

$$-\frac{\partial}{\partial t}(qf_0) = -\frac{d}{dt}(qf_0) + W\frac{\partial}{\partial z'}(qf_0)$$

$$\cong -f_0^* D_L \frac{\partial^2 q}{\partial z'^2} + W\frac{\partial}{\partial z'}(qf_0)$$

The approximation sign indicates that a term in $\frac{\partial^3 q}{\partial z'^3}$ has been ignored.

Having removed the time term in equation A.1 (by employing moving axes), it is now possible to substitute for $f_0 q$ from equation A.2 in the remaining terms. This is a clumsy but straightforward procedure leading to an equation in the form

$$A(c)q + B(c)\frac{\partial q}{\partial z} + C(c)\frac{\partial^2 q}{\partial z^2} = 0 \qquad (A.3)$$

where again third derivatives have been ignored, and for simplicity the prime on z' has been removed. In equation A.3 the coefficients A, B and C must each be zero. Thus the following three equations are obtained.

$$c^2\frac{df_0^*}{dc}\left(\frac{VV'\nu_{el}}{3N} + \frac{kT\nu_{el}}{NM}\right) + \frac{c^3 m\nu_{el}}{N}\frac{f_0^*}{M} + I_1 = 0 \qquad (A.4)$$

$$Wf_0^* + \frac{cV'}{3}\frac{df_0^*}{dc} + \frac{1}{c^2}\frac{\partial}{\partial c}\left\{\frac{c^3}{3}V'f_0^* + c^2\frac{d}{dc}(f_0^* b)\left(\frac{VV'\nu_{el}}{3} + \frac{kT\nu_{el}}{M}\right) + \frac{c^3 m\nu_{el}}{M}f_0^* b + NI_2\right\} = 0 \qquad (A.5)$$

$$-f_0^* D_L + Wf_0^* b + \frac{cV'}{3}\frac{d}{dc}(f_0^* b) + \frac{c^2}{3\nu}f_0^* + \frac{1}{c^2}\frac{\partial}{\partial c}\left\{\frac{c^3\nu_{el}}{\nu}V'f_0^* b\right\} = 0 \qquad (A.6)$$

where

$$I_1 = \int_c^{c_1} f_0^*(x) q_{0\ inel}\, x^3 dx \qquad \text{and}$$

$$I_2 = \int_c^{c_1} f_0^*(x) b(x) q_{0\ inel}\, x^3\, dx$$

It can be seen that the first equation A.4, is simply the equation, 3.19, developed in section 3.3.6 describ--ing the velocity distribution function for the 'uniform steady stream' conditions. The third equation A.6 may be multiplied throughout by $4\pi c^2 dc$ and integrated over all velocities. Then, since

$$\int_0^\infty 4\pi f_0^* c^2 dc = 1 \quad \text{and} \quad \int_0^\infty 4\pi f_0^* b c^2\, dc = 0$$

$$D_L = \frac{4\pi}{3} \int_0^\infty \frac{c^4}{\nu} f_0^* dc + \frac{4\pi}{3} \int_0^\infty c^3 V' \frac{d}{dc}(f_0^* b) dc \qquad (A.7)$$

The first term above is the isotropic diffusion coefficient, it is seen that only if b is zero is isotropic diffusion obtained. Equation A.5 differs somewhat from that implied by the equations and discussion given by Huxley and Crompton[1].

In principle it should be possible to calculate the function b(c) from the two equations A.4 and A.5. Work on this problem is still in hand. It has been found difficult to obtain convergence in iterative procedures, although some limited success has now been achieved.

CHAPTER 4.

REVIEW OF TRANSPORT COEFFICIENT PREDICTION BY MONTE - CARLO SIMULATION OF ELECTRON MOTION IN GASES.

4.1 INTRODUCTION.

The experimental results obtained in this work are compared with theoretical predictions in chapter 8. The Monte-Carlo simulations of Mathieson were made to obtain firstly predictions of the longitudinal diffusion coefficient D_L, and secondly D/μ and W values for comparison with the results of Boltzmann calculations. The same cross-section data were used in the simulations and the Boltzmann calculations, and so the validity of the two-term approximation could be judged.

There has been considerable work in this field using Monte-Carlo simulations. Most of these simulations have been for high E/p values where ionisation is significant and the Boltzmann two-term expansion is most unreliable. The field of interest of this work, that is counter gases at low E/p values has not been studied to any depth by Monte-Carlo simulations.

The principles of a Monte-Carlo simulation will be discussed in this chapter. Two approaches have been used by different workers. The approach which will be discussed here simulates the motion of a single electron in a uniform electric field and a particular gas undergoing many collisions (Lucas and Saellee, 1975; Itoh and Musha, 1960; Milloy and Watts, 1977; Mathieson et al, to be published). The other approach simulates the motion of a group of electrons, the number in the group

varies considerably from 150 (McIntosh, 1974) to 2500 (Braglia 1977). The simulation involves many collisions for each electron, (Braglia and Baiocchi, 1978; Reid, 1979).

The Monte-Carlo simulation will be discussed here in its distinct stages.

4.2 COLLISION CROSS-SECTIONS AND CHANGES BETWEEN COLLISIONS.

The intensity I of a beam of electrons emerging from material of thickness x can be given in terms of the incident intensity I_0 as

$$I = I_0 e^{-\sigma n x}$$

σ is the collision cross-section and ndx is the number of scattering centres per unit area, so

$$dI = I\sigma n dx.$$

dI is the number of particles involved in a collision between x and x + dx and so is the number having a free path length x.

$$\text{Mean free path} = \frac{1}{I_0}\int_0^\infty I\sigma n x.dx$$

$$= \sigma n \int_0^\infty x e^{-\sigma n x}.dx$$

$$= \frac{1}{\sigma n}$$

and so the mean free time = $1/(\sigma nc)$

and the collision frequency $\nu = \sigma nc$.

The probability of a collision occurring between the times t and t + dt is $\nu.dt$. For a gas mixture with k components the collision frequency is given by

$$\nu = \sum_k \nu_k \qquad (4.1)$$

where $\nu_k = \sigma_k n_k c$

and $c = (2\varepsilon/m)^{\frac{1}{2}}$

Electrons are accelerated by an electric field in this specific simulation and so ν is a function of time, and so

$$\nu(c) = \nu(\varepsilon) = \nu(t).$$

The number of collisions between t and t + dt is given by

$$dN = -N\nu(t)dt$$

$$\text{then } [\ln N]_{N_0}^{N} = -\int_0^{t_c} \nu(t)dt \quad \text{by integration}$$

$$\text{and} \quad \frac{N}{N_0} = \exp\left(-\int_0^{t_c} \nu(t)dt\right)$$

$\frac{N}{N_0}$ is the probability of a collision being avoided between $t = 0$ and $t = t_c$, so the probability of a collision occurring between these times is

$$1 - \exp\left(-\int_0^{t_c} \nu(t)dt\right)$$

t_c is determined by generating a pseudo-random number R_1 where $0 \leq R_1 \leq 1$ and letting

$$1 - \exp\left(-\int_0^{t_c} \nu(t)dt\right) = R_1$$

$$\text{then} \int_0^{t_c} \nu(t)dt = \ln \frac{1}{1 - R_1} \tag{4.2}$$

The collision frequency is integrated numerically with respect to time until this is satisfied and t_c, the free time follow--ing a collision is found.

Direction cosines are used to describe the direction and changes in coordinates of the electron, see figure 4.1. Initially the direction cosines are

$$\begin{aligned} d_{x1} &= \sin\theta\cos\phi \\ d_{y1} &= \sin\theta\sin\phi \\ d_{z1} &= \cos\theta \end{aligned} \tag{4.3}$$

The initial energy of the electron is ε_1 and $c = (2\varepsilon_1/m)^{\frac{1}{2}}$

Let E accelerate the electron parallel to the z-axis, the components of the velocity initially are :-

$$
\begin{aligned}
c_{x1} &= (2\varepsilon_1/m)^{\frac{1}{2}} d_{x1} \\
c_{y1} &= (2\varepsilon_1/m)^{\frac{1}{2}} d_{y1} \\
c_{z1} &= (2\varepsilon_1/m)^{\frac{1}{2}} d_{z1}
\end{aligned}
\tag{4.4}
$$

After some time t the velocity components are

$$
\begin{aligned}
c_x &= c_{x1} \\
c_y &= c_{y1} \\
c_z &= (2\varepsilon_1/m)^{\frac{1}{2}} d_{z1} + at
\end{aligned}
\tag{4.5}
$$

Then if $t = t_c$, from R_1, the energy ε just before the collision is

$$
\varepsilon = \frac{m}{2} \left(c_x^2 + c_y^2 + c_z^2 \right)
$$

$$
\varepsilon = \varepsilon_1 + m\sqrt{\frac{2\varepsilon}{m}_1} d_{z1} a t_c + (a t_c)^2 \frac{m}{2} \tag{4.6}
$$

The new direction cosines just before the collision are

$$
\begin{aligned}
d_x &= (\varepsilon_1/\varepsilon)^{\frac{1}{2}} d_{x1} \\
d_y &= (\varepsilon_1/\varepsilon)^{\frac{1}{2}} d_{y1} \\
d_z &= (\varepsilon_1/\varepsilon)^{\frac{1}{2}} d_{z1} + \frac{a t_c}{(2\varepsilon/m)^{\frac{1}{2}}}
\end{aligned}
\tag{4.7}
$$

and the coordinates just before the collision are

$$
(x, y, z) = (t_c c_{x1}, t_c c_{y1}, t_c c_{z1} + \tfrac{1}{2} a t_c^2) \tag{4.8}
$$

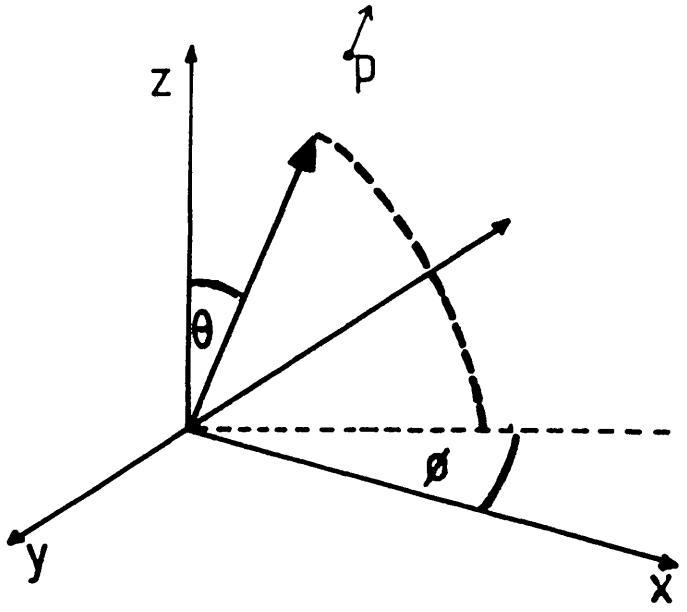

FIG 4.1

The direction cosines for an electron, projections of a unit vector.

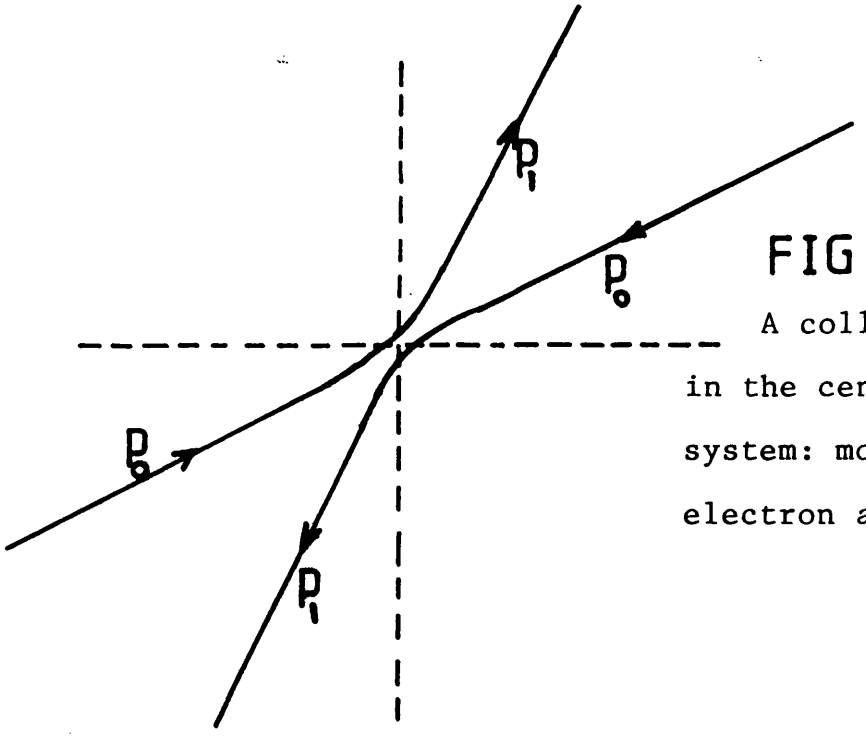

FIG 4.2

A collision observed in the centre-of-mass system: motion of the electron and the molecule.

4.3 THE COLLISION.

4.3.1 Determining the Type of Collision.

From equation 4.1 $\nu_k = \sigma_k n_k c$ for the k^{th} gas component, this can be rewritten as

$$\nu_k = (p_k/kT)\sigma_k c$$

where $p_k = n_k kT$ is the partial pressure of this component, so

$$\nu_k = \frac{p}{kT} f_k \sigma_k c \qquad (4.9)$$

where f_k is the fraction represented by the k^{th} component. So

$$\nu = \frac{p}{kT}(2\varepsilon/m)^{\frac{1}{2}} \sum_k f_k \sigma_k .$$

For each component the cross-section is the sum of a momentum transfer cross-section and a number of inelastic cross-sections, i.e.

$$\sigma_k = q_{mk} + \sum_i q_{ik} \qquad (4.10)$$

q_{mk} = momentum transfer cross-section for the k^{th} component,

q_{ik} = inelastic cross-section for excitation to the energy level ε_{ik}.

Then,

$$\nu(\varepsilon) = \frac{p}{kT}(2\varepsilon/m)^{\frac{1}{2}} \sum_k f_k \{ q_{mk}(\varepsilon) + \sum_i q_{ik}(\varepsilon) \} \qquad (4.11)$$

A second random number R_2 is used to determine the type of collision. Each elastic and inelastic cross-section contributes a single term to the sequence of fractional collision frequencies s_j, where

$$s_j = \sum_{l=1}^{j} \nu_l / \nu \qquad (4.12)$$

The collision is type j if $s_{j-1} < R_2 \leq s_j$

4.3.2 Kinematics of the Collision.

The changes occurring during a collision in direction and energy are considered using both the centre of mass reference system (C-system) and the laboratory reference system (L-system).

In the L-system the target molecule of the collision is assumed to be at rest and the electron approaches with momentum p_0 and energy $\varepsilon_0 = p_0^2/2m$. After the collision the electron moves along a path at an angle with the original direction and with a new velocity. The molecule gains momentum in this system and moves with some velocity at some angle to the original direction of the electron. The velocity of the centre of mass before the collision is given by

$$V = p_0/(M+m) \qquad (4.13)$$

Both the electron and the target molecule approach the centre of mass in the C-system. The velocity of the electron before the collision is

$$\frac{p_0}{m} - V = \frac{p_0}{m}(M/M+m),$$

the total momentum is zero in the C-system before and after the collision. An observer only sees the changes in the direc--tions of the electron and the molecule as a result of the collision, and the two move away from the centre of mass in opposite directions, see figure 4.2.

For an elastic collision, when kinetic energy is conserved, the speeds of the electron and the molecule are the same before and after the collision, so only the directions of the velocities change.

$$\text{Energy of electron \& molecule before collision} = \frac{1}{2m}p_0^2\,(M/M+m)^2 + \frac{1}{2M}p_0^2\,(M/M+m)^2 \qquad (4.14)$$

$$\text{Energy of electron \& molecule after collision} = \frac{1}{2m}p_1^2 + \frac{1}{2M}p_1^2 \qquad (4.15)$$

The energy difference is ε_{ik}, the excitation energy of the particular inelastic collision, so

$$p_1 = \{(p_0 M/M+m)^2 - (2\varepsilon_{ik} mM/M+m)\}^{\frac{1}{2}} \qquad (4.16)$$

$$\text{and } \varepsilon_1 = p_1^2/2m$$

Two more random numbers R_3 and R_4 are used to determine the new direction cosines in the C-system. A polar angle θ_0 and an azimuthal angle ϕ_0 fix the new electron direc--tion relative to the original direction, see figure 4.3.

θ_0 is in the range 0 to π. Each element $d\omega$ of the solid angle has equal probability,

$$d\omega = 2\pi \sin\theta \, d\theta$$

$$p(\omega)d\omega = \frac{2\pi \sin\theta d\theta}{4\pi} = \tfrac{1}{2}\sin\theta d\theta$$

$$\int_0^{\theta_0} \tfrac{1}{2}\sin\theta d\theta = R_3 \text{ where } 0 \leq R_3 \leq 1 \qquad (4.17)$$

$$\text{so } \theta_0 = \arccos(1 - 2R_3) \quad 0 \leq \theta_0 \leq \pi$$

ϕ_0 is generated by R_4. All ϕ_0 are equally probable in isotropic scattering, $0 \leq \phi_0 \leq 2\pi$, R_4 is generated so that $0 \leq R_4 < 1$, so

$$\phi_0 = 2\pi R_4 \qquad (4.18)$$

The new situation just after the collision is now obtained by transferring to the L-system.

See figure 4.4, p_1/m is the velocity in the C-system and V is the velocity of the centre of mass, equation 4.13.

From figure 4.4,

$$(p/m)^2 = (p_1 \sin\theta_0/m)^2 + ((p_1 \cos\theta_0/m) + (p_0/M+m))^2$$

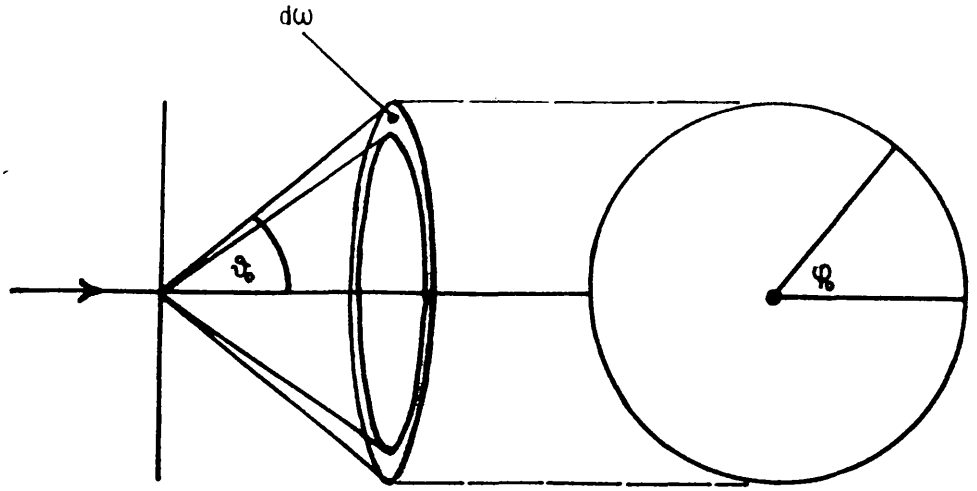

FIG 4.3 The polar and azimuthal angles, θ_0 and ϕ_0, for an electron after a collision.

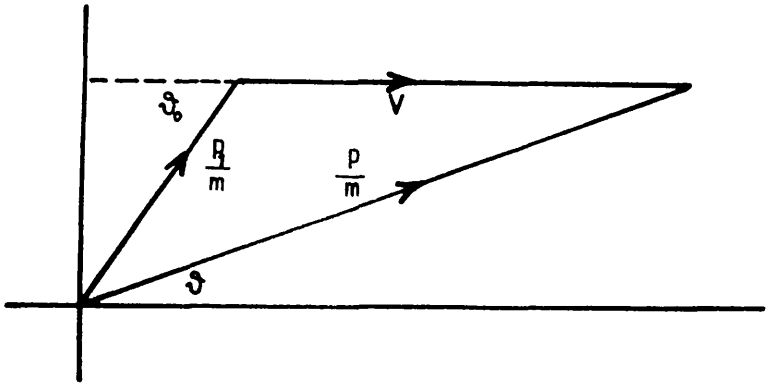

FIG 4.4 Transferring from the C-system to the L-system, p_1/m = velocity in the C-system of the electron, V = velocity of the centre of mass.

so,

$$(p/m)^2 = (p_1/m)^2 + (p_0/M+m)^2 + 2(p_1/m)(p_0/M+m)\cos\theta_0 \tag{4.19}$$

The energy of the electron in the L-system after the collision is given by

$$\varepsilon_0 = \frac{m}{2}(p/m)^2$$

and before the collision the energy is

$$\varepsilon_0 = \frac{m}{2}(p_0/m)^2.$$

Substituting into equation 4.19 this yields

$$\varepsilon = \varepsilon_0\left[1 - \frac{M}{(M+m)}\frac{\varepsilon_{ik}}{\varepsilon_0} + \frac{2mM}{(M+m)^2}\left\{\cos\theta_0\left[1 - \frac{(M+m)}{M}\frac{\varepsilon_{ik}}{\varepsilon_0}\right]^{\frac{1}{2}} - 1\right\}\right] \tag{4.20}$$

This is ε_1 for the next collision.

The angles in the L-system, relative to the direction before the collision are θ and ϕ.

$$\phi = \phi_o$$

and from figure 4.4,

$$\frac{p}{m}\sin\theta = \frac{p_1}{m}\sin\theta_0$$

then as $p = (2\varepsilon m)^{\frac{1}{2}}$,

$$\sin\theta = \left[\left(\frac{2\varepsilon_0 mM^2}{(M+m)^2} - \frac{2\varepsilon_{ik}mM}{(M+m)}\right)\frac{1}{2m\varepsilon}\right]^{\frac{1}{2}} \times \sin\theta_0$$

$$= \frac{M}{M+m}\left(\frac{\varepsilon_0}{\varepsilon}\right)^{\frac{1}{2}}\left[1 - \frac{(M+m)}{M}\frac{\varepsilon_{ik}}{\varepsilon_0}\right]^{\frac{1}{2}} \times \sin\theta_0 \tag{4.21}$$

If $\theta_0 > \pi/2$, $\theta > \pi/2$ if $\cos^2\theta_0 > (m/M)^2 \dfrac{1}{\left[1 - \dfrac{(M+m)}{M}\dfrac{\varepsilon_{ik}}{\varepsilon_0}\right]}$

The new direction cosines, with respect to the original coordinate system, can be stated as the initial ones for the next free time, i.e. d_{x1}, d_{y1}, d_{z1}.

$$d_{x1} = d_x\cos\theta - \frac{d_y}{A}\cos\phi\sin\theta - \frac{d_x d_z}{A}\sin\phi\sin\theta$$

$$d_{y1} = d_y\cos\theta + \frac{d_x}{A}\cos\phi\sin\theta - \frac{d_y d_z}{A}\sin\phi\sin\theta \quad (4.22)$$

$$d_{z1} = d_z\cos\theta + A\sin\phi\sin\theta$$

where $A = (d_x^2 + d_y^2)^{\frac{1}{2}}$ and d_x, d_y, d_z are the direction cosines just before the collision.

The new coordinates of the electron can now be calculated.

4.4 DETERMINATION OF THE TRANSPORT PARAMETERS.

The continuity equation, equation 3.5, for electron density n(x,y,z,t) may be solved to describe an isolated group of n_0 electrons drifting with mean velocity W along the z-axis (the field direction). The solution, equation 3.6, assumes that at time t = 0 the n_0 electrons are at the coordinate origin,

$$n = \frac{n_0}{4\pi Dt(4\pi D_L t)^{\frac{1}{2}}} e^{\frac{-(x^2+y^2)}{4Dt}} e^{\frac{-(z-Wt)^2}{4D_L t}} \qquad (3.6)$$

In the present Monte-Carlo calculations, as described above, the x, y and z displacements of a single electron were repeatedly calculated for a constant time interval τ. Thus the lateral diffusion coefficient D is calculated from the expression

$$D = \frac{1}{4\tau} \{\rho^2\}_{av} \qquad (4.23)$$

where $\rho^2 = \{x(t+\tau) - x(t)\}^2 + \{y(t+\tau) - y(t)\}^2$

The time interval τ must be chosen to ensure that no signifi--cant correlation remains between $x(t+\tau)$ and x(t). For all calculations presented here τ was chosen as 1000 mean free times. The total number of simulated collisions for each determination was $3 \cdot 10^6$, this being the maximum number that could be reached within the maximum time available (1280 seconds) on the CDC 7600 computer at the University of Manchester Regional Computing Centre. Drift velocity W is calculated simply as the total displacement along the field direction divided by the total time. The longitudinal diffusion coefficient D_L is calculated from the expression

$$D_L = \frac{1}{2\tau} (\overline{z^2} - \overline{z}^2) \qquad (4.24)$$

where $\overline{z^2} = \left(\{ z(t+\tau) - z(t) \}^2 \right)_{av}$

and $\overline{z} = \{ z(t+\tau) - z(t) \}_{av}$

It is seen from the above that averages were taken over $3 . 10^3$ samples (each sample representing the result of 10^3 collisions). So that the stability of the results could be examined, averages were in fact calculated, and printed, every 50 samples. It was found that the drift velocity always stabilised very rapidly; the mean energy and the ratio D/μ generally fluctuated more seriously but these fluctuations remained within 2 % for the second half of the run for all the cases presented here.

The simulation programme was tested to a certain degree by examining in detail an artificial gas in which the molecular weight M = 0.2 amu, $q_m(\varepsilon) = 3 . 10^{-16} / \varepsilon^{\frac{1}{2}}(eV)$ cm^2 (constant collision frequency), zero inelastic scattering and for E/p in the range up to 1.5 V/cm torr. Simple analysis of the Boltzmann equation (see equation 3.24) is then possible for comparison. Very close agreement (within 0.2 %) was obtained for both W and D/μ. Both forms of calculation were also tested by examining W and D/μ in pure argon, the results were compared with Robertson's experimental values for W (Robertson, 1977) and the experimentally determined values for D/μ of Milloy and Crompton (1977). The argon momentum transfer cross-section data was obtained by cubic spline interpolation of the tabulated data of Milloy et al (1977), derived by analysis of the experiments of Robertson and of Milloy and Crompton. Table 4.1 gives the comparison, there is good agreement between experiment and both forms of calculation.

TABLE 4.1 COMPARISON OF CALCULATIONS AND EXPERIMENT IN PURE ARGON.

E/p (V/cm torr) x 10^2	W (cm/μs)			D/μ (V)		
	EXPERIMENT 1	BOLTZMANN	MONTE-C	EXPERIMENT 2	BOLTZMANN	MONTE-C
0.0825	(0.204)	0.18	0.19	0.1234	0.005 0.125	0.006
0.165	(0.71)	0.75	0.70	0.2865	0.284	0.261
0.33	0.94	0.98	0.97	0.5060	0.497	0.437
0.66	1.08	1.08	1.14	0.7659	0.751	0.719
0.99	1.20	1.19	1.23	0.9355	0.918	0.921
1.65	1.37	1.36	1.41	1.163	1.15	1.12
2.64	1.56	1.54	1.58	1.391	1.39	1.39
3.30	1.66	1.64	1.69	1.508	1.52	1.48
3.96	1.74	1.72	1.78		1.63	1.59
4.95	1.85	1.83	1.88		1.77	1.72
5.94	1.95	1.92	1.97		1.91	1.93
6.60	2.00	1.98	2.00		1.99	2.05

Experiment 1 (Robertson, 1977) Experiment 2 (Milloy and Crompton, 1977)

CHAPTER 5.

EXPERIMENTAL ARRANGEMENT.

5.1 INTRODUCTION.

Two distinct experimental arrangements have been used to measure the three parameters D/μ, W and D_L/μ, a review of previous methods of measuring these appears in chapter 2. One arrangement, based on the Townsend method has been used to measure D/μ, the other, an electron pulse arrangement, to measure W and D_L/μ.

Both experiments were carried out using the same drift chamber, which contains a uniform electric field assembly 15 cm long. A special feature of the system is the variable drift length between 2 cm and 15 cm in 1 cm steps, this was possible by allowing the electron source to move parallel to the electric field direction. For longitudinal diffusion measurements it was desirable to be able to use long drift lengths as the amount of diffusion increases with drift length. Diffusion also increases with decreasing gas pressure, a simple but effective gas control system was used which allowed pressures between 5 torr and 1 atmosphere to be maintained precisely while keeping a steady flow of gas through the chamber to reduce contamination.

The main difference between the two arrangements is in the means of detection of the electrons after they have drifted the length of the drift chamber and in the associated electronics.

All the features of the common parts of the system and the different components and electronic arrangements will be discussed here.

5.2 THE DRIFT CHAMBER.

The drift chamber was constructed in stainless steel in three sections. The chamber is a cylinder with an internal diameter of 124 mm, outside diameter 130 mm and overall length 275 mm. The two upper sections of the chamber are illustrated in figure 5.1. These two sections are common to both arrangements and form the housing for the field assembly and electron source as shown. The third section either contains the plane collector for D/μ measurements or is a gas-filled counter for W and D_L/μ measurements.

The sections are bolted together through 10 mm flanges recessed for standard 3 mm diameter section by 139.5 mm internal diameter 'O' rings, BS 4518 No. 1395-30. The section carrying the field assembly is 215 mm in length, the top section 60 mm. For lateral diffusion measurements the third section housing the plane collector is added at the bottom, this section is 55 mm long. Both this section and the counter contain welded 6.4 mm diameter stainless steel tubes, these provide a gas outlet and a point to which pressure gauges can be attached. The gas inlet is a similar tube welded into the top plate illustrated in figure 5.1.

The section housing the field assembly has 15 glass-to-metal seals fixed by epoxy resin into holes in the side. These are closely spaced around the top of the section within 25 mm of the flange. The glass-to-metal seals are connected to alternate field rings, i.e. to points spaced at 1 cm intervals along the field.

Two 23 mm diameter window ports, figure 5.2, are welded into the side of this section, 40 mm and 140 mm

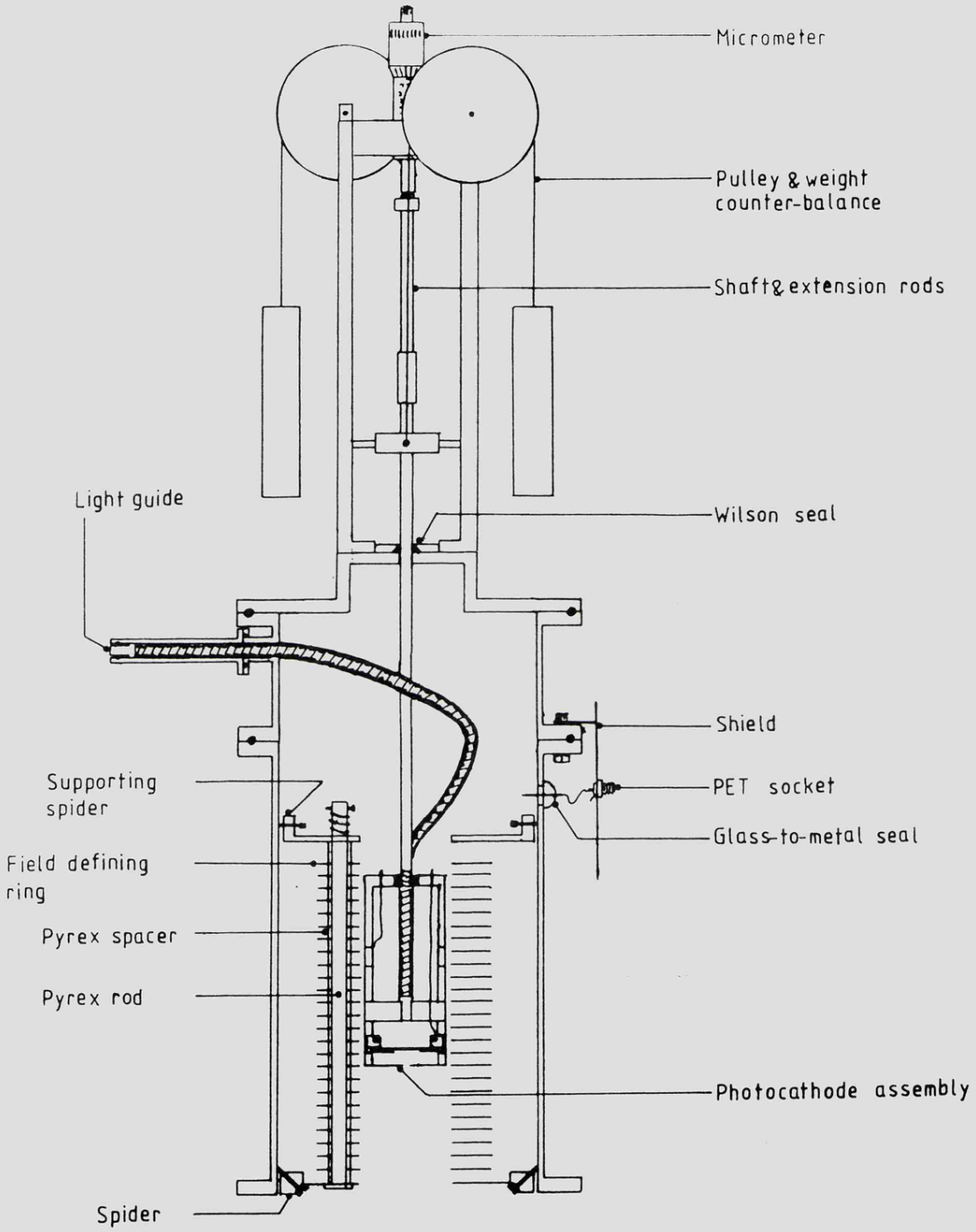

FIG 5.1 The drift field and electron source sections of the chamber.

Figure 5.2 Chamber drift field section, showing window ports, top spider and glass to metal seals.

from the bottom. Each port contains plate glass clamped against a rubber 'O' ring. The ports are used to line up the source head with the field rings to determine accurately the drift length.

The top section has a port to carry a light guide out of the chamber. Electrons are produced in the source head by photoemission from gold, the light guide transmits UV light from an external lamp to the photocathode. A stainless steel tube bolted to the port by an 'O' ring sealed flange, carries the light guide, the ferrule on the end of the light guide is packed inside the end of the tube with small 'O' rings which produce a good seal between the ferrule and the inside of the tube. The light guides used were not designed for this type of arrangement, at least one was found to introduce a leak into the system which could not be tolerated. This leak was along the light guide between the fibres of glass, it was remedied by rubbing the face of the light guide with Apiezon vacuum grease, repeated application over a few days with a vacuum inside the chamber produced a permanently leak tight system.

The top-plate supports the micrometer adjust-ment and counter-balance arrangement used to set the position of the electron source in the electric field, and thus the drift length for the electrons from the source to the collector or counter. The shaft carrying the source head passes through an 'O' ring seal in the centre of the plate and a brass bearing in the recess inside the chamber. The horizontal part of the plate contains 'O' ring sealed P.E.T. sockets for connections to the electron source. Figure 5.3 shows this section, complete with source head.

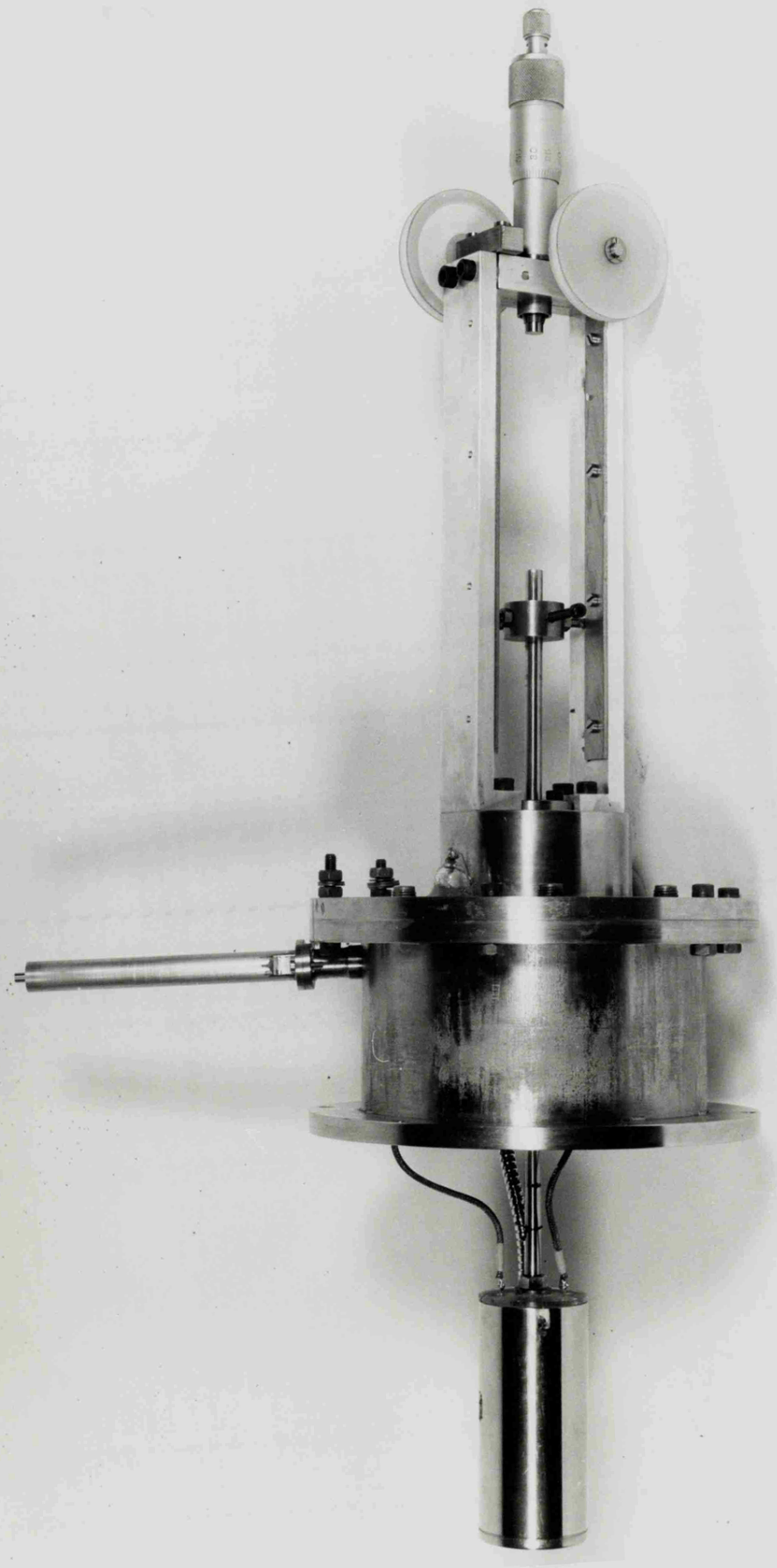

Figure 5.3 Chamber top section, showing the source head, light guide and micrometer.

5.3 ELECTRIC FIELD ASSEMBLY.

To measure the transport coefficients of electrons in gases it is necessary to allow the electrons to drift through a uniform electric field, in this case over a distance of up to 15 cm. The uniform field was set up in a cylindrical region bounded at the ends by the grid of the electron source and by the plane collector or counter. In addition the drift length was made variable.

The field was established by a series of parallel flat electrodes, held at voltages appropriate to their position along the drift length by a potential divider. The divider was a chain of 1 MΩ, 0.25 W carbon film resistors matched to within 0.2 %. The resistor chain was earthed at one end by connecting it to the bottom field defining electrode for D/μ measurements, and to the counter wall in the electron pulse arrangement. The other end of the chain was connected to the top field ring. The electrodes were in the form of annuli, the uniform field being established through the central hole through the assembly of parallel field rings. The annuli were spaced at 0.5 cm intervals, each being connected to the next by a resistor of the potential divider chain. The resistor chain was tapped at 1 cm intervals from the bottom of the field region, the connections were taken out of the chamber to P.E.T. sockets fixed to the metal shield shown in figure 5.1, via the glass-to-metal seals in the side of the chamber. When a particular drift length is chosen, the appropriate field ring is held at the required voltage, a uniform field would then be produced down the centre of the chamber by the resistor chain to earth and the field defining rings. The rings and resistor chain above the required drift

length were held at the same potential as the tapped ring by connecting the 15 cm ring and the tapped ring externally.

Crompton and Jory (1962) and Crompton, Elford and Gascoigne (1965) considered the problems of setting up a uniform field and the effects of non-uniformities. They found no significant errors associated with their arrangement of field rings at 1 cm intervals. They recommended precision spacing of the rings and corresponding precision in the applied voltage, they achieved a drift length accuracy of +/- 0.05 mm over 10 cm and voltage accuracy of +/- 0.1 %. Because of the possibility of field distortion due to the earthed chamber wall they favoured the use of numerous electrodes with a large diameter.

The field rings used in this work were made from 0.5 mm beryllium-copper sheet. In the completed assembly the rings were separated by lengths of Pyrex glass tubing, ground individually by hand so that each ring and spacer unit was 5+/-0.02 mm thick. The central holes in the rings were 42 mm in diameter allowing 1 mm clearance all around the electron source head, see section 5.4. The outside diameter of the rings was 80 mm, giving considerable lateral depth to the chamber wall. Each ring also had a 2.5 mm tag at a point on the edge for connecting the divider chain and tapping connections. The minimum clearance between the rings and the chamber wall was 19.5 mm, except for the 0.5 cm drift length ring described below.

In order to assemble and make connections to the field assembly it was convenient to design it in a form that could be mounted in the chamber as a complete wired and mechanically rigid unit. This was achieved by the use of

two 'spider' gigs to support the field rings in the chamber. These had vertical edges (lips) which contained threaded holes and screws which moved out towards the chamber wall when rotated. The assembly of rings has a spider at each end so the entire unit is placed in position in the chamber and the gigs are then accessible from each end of the section and are operated to fix the assembly. The top spider positions the top of the assembly centrally and carries the weight of the assembly. The bottom spider is only a positioning device, however the screws it carries are nylon as it is the 0.5 cm field ring, apart from the edge near the chamber wall it is just 0.5 mm thick. Each spider carries six screws spaced at 60^{o} intervals. The stainless steel screws in the top spider are pointed and engage with a groove machined inside the chamber section. Figure 5.4 gives a view down the chamber, the top spider, field ring tapping connections and glass-to-metal seals can be clearly seen.

All the annular field rings and spiders have three holes, 7 mm in diameter, 33.5 mm from the centre and spaced at 120^{o} intervals. These are used to thread the rings onto rigid supports with Pyrex spacers between each.

Pyrex rods were ground down to a uniform 7 mm diameter and until straight. 3 mm at one end of each was left at 9 mm diameter, this section was faced on the rod side until the edge was perpendicular to the length of the rod. The finished rods had an overall length of about 180 mm, with a 1.5 mm hole ultrasonically drilled along a diameter 10 mm from the 7 mm diameter end.

Three of these rods were used to mount the rings and spiders into a unit. The assembly was built up from the bottom spider by threading a ring followed by a Pyrex spacer

on each rod, until the 15 cm drift length was built up. Finally longer spacers followed by the top spider and then springs were threaded onto the rods. The three springs were compressed and kept compressed by metal pins pushed through the holes drilled through the rods. The springs clamped the rings, spacers and spiders together.

After soldering the resistor chain and connections to the field ring tags the assembly was placed inside the chamber section and fixed in position with the spider screws.

Crompton and Jory (1962) expressed concern regarding contact potential differences on metal surfaces. This is particularly significant at the collector in lateral diffusion measurements, as field distortion here would effect the current ratio for the two parts. Precautions to avoid large contact potential differences were taken with the collector, see section 5.5, and were extended to the field system as a whole. Parker and Warren (1962) considered and measured contact potential differences on a number of surfaces for various treatments. It was found that contact potential variations for colloidal graphite (about 50 mV without baking) are about the same or better than for gold (about 65 mV without baking). Applying graphite coatings is far more convenient than gold evaporation or plating for large areas and large numbers of components. All the field rings were sprayed with a colloidal graphite suspension, as were the electron source grids for D/μ measurement and the counter hole for D_L/μ and W measurement, the Townsend collector was evaporated with gold.

Once assembled the chamber required long periods of pumping when ever opened to the air, mainly due to

to gas trapped in this section, in the large areas of graphite coating, ceramic fish-beads used to insulate the tapping connections and so on, as no baking was possible.

5.4 THE ELECTRON SOURCE HEAD.

The electron source assembly in its final form is described here. The development and optimisation of this component are discussed in chapter 6.

Figure 5.5 shows the electron source head in the form used for the measurement of lateral diffusion. The photocathode (10) is held in position by fibre-glass spacers/ insulators (7,8,11) in a stainless steel cylindrical casing (6), (40 mm in diameter, 85 mm in length and with 1 mm wall thickness). The grid (13) containing a central source hole (14) for lateral diffusion and a micromesh for longitudinal diffusion measurements, is supported by the push-fit end cap (12) gripping the stainless steel case. The casing and the grid are at the same potential. The casing is secured to the fibre-glass base (5) by three screws, the screw heads lie flush with the surface of the casing when tightened. The light guide (4) passes through a hole in the base and its ferrule is held in the ceramic carriage (9), a fixed distance from the photocathode. All the components of the head are held in position by fibre-glass spacers clamped between the end cap and the base. The connection to the photocathode (2) with PTFE sleeving passes through the base. The casing connection which is also the grid connection is made by a nickel tab (1) spot-welded in a recess of the casing where it meets the base.

The base is held to the threaded end of a 6 mm shaft (3) by a nut. The shaft passes through a bearing and an 'O' ring seal and emerges through the top of the drift chamber. The shaft has been mentioned in section 5.2, and is used to vary the drift length. The light guide used is very flexible

and sufficiently long to achieve a range of drift lengths from 1 to 15 cm. The light guide, supplied by Schott Glass Ltd., was 500 mm long with a quartz fibre bundle 3 mm in diameter.

Several combinations of fibre-glass spacers (7 and 8 in figure 5.5) were available so the spacer separating the photocathode and the grid (11, figure 5.5) could be replaced by one of a different height.Consequently the cathode-grid separation could be varied from 0.5 mm or even less to a large separation only limited by the length of the source head. For all the lateral diffusion measurements a cathode-grid separation of 2 mm was used. A source hole 0.72 mm in diameter was chosen, this was considered sufficiently small in comparison to the collector diameter, and at the same time gave sufficient current to obtain reasonable reproducibility in the results. El-Hakeem (1978) showed that holes slightly less than 1 mm in diameter are small enough when used with a smaller collector and shorter drift lengths. Also Crompton and Jory (1962) found the maximum error for a 1 mm hole and $b = 0.5$ cm, $h = 2$ cm and $R = 0.5$ is 0.4 %, see figure 7.1.

The grid (13, figure 5.5) is made from beryll--ium-copper, 1 mm thick and is a tight fit inside the stainless steel casing. The outside surface was coated with colloidal graphite, as were the field rings discussed in section 5.3.

The modified cathode-grid region for drift velocity and longitudinal diffusion measurements is shown in figure 5.6. In this arrangement the cathode-grid separation is 5 mm. The grid consists of a copper micromesh supplied by EMI Electron Tubes. The mesh diameter is 18 mm, the mesh pitch is 67.73 μ (14.8 cells per mm) with a nominal aperture of 57 μ and transparency 71 %. The Ferri mounting ring of the micro-

Fig. 5.5 KEY.

1	Grid connection	8	Fibre-glass spacer
2	Photocathode connection	9	Ceramic ferrule carriage
3	Shaft	10	Photocathode assembly
4	Light guide	11	Fibre-glass spacer
5	Fibre-glass base	12	Push-fit end cap
6	Stainless steel case	13	Grid
7	Fibre-glass spacer	14	Source hole.

Fig. 5.6 KEY.

1	Light guide	6	Photocathode assembly
2	Stainless steel case	7	Push-fit end cap
3	Fibre-glass spacer	8	Fibre-glass spacer
4	Fibre-glass spacer	9	Fibre-glass spacer
5	Ceramic ferrule carriage	10	Copper micromesh
		11	Ferri micromesh mounting

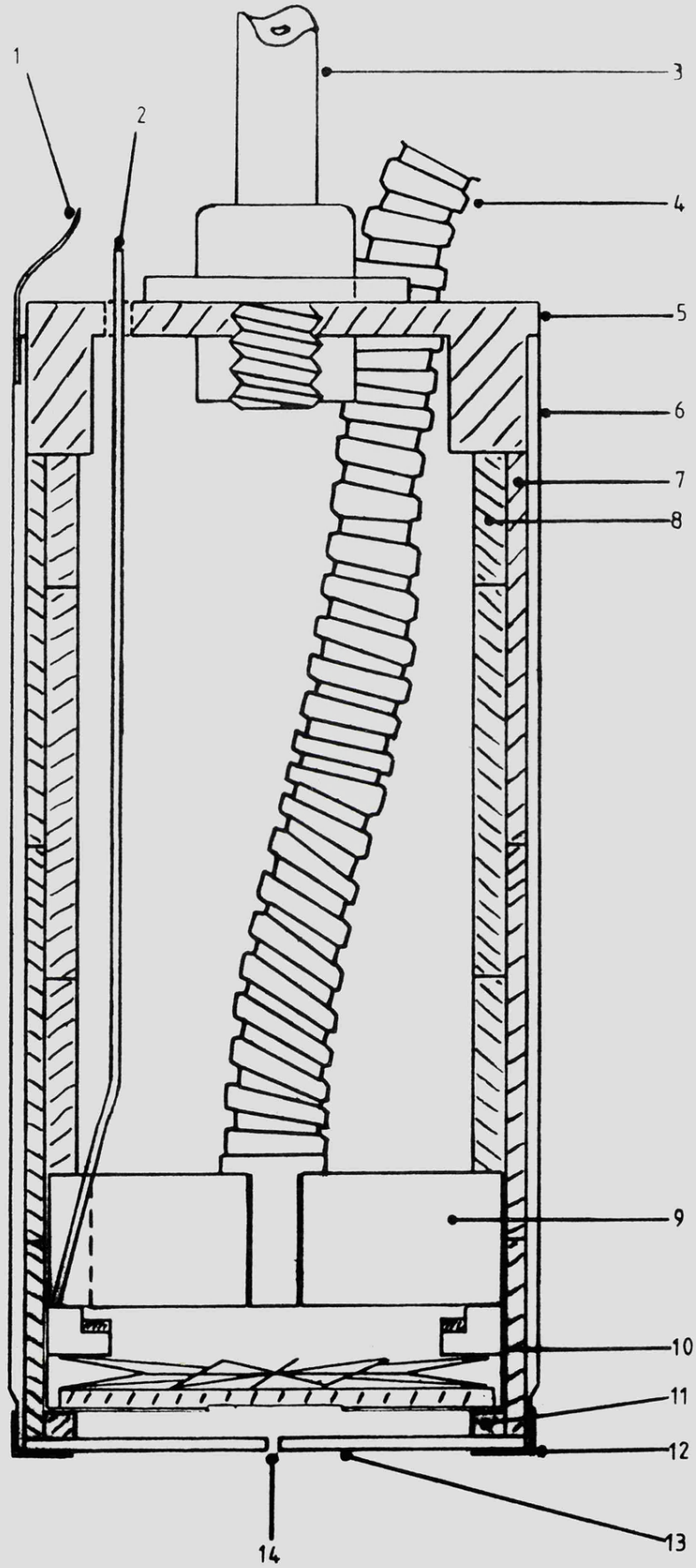

FIG 5.5 Internal construction of the electron source head.

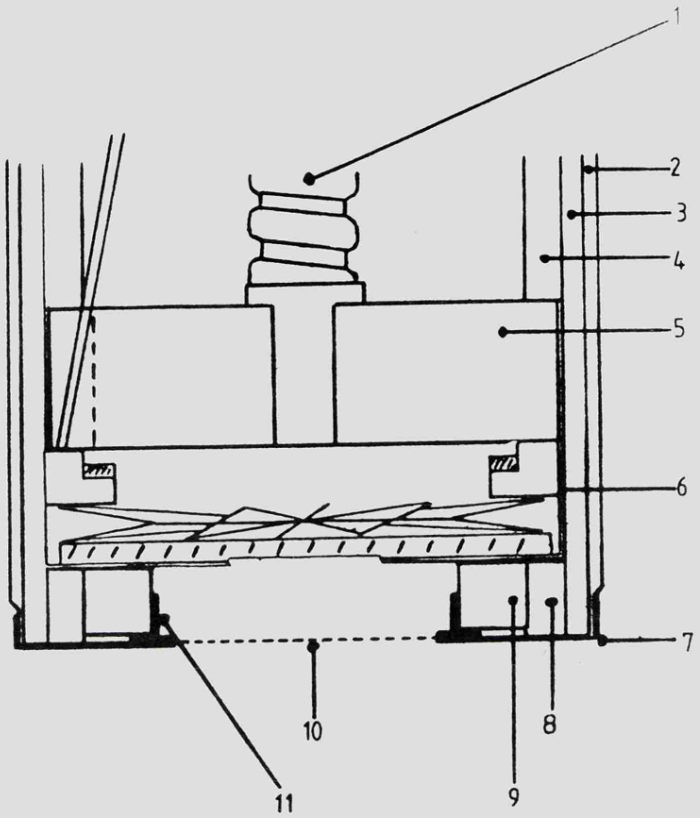

FIG 5.6 Modified source head for drift velocity and longitudinal diffusion.

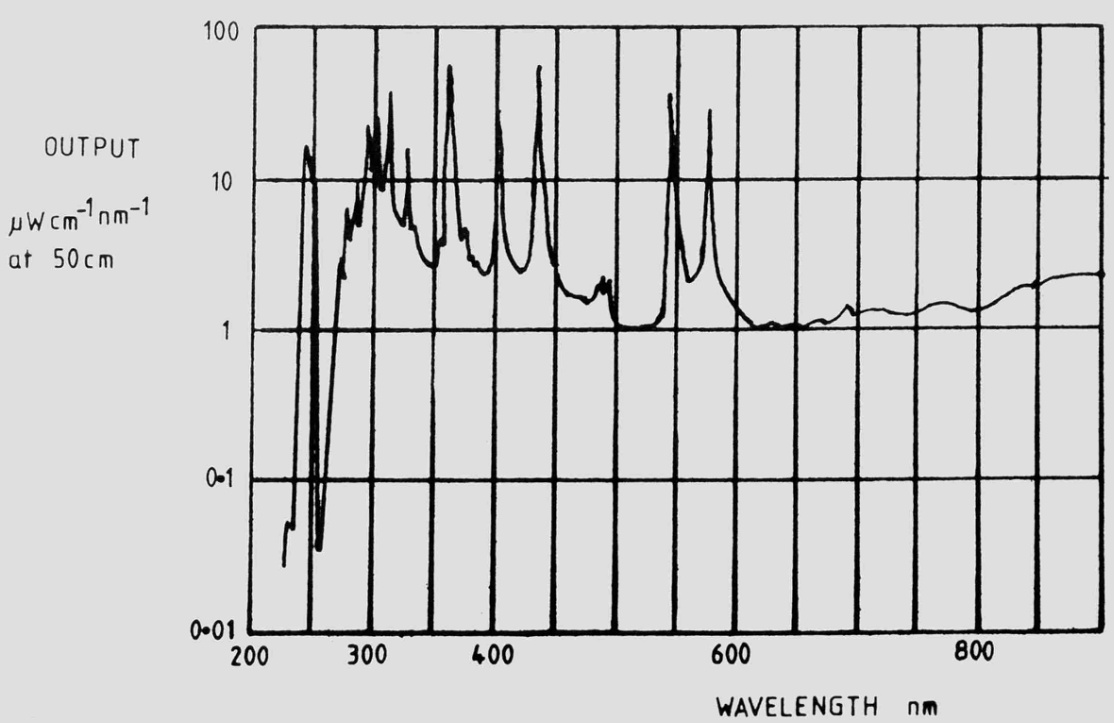

FIG 5.7 Typical high pressure mercury lamp emission spectrum.

-mesh was soldered to the stainless steel end cap of the source head. The central aperture in the end cap is 18 mm in diameter to match the micromesh.

The electrons produced by photoemission from the gold cathode cross the cathode-grid region under the forward bias condition which exists when the photocathode is pulsed. The electrons are assumed to emerge from a fairly large area of the mesh, so the electron source is assumed to be extended. This is a fair assumption as the light guide specifications quote an angle of aperture $2\alpha = 32^{o}$ at a wavelength of 254 nm. The light guide to photocathode separation was 8 mm, therefore the diameter of the illuminated region of the photocathode is approximately 8 mm, out of the 10 mm diameter region exposed by the contact.

Electrons were produced by photoemission from a thin layer of gold evaporated onto a quartz disc forming the cathode. Gold has a work function of 4.9 eV (Kaye and Laby, 1960), photons of this energy or greater can release electrons from the gold, this energy is equivalent to a wavelength of approximately 250 nm.

A typical high pressure mercury lamp spectrum is shown in figure 5.7. A mercury lamp of this kind, with a quartz glass envelope, is a good source of UV light of short wavelength. The quartz disc used as the base of the photo-cathode transmits low wavelength UV light well, about 86 % transmission. The cathode can be used in a transmission mode with a suitable gold thickness, see sections 6.2 and 6.3. The transmission curve for the light guide used, provided by the manufacturer, is shown in figure 5.8. Tests carried out on light guides as part of this work suggest the transmission of useful UV is about 35% for the 500 mm guide used and 65% for a 250 mm guide.

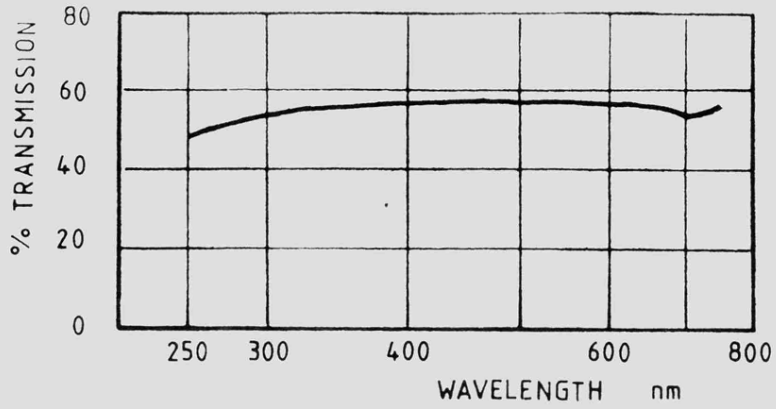

FIG 5·8

Transmission curve for 500 mm

UV light guide (Schott Glass Ltd.)

5.5 THE PLANE COLLECTOR.

The method of measuring the lateral diffusion coefficient to mobility ratio D/μ is that of Townsend using a divided collector. The method is reviewed in section 2.1.

Figure 5.9 shows the collector used in this work, viewed from above and in section. It consists of a central circular collector, 5 mm in diameter, and an outer concentric annular collector, 42 mm in diameter. These dimensions were selected on the basis of the other chamber dimensions, the gases to be studied and their estimated D/μ values.

Let the current collected on the central collector be i_c and the current to the outer part of the collector be i_o. Then the total collected current $i = i_c + i_o$. The ratio R of currents is given, as an approximation valid when $(b/d)^2 \ll 1$, by

$$R = i_c/i = 1 - \frac{h}{d} e^{\frac{-W(d - h)}{2D}} \qquad (5.1)$$

where h is the drift length, b is the radius of the central collector and d is the hypotenuse to these perpendicular distances, i.e. $d = (h^2 + b^2)^{\frac{1}{2}}$.

If $(b/h)^2 \ll 1$ then equation 5.1 can be written as

$$R = 1 - \frac{h}{d} e^{\frac{-W}{2D} \cdot \frac{b^2}{2h}} \qquad (5.2)$$

In the present system h is variable from 2 to 15 cm. The range of D/μ values to be measured was estimated to be from the thermal agitation minimum value of 0.026 V (e.g. 100 % carbon dioxide at $E/p = 0.1$ V cm^{-1} torr^{-1}) to about 1.5 V (e.g. argon + 10 % methane at $E/p = 1.0$ V cm^{-1} torr^{-1}). The value of b had to be chosen bearing in mind these factors. According to the work of El-Hakeem (1978) and Huxley and

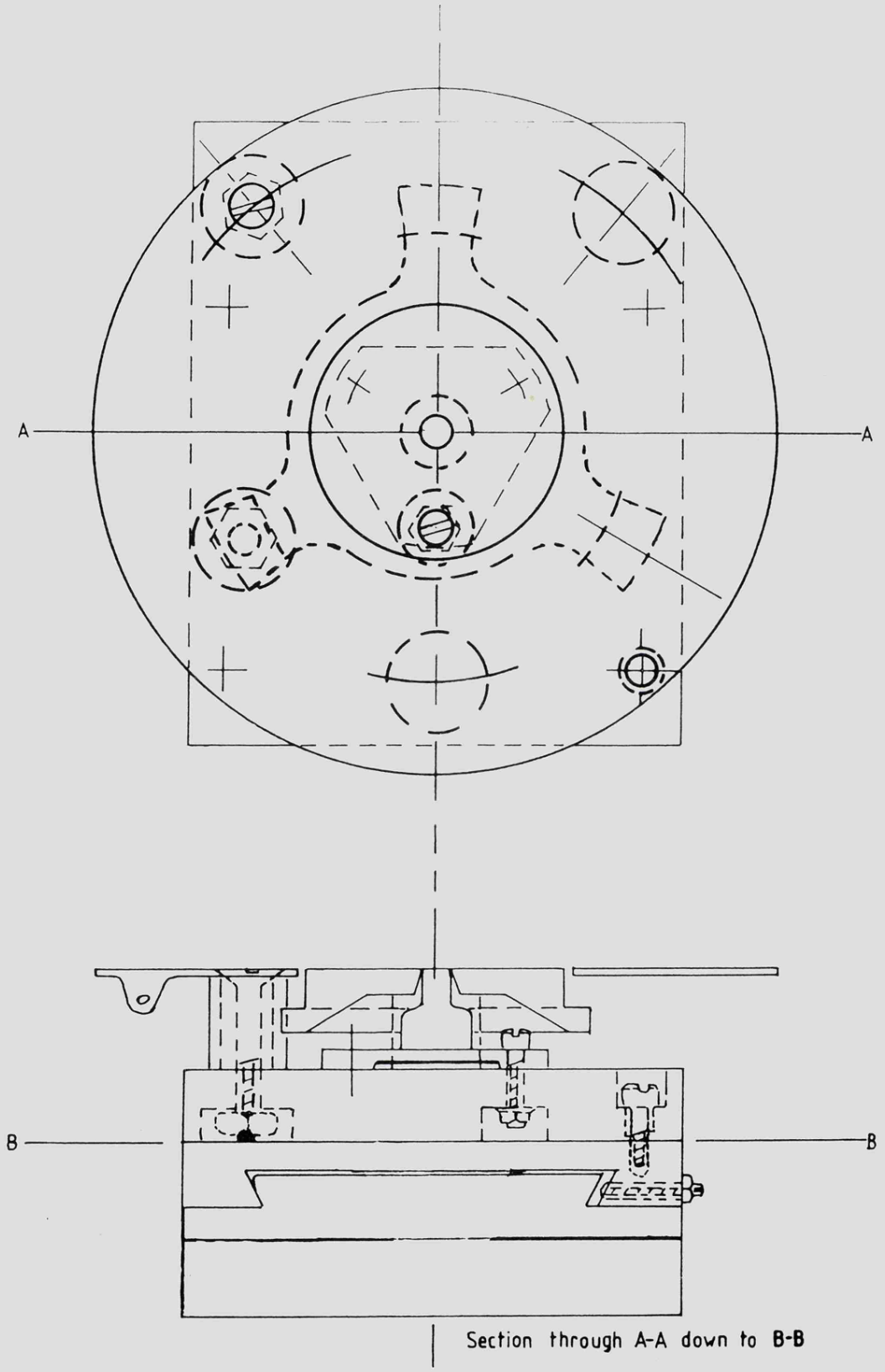

FIG 5·9 THE COLLECTOR PLATE ASSEMBLY.

Crompton (1974) greatest accuracy is achieved when the current ratio R is in the range 0.5 to 0.6.

As the value of D/μ is obtained by plotting a term involving the measured current ratio against the drift length, it is necessary to have, for a particular gas at each value of E/p, several current ratio measurements scattered about 0.5 corresponding to several drift lengths. A simple computer program was run on a PDP-11, this used predicted values of D/μ over a range of E/p for a certain gas, to tabulate the current ratio against drift length for particular values of b and gas pressure p.

The central collector diameter chosen, 5 mm, would be able to cover the range of D/μ from 0.026 to 1.5 V satisfactorily. In practice however the range of E/p which could be used was limited by electrical breakdown in the system. Current ratios of 0.5 could not be achieved in gases with D/μ values as high as those of argon + 10 % methane, ratios between 0.1 and 0.2 had to be accepted.

The collectors were made from solid stainless steel. The central collector was in the form of a cylinder rising up from a triangular base with three holes for mounting. The top of the cylinder was turned down to fit through the hole in the centre of the outer collector, with a clearance of less than 10 μm. The outer collector mounted by three legs was cut away below, the central hole was bevelled so that its diameter reached a minimum on the collecting face.

The collectors were bolted to a block of insulating Aremcolox (a very rigid and strong mica based material). The screws mounting the outer collector were loose fitting in the holes in the Aremcolox and carried crinkle washers. A gig was made so that the outer collector could be

moved relative to the central collector, the gig had brass screws with very fine (micrometer) threads which were turned to push against the mounting legs. The outer collector was moved in this way until the collectors were optically concentric and electrically separated. With the gig still in place the outer collector was firmly screwed down. This was done in a flow cabinet after thorough cleaning, for the final assembly. The arrangement was transferred to the vacuum chamber of an evaporation plant for coating with gold. It had proved impossible to either coat the collector in graphite as the field rings were or to evaporate gold onto the components before final assembly, without permanently short-circuiting the two parts of the collector together.

A graphite coated beryllium-copper guard ring, almost identical to those in the field assembly, but 110 mm in diameter with a 44 mm diameter central hole, was mounted concentrically with the collector on the Aremcolox block. The top face of the guard ring is coplanar with the collector. Ceramic tubing accurately cut and ground to length supports the guard ring. This ring is the final ring on the potential divider chain and was held at earth potential.

The Aremcolox block was bolted onto a three-part aluminium slide arrangement, and this was fixed to the base of the chamber. The line B-B in figure 5.9 shows the Aremcolox/slide interface. The slide arrangement permitted the movement of the whole collector assembly in the plane of the collector face in two perpendicular directions by up to 1.5 cm. Two micrometers mounted on the side of the bottom section of the chamber, with their shafts passing inside the chamber through 'O' ring seals, pushed on hard steel plates fixed to the slide arrangement. The slides were pulled back by springs

when the micrometers were withdrawn. The shafts of the micro--meters were tipped with ball-bearings to prevent sticking. Figure 5.10 shows the slide arrangement, the sliding aluminium faces were separated by thin strips of brass to prevent sticking and lubrication was provided by a light smear of Apiezon high vacuum grease. All enclosed holes, faces etc were linked to the outer surface by slots to assist efficient pumping and out-gassing. Figure 5.11 shows the micrometers used to move the collector (the units engraved on them are arbitrary).

5.6 THE SINGLE ELECTRON DETECTOR.

A coaxial gas filled detector, operated in the Geiger mode was used in the time-of-flight experiment.

The counter is a square cross-section 25 x 25 mm and is 70 mm long, with a 50 μm diameter tungsten wire anode stretched between two glass-to-metal seals. The counter was housed in a gas-tight stainless steel pill box shaped section which bolted directly to the field section of the drift chamber by an 'O' ring sealed flange. Several holes were drilled through the top of the detector section for gas flow from the chamber.

The detector section carried the pumping outlet and the pressure gauge port. A 1 mm diameter aperture positioned centrally below the uniform field region allowed electrons to enter the detector after drifting and diffusing from the electron source.

The chamber and therefore the detector was filled with gas at low pressure for the measurement of longitudinal diffusion. At first the detector was operated as a proportional counter, but a very strong dependence of arrival time spectrum peak and width upon count rate and counter voltage was observed. This dependence was not observed in the Geiger mode of operation. The detector was operated throughout this experiment well into the Geiger mode.

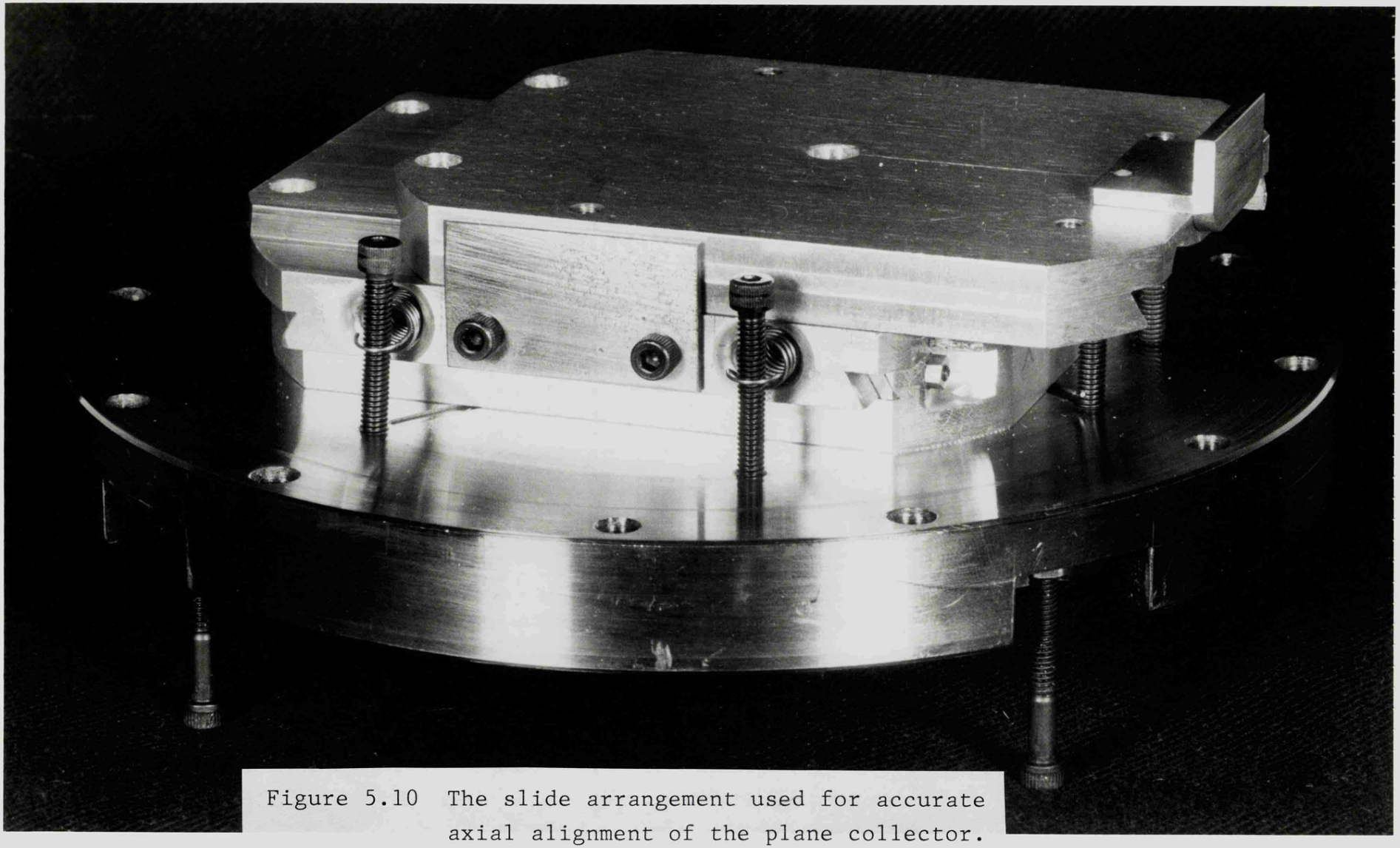

Figure 5.10 The slide arrangement used for accurate axial alignment of the plane collector.

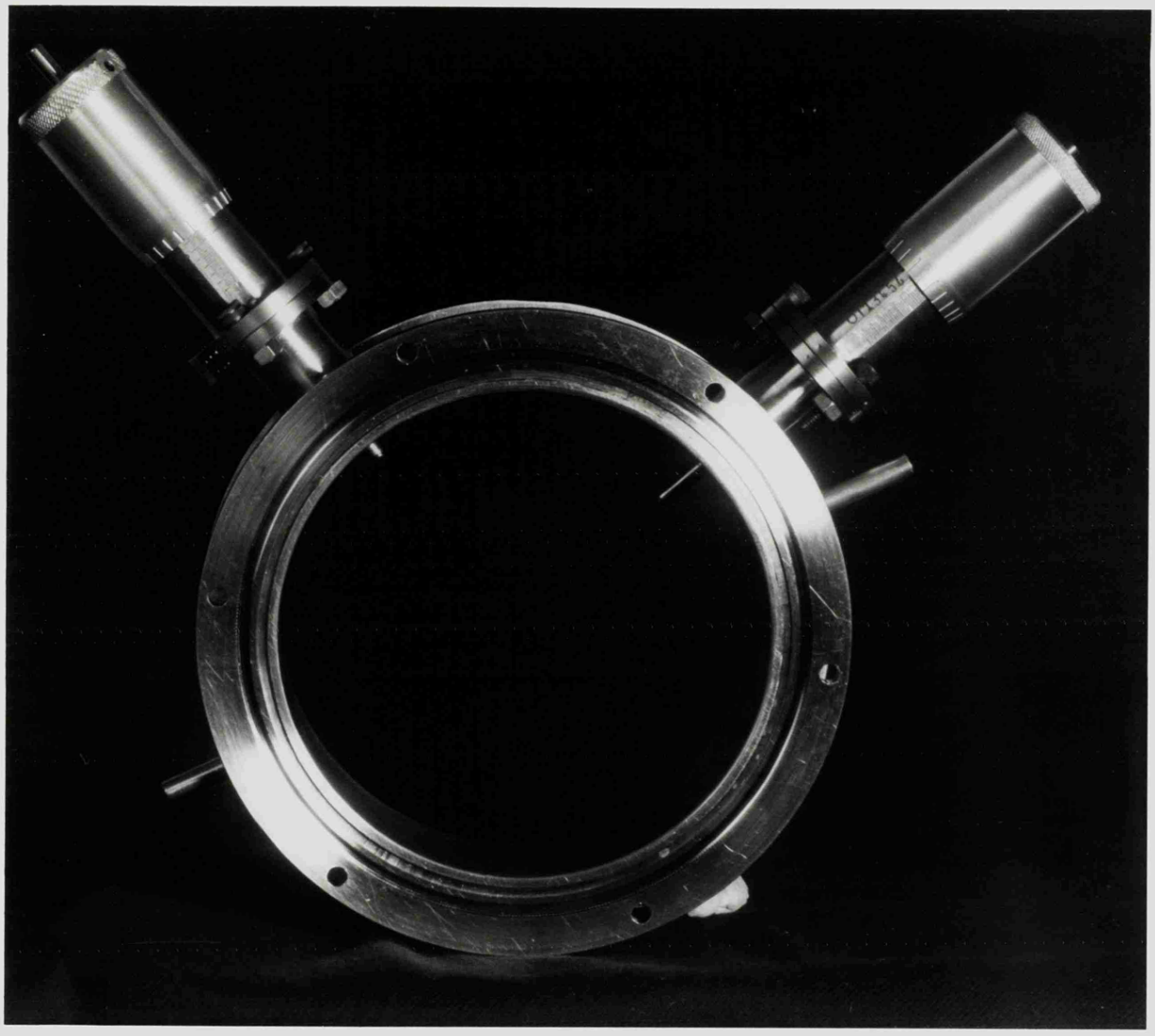

Figure 5.11 The micrometers used to operate the slide arrangement when aligning the plane collector.

5.7 GAS CONTROL.

The experimental arrangements for both experiments requires a flow of gas through the chamber to reduce the level of impurities due to leaks in the system and outgassing of porous and organic materials used. To increase the amount of diffusion to a measurable magnitude in some gases reduced pressure is essential. In carbon dioxide for example a low pressure is required for lateral diffusion measurement to produce currents of the same order on the two parts of the collector. As the pressure is reduced the diffusion coefficient D increases, Dp remains constant.

Having decided upon a particular pressure and flow rate, these have to be maintained for long periods of at least 8 hours to complete a run.

The required pressure and flow rate were achieved by adjusting the pumping rate and gas flow rate by means of fine control needle valves (Edwards LB2B; 18 turn, 0 - 100 divisions per turn, 0 - 0.09 litres per second atmosph--eric flow) until they balanced at the required pressure and flow rate, see figure 5.12.

In practice one needle valve was used as a fixed resistance to flow in the pumping line from the chamber. The required pressure was then set up by adjusting the needle valve in the gas line to the chamber. In this way any pressure, virtually from 0 to 1000 torr could be accurately selected quite quickly and would be subject to no visible fluctuation over periods of many hours.

For pumping down the chamber or flushing it through with gas both needle valves were put in parallel with stop-cocks which could provide high flow rates or low

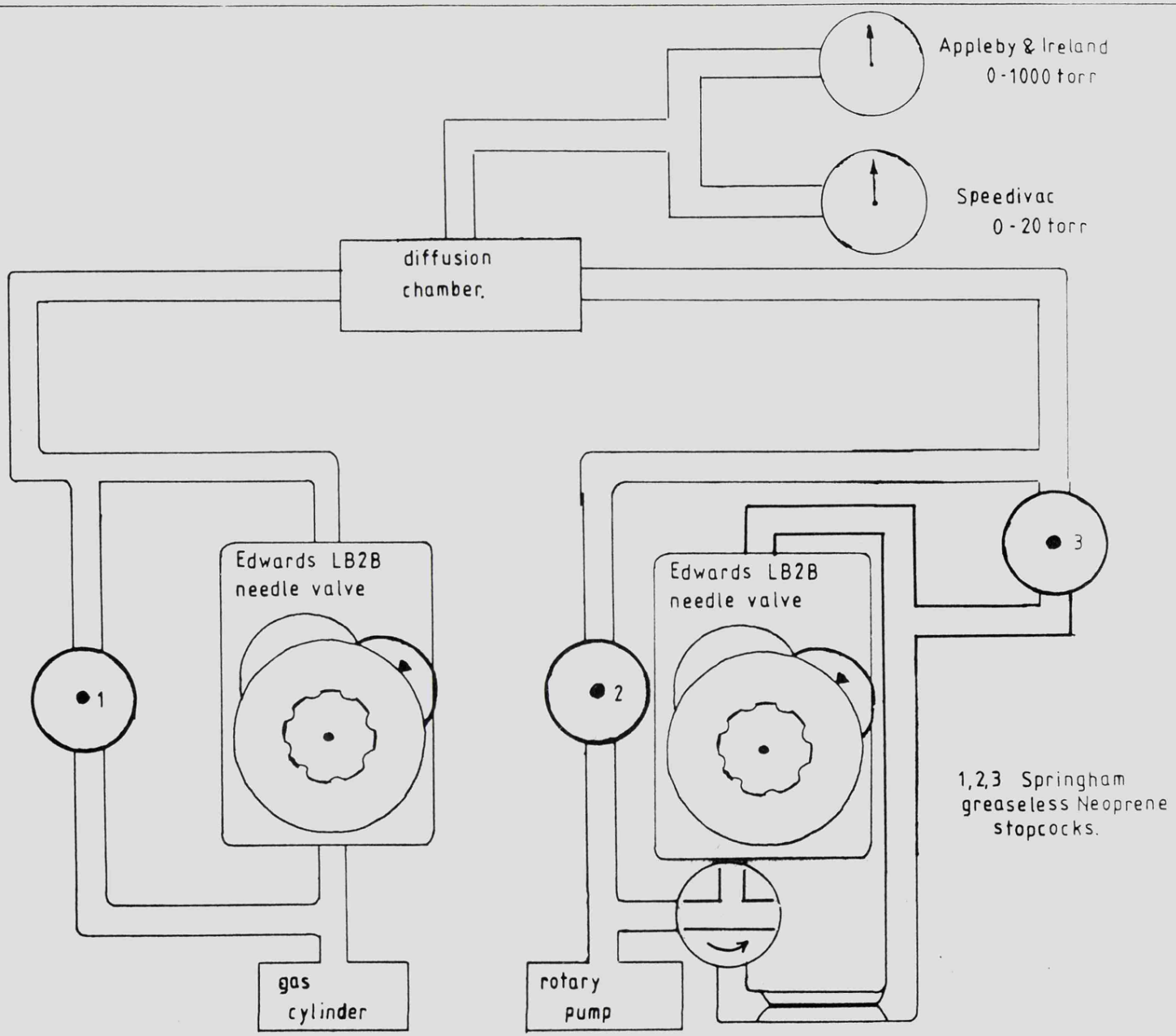

FIG 5.12 THE GAS CONTROL SYSTEM.

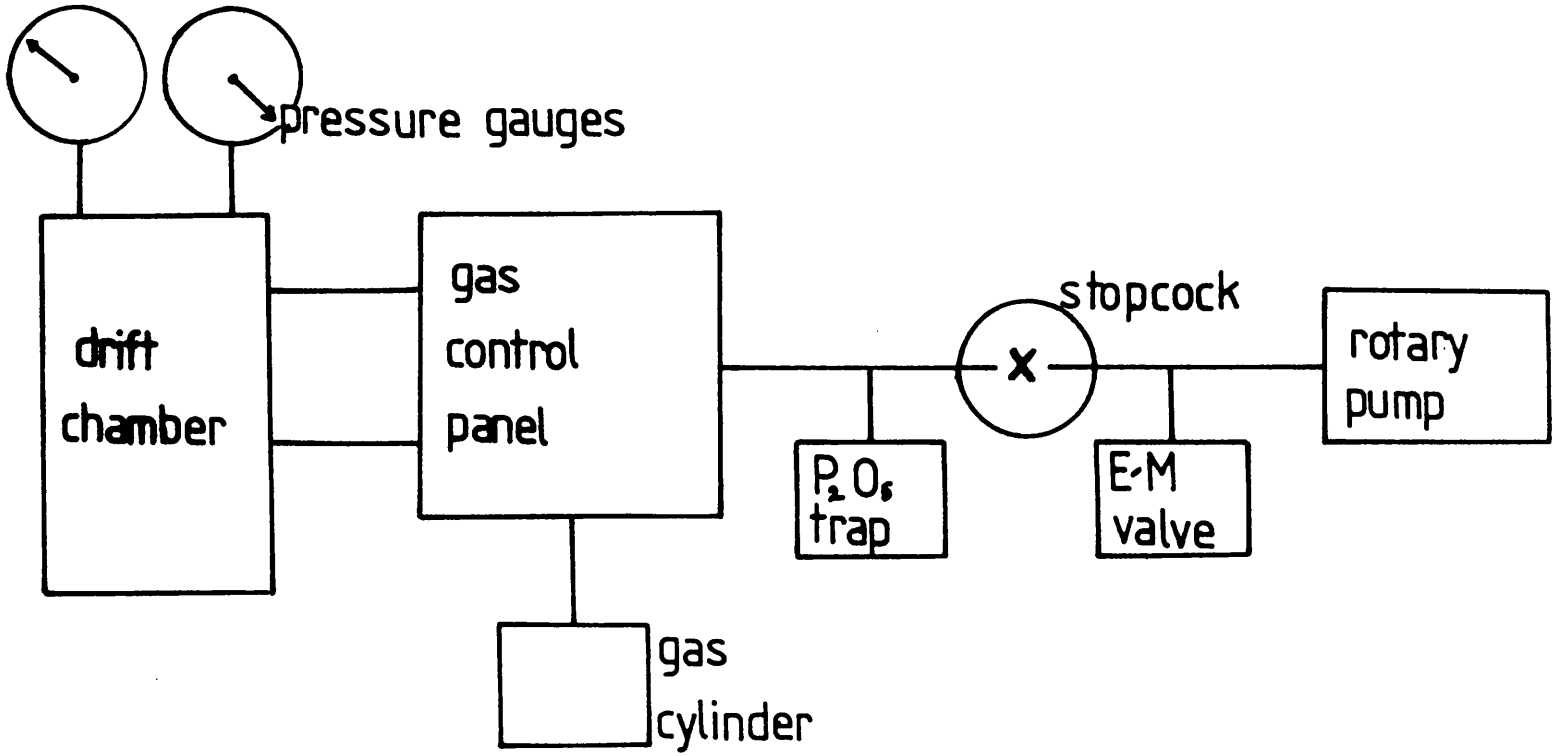

FIG 5.13 The full gas system.

resistance to pumping (Springham High Vacuum Greaseless Stop-cocks, 3 mm bore).

The chamber pressure was monitored with an Appleby and Ireland AI.101, 0 - 1000 torr precision absolute pressure gauge and a Speedivac 0 - 20 torr gauge, giving pressure measurements to within 0.5 torr.

The chamber was pumped by a Speedivac rotary pump.

Figure 5.13 shows the gas control arrangement, including the phosphorous pentoxide drying trap and an electromagnetic air admittance valve to protect the chamber from any oil suck back from the pump in the event of a power failure.

Stainless steel or glass tubing was used throughout the gas supply, pumping and pressure monitoring arrangement, except for on the pump side of the control system where rubber tubing was used to prevent the transmission of pump vibration to the chamber. The lateral diffusion arrangement was particularly microphonic and the chamber had to be rested on foam rubber.

At low pressures up to 20 torr the error in pressure readings is +/-0.5 torr, at higher pressures it is better than +/-1 torr. This error produces an error in E/p according to

$$\frac{E}{p} \pm \beta = \frac{E}{p \pm \Delta p}$$

the percentage error in E/p is therefore

$$\% \text{ error} = \pm \frac{\Delta p}{(p + \Delta p)} \times 100$$

Table 5.1 gives some examples of the error in E/p which apply to results given in this work, but which are not very signifi--cant.

TABLE 5.1 % ERROR IN E/p DUE TO PRESSURE READING INACCURACY.

PRESSURE (torr)	ERROR IN E/p (%)
10	4.8
50	1.0
100	1.0
150	0.7
200	0.5

5.8 ELECTRONICS.

Two distinct electronic arrangements were used, these are discussed separately.

5.8.1 Lateral diffusion measurements.

Figure 5.14 shows a block diagram of the electronic arrangement.

The asterisk represents the continuous source of UV above the photocathode, this is discussed in chapter 6. The 10 Hz square wave generator draws the electrons to the source hole in the grid and sets up the same magnitude electric field in the cathode-grid space as in the drift region of the chamber. The square wave generator was purpose built to give a large amplitude range fairly accurately controlled by a helipot and vernier, it also had a separate low fixed amplit--ude output to provide the reference signal for the phase-sensitive detector.

The electrons are collected on the plane Townsend collector after drifting and diffusing in the uniform field of the drift region. The lateral diffusion coefficient to mobility ratio D/μ is determined from the current distrib--ution on the collector by measuring the ratio of the currents to the central and the outer parts of the collector. This is discussed in chapter 7.

The currents involved in this experiment are very small (10^{-14} to 10^{-13} A). Low noise operational amplifiers with very large value feedback resistors ($2 \times 10^{9}\Omega$) were used. The inputs to these amplifiers are virtual earths, it was checked that the input potentials were at earth potential.

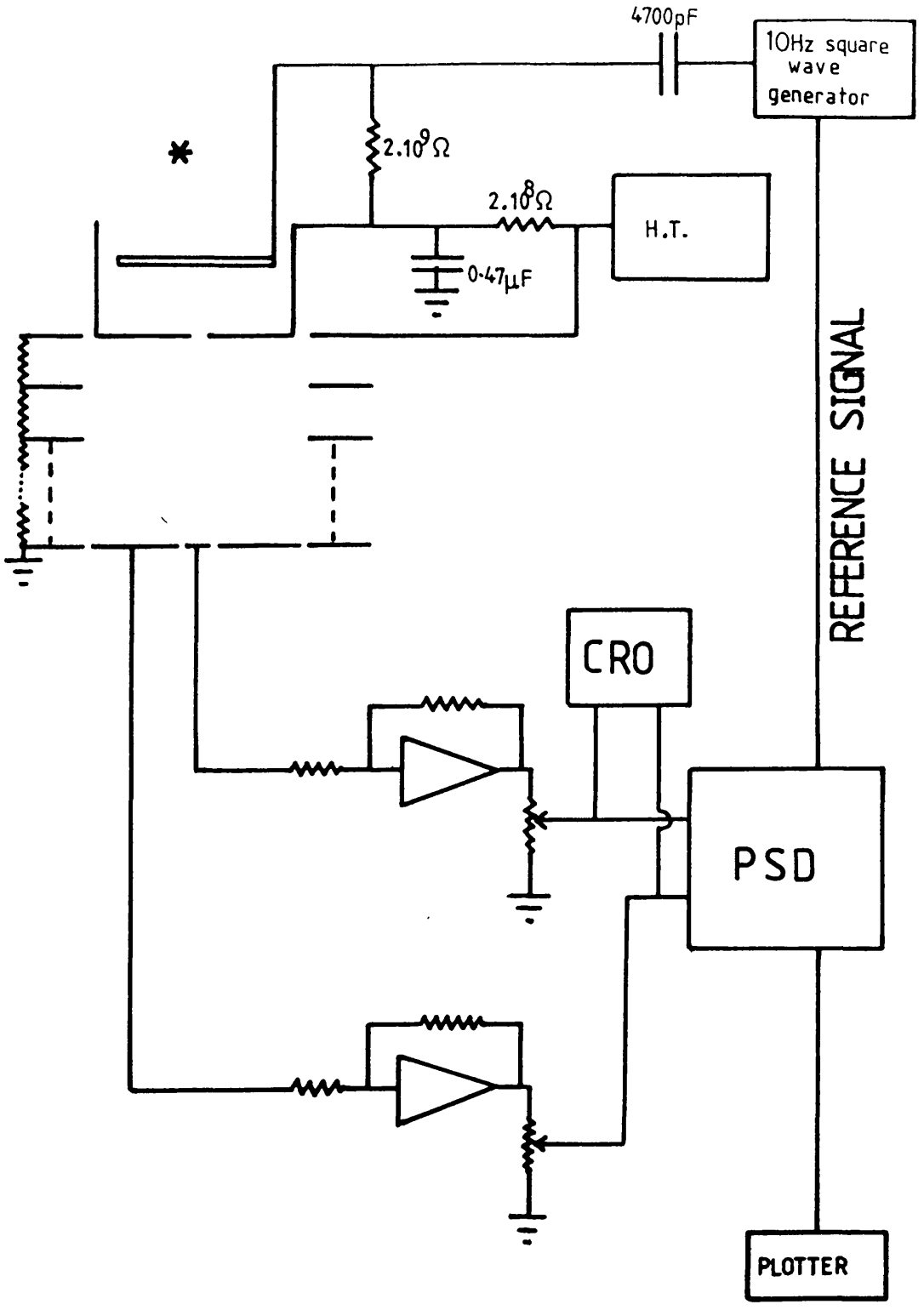

FIG 5·14 Block diagram of the electronic arrangement for lateral diffusion measurements.

With the series resistor on an amplifier output at its central adjustment position a collected current of 10^{-13} A produces an output of 0.1 mV. These series resistors are 10 kΩ helipots adjusted by verniers.

The outputs of the amplifiers were continuously monitored on an oscilloscope to check for increases in noise, pick-up etc.

The operational amplifiers were PMI OP-15G, which have low noise performance with a high signal gain

Input noise current density: 0.01 pA/√Hz

Input impedance: 10^{12} Ω

Signal voltage gain: 200 V/mV.

The amplifier outputs were fed to the differential inputs of a phase sensitive detector ORTEC 9501E, which selects signals modulated in phase with a reference signal. This model has a phase difference control allowing adjustment for the change in phase resulting from the drift time of the electrons to the collector and the amplifier. In the differential mode the phase sensitive detector produces a D.C. output proportional to the difference between the two inputs. The output fluctuations were attenuated by selecting a suitably long time constant on the phase sensitive detector.

The manufacturers give the following specifications

Sensitivity: 1μV

Frequency range: 2 Hz to 100 kHz

Time constant: 1 ms to 30 s (10 settings).

Fluctuations in P.S.D. output were a combination of very rapid changes due to noise which were easily attenuated by using a time constant of a few seconds and much slower changes. The output of the P.S.D. was monitored on a Y-T paper

plotter for long periods of time while the operational amplifier series resistors were adjusted, until the P.S.D. output was judged to be zero. A zero output from the P.S.D. indicates that the two inputs are equal. The plotter used was a Heath Servo-recorder EUW-20A.

The field voltage in this and the other arrange--ment was provided by a Brandenburg 45-B High voltage power supply which provides voltages in the range 0 to $\pm$3 kV.

5.8.2 Drift Velocity and Longitudinal Diffusion Coefficient Measurements.

Figure 5.15 shows a block diagram of the electronic arrangement for these measurements.

Electrons were released from the photocathode by pulses of UV from a flash-tube. A very narrow electron pulse was required so a narrow pulse was applied to the photocathode superimposed on a D.C. reverse bias of the cathode -grid space (not illustrated in figure 5.15). The amplitude of this pulse was adjusted to produce the same field in the cathode-grid region as in the drift region. The width of this pulse is just greater than the time taken for electrons produced at the photocathode to drift to the grid. In practice this width could be made equal or slightly less than the transit time without reducing the number of counts in the detector to zero, this is because of penetration of the drift field through the grid. Both the UV flasher and the cathode pulser were triggered by a master pulser producing positive 30 µs pulses of 20 V amplitude at a rate of 100 Hz.

A second pulser produces pulses delayed behind the pulses from the master pulser. The delay is measured by

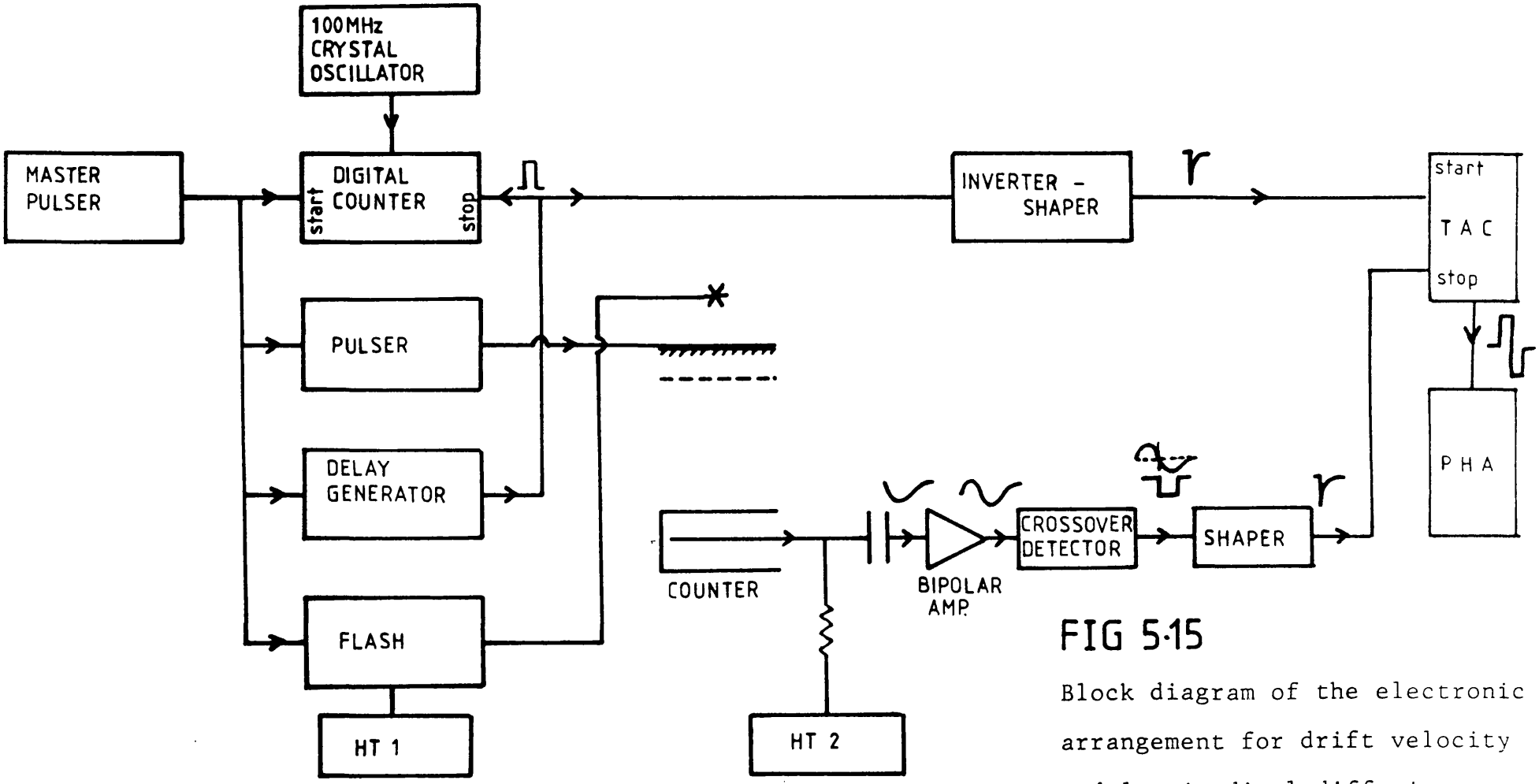

FIG 5.15

Block diagram of the electronic arrangement for drift velocity and longitudinal diffusion coefficient measurements.

a digital counter which monitors the number of oscillations of a 100 MHz crystal oscillator between a start signal from the master pulser and a stop signal from the delayed pulser. The delayed pulse was +20 V, 0.4 μs. Both the master pulser and the delayed pulser were Venner TSA 628 pulse generators.

The cathode pulse was provided by a Hewlett Packard 214A pulse generator capable of providing pulse amplitudes up to 100 V and as narrow as 0.05 μs.

The delayed pulse after inverting and shaping provides the start signal for a time-to-amplitude converter.

The electrons drift to the Geiger counter. The signal from the counter is amplified and fed to a cross-over detector which produces a negative pulse coinciding with the zero voltage cross-over point of the bipolar input. After shaping this pulse provides the stop signal for the T.A.C.

The inverter/shaper and the shaper are shown in figure 5.16, these are used to alter the square pulses in the start and stop circuits to the pulse shape required by the T.A.C.

The E.H.T. for the Geiger counter is supplied by an Isotope Development 532/D E.H.T. Unit through a 12 MΩ coupling resistor. The E.H.T. is decoupled from the stop channel electronics by a 5000 pF series capacitor.

The counter signal is shaped by a linear amplifier, ORTEC 571 operating in the bipolar mode with a gain setting of 300 and a 1 μs shaping time. The cross-over detector used is described by T. Harris (1972).

The ORTEC 437A time-to-amplitude converter is used to provide a bipolar pulse for each detected electron with an amplitude proportional to the time difference between the arrivals of the start and stop inputs.

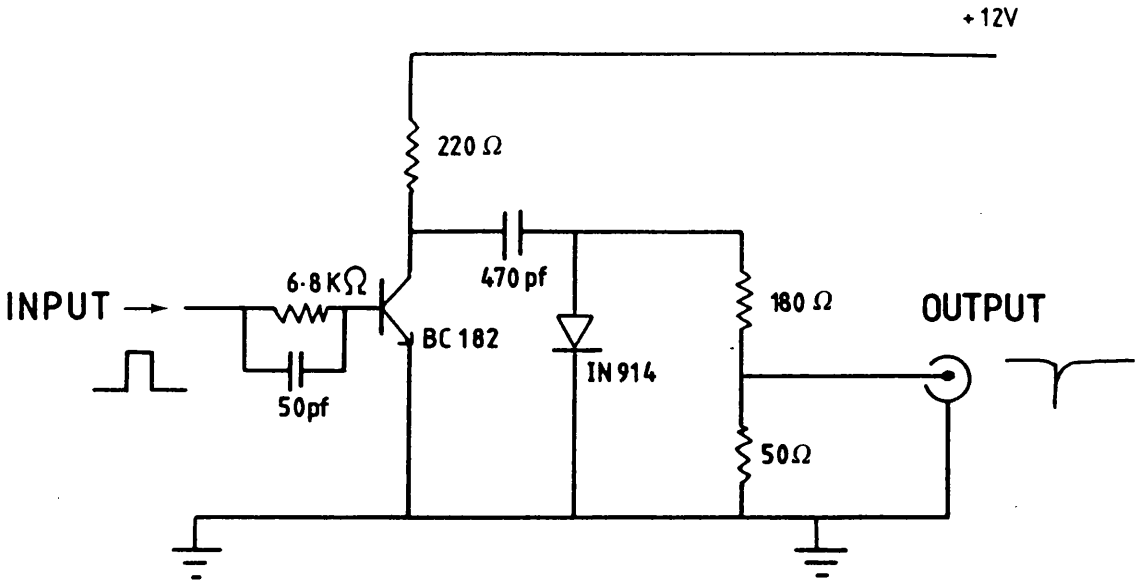

(a) Circuit diagram of inverter/shaper.

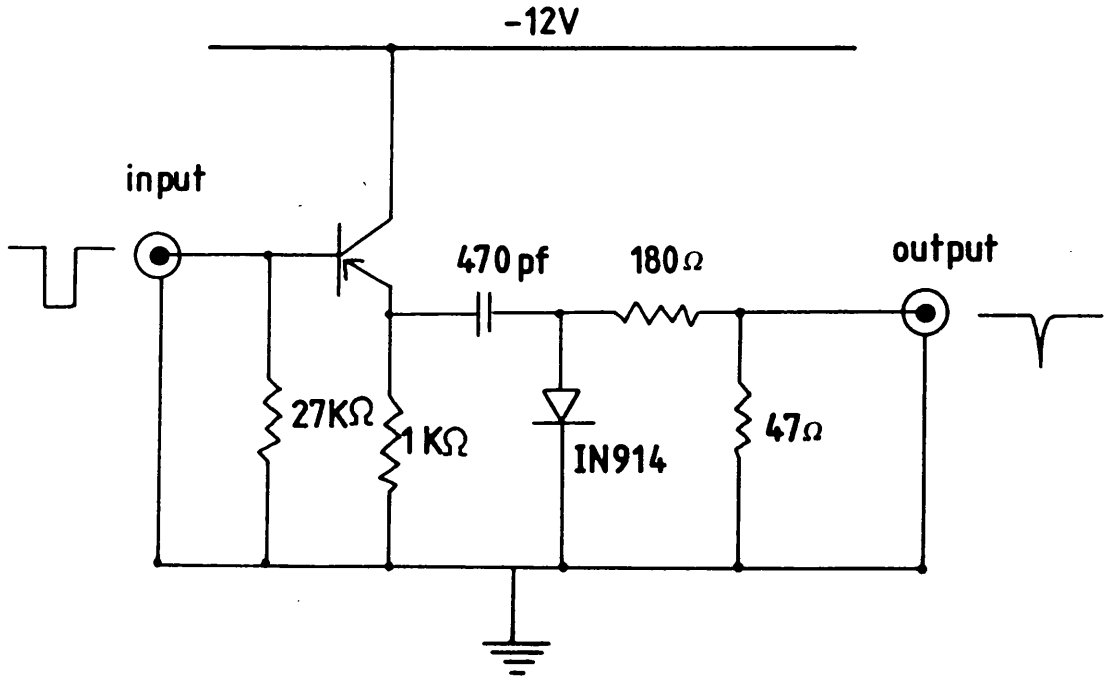

(b) Circuit diagram of the shaping network used in the stop channel.

FIG 5·16

The T.A.C. pulses are collected by an E.G.&G. Northern NS600, 256 channel pulse height analyser. This instrument has digital zero-offsets providing a resolution equivalent to 2048 channels. Further discussion will be found in section 7.3.

Figure 5.17 shows the circuit diagram of the UV flash-tube trigger arrangement. The flash-tube used is an E.G.&G. 108-AU xenon flash-tube. Typical operating characteristics quoted by the manufacturer are

Energy input per flash: 0.01 J

Arc length: 8 mm

Maximum repetition rate: 500 Hz

Pulse duration: 0.8 μs

Life in free air: 6×10^8 flashes.

Figure 5.18 illustrates the time relationships between the different signals in the experiment.

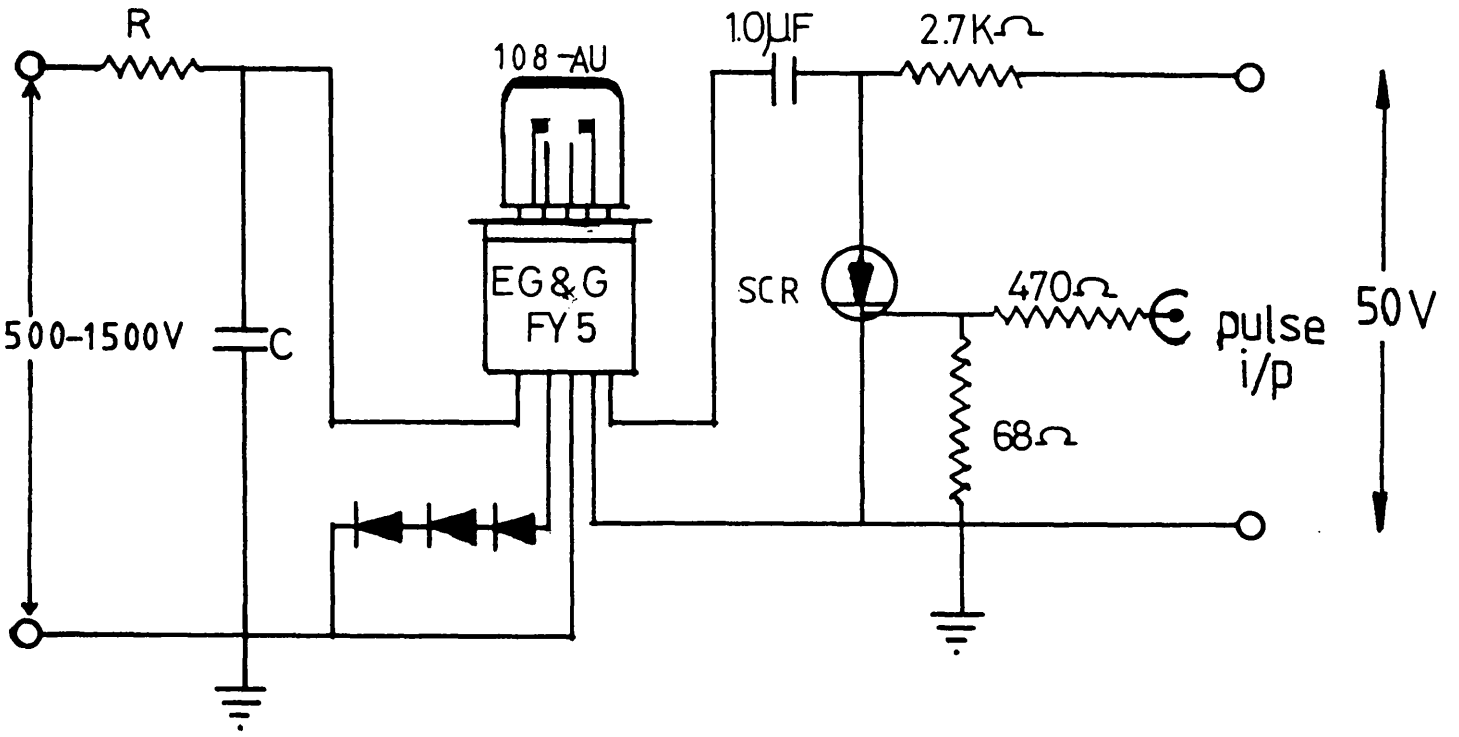

FIG 5·17 Circuit of the UV flash-tube trigger.

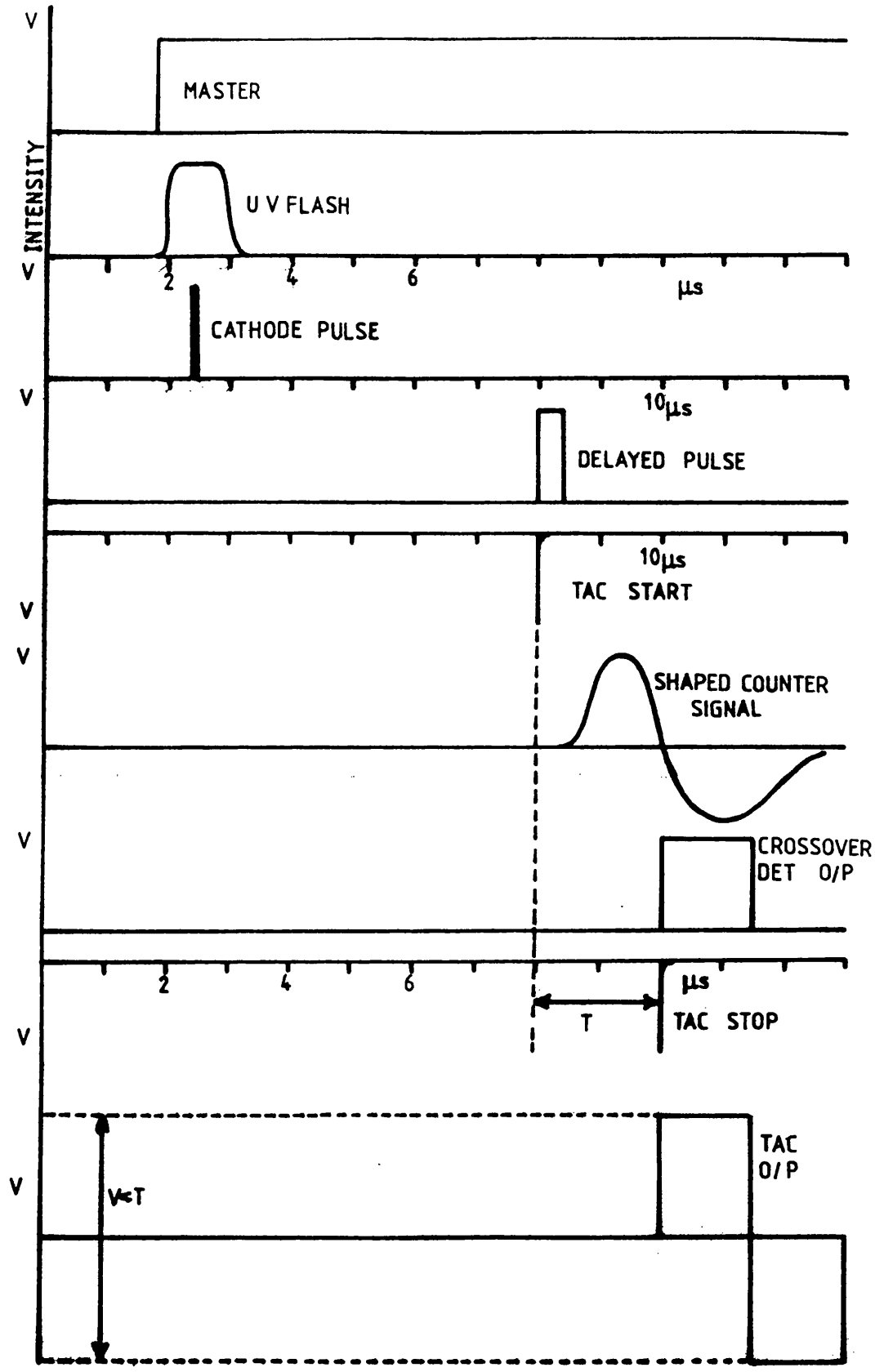

FIG 5.18 Time relationships between signals.

CHAPTER 6.

ELECTRON PRODUCTION.

6.1 INTRODUCTION.

The electron source assemblies used in this work have been described in chapter 5. This part of the apparatus was given considerable attention aimed at improving and optimising its operation.

The requirements of the experiments in regard to the electron source, and the development of a practical source fulfilling these as far as possible are considered here. Methods of electron production which did not show themselves to be appropriate to this work and which were rejected are also referred to, but in less detail.

6.2 THE ELECTRON SOURCE FOR LATERAL DIFFUSION MEASUREMENTS.

The experimental arrangement for lateral diffusion measurement was based upon the measurement of small currents arriving at a plane collector by means of high gain low noise amplifiers and a phase sensitive detector. The arrangement is described fully in chapter 5 and the procedure for operation in chapter 7.

The electron current flowing through the gas could be as large as 10^{-12}A without producing errors in the measurements due to the space-charge effects (Huxley and Crompton, 1974). A time varying signal is required for the phase sensitive detector to eliminate random noise which appears superimposed on the electron signal. The optimum frequency of this variation being 10 Hz.

6.2.1 Electron production by photoemission.

The method used by El-Hakeem (1978) in a very similar experimental arrangement was an obvious choice for this work. The method involved a transmission gold photocathode evaporated onto a quartz disc similar to that of Moruzzi(1967). The uncoated side of the quartz disc was illuminated with low wavelength UV light from a mercury lamp (the 254 nm line of the mercury spectrum and the continuum below this wavelength). This UV light has enough energy to release electrons from the gold layer, the photoelectric effect.

The assembly of the electron source head suspended in the drift chamber, and the use of a flexible light guide to transmit the UV light from the mercury lamp outside the chamber to the photocathode is illustrated and

described in section 5.3.

Several factors had to be considered in order to optimise the photoelectric method

a) electrical contact to the gold layer

b) optimum thickness of gold for efficient electron production

c) physical arrangement in the source head,i.e. the relative positioning of the light guide, cathode and grid within the head.

Previously electrical contact to the gold layer on the quartz disc was made by pushing the disc against a metal annulus carrying the connection with a fairly weak extension spring (El-Hakeem, 1978). This was not satisfactory as the quality of the contact was variable as a result of dismantling, which could also damage the photocathode, repeat--ed reassembly was often necessary until a good contact and cathode condition were proved by a trial run.

An unsuccessful attempt was made to produce a photocathode with a rigid permanent contact. A thin stainless steel annulus was fixed to the gold layer with conducting epoxy resin. Although a thick gold layer was evaporated onto the part of the quartz disc which would be fixed to the metal contact the gold developed discontinuities during the curing of the resin. Even after extended ion bombardment of the quartz before evaporation, the adhesion of the gold was insufficient for the thin emission layer to withstand the forces present during the curing of the resin.

In the final design the photocathode and the contact were pressed together in a unit which could be removed from the source head without affecting the contact between them or exposing the fragile cathode enough to damage it.

The contact was in the form of a stainless steel can with a 1.0 cm diameter hole in the bottom. The photocathode was held against the bottom of this using a crinkle spring and a circlip, see figure 6.1.

The quartz disc is coated around the edge with a thin layer of graphite before evaporation with gold. This arrangement produces a very good electrical contact and is easily assembled and installed in the source head. Far more pressure can be applied between the photocathode and the contact than in the previous arrangement, in which a strong spring would have tended to push the grid out of the end of the source head.

In order to find the optimum thickness of gold for the photocathode, quartz discs were evaporated with a range of thicknesses, 60 Å, 100 Å, 200 Å, 300 Å and 400 Å. Previously 400 Å was the thickness used (El-Hakeem, 1978). The percentage transmission of 254 nm UV light, the resistance edge to centre and the relative photoemission currents were obtained for each disc, Table 6.1. The optimum thickness for efficient electron production is clearly about 100 Å of gold, this thickness was used throughout the experiments.

The remaining concern was the separation of the grid and the photocathode in the source head. The forward bias required to produce saturation was investigated for several gases and pressures over a range of photocathode-grid separations from 1 mm to 10 mm, by measuring the cathode-grid current as a function of the bias voltage. Figure 6.2 shows clearly that a 10 mm separation requires a far larger applied voltage to produce saturation, particularly in methane, than a 1 mm separation. A photocathode-grid separation of 2 mm has been used throughout this work. This separation requires a square

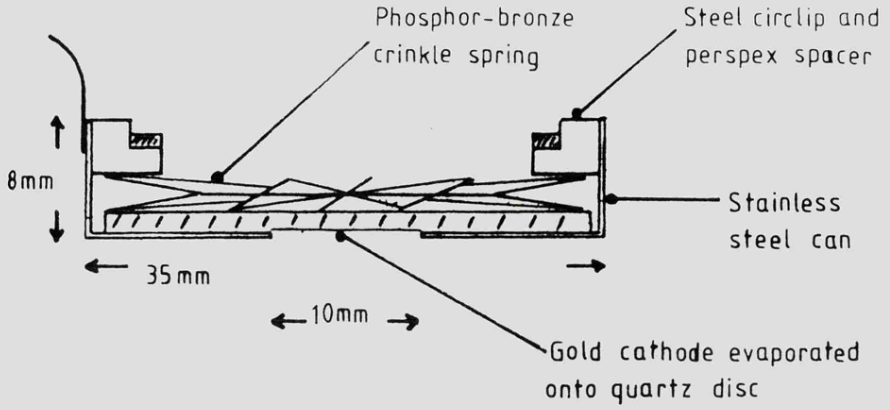

FIG 6.1 The photocathode contact arrangement

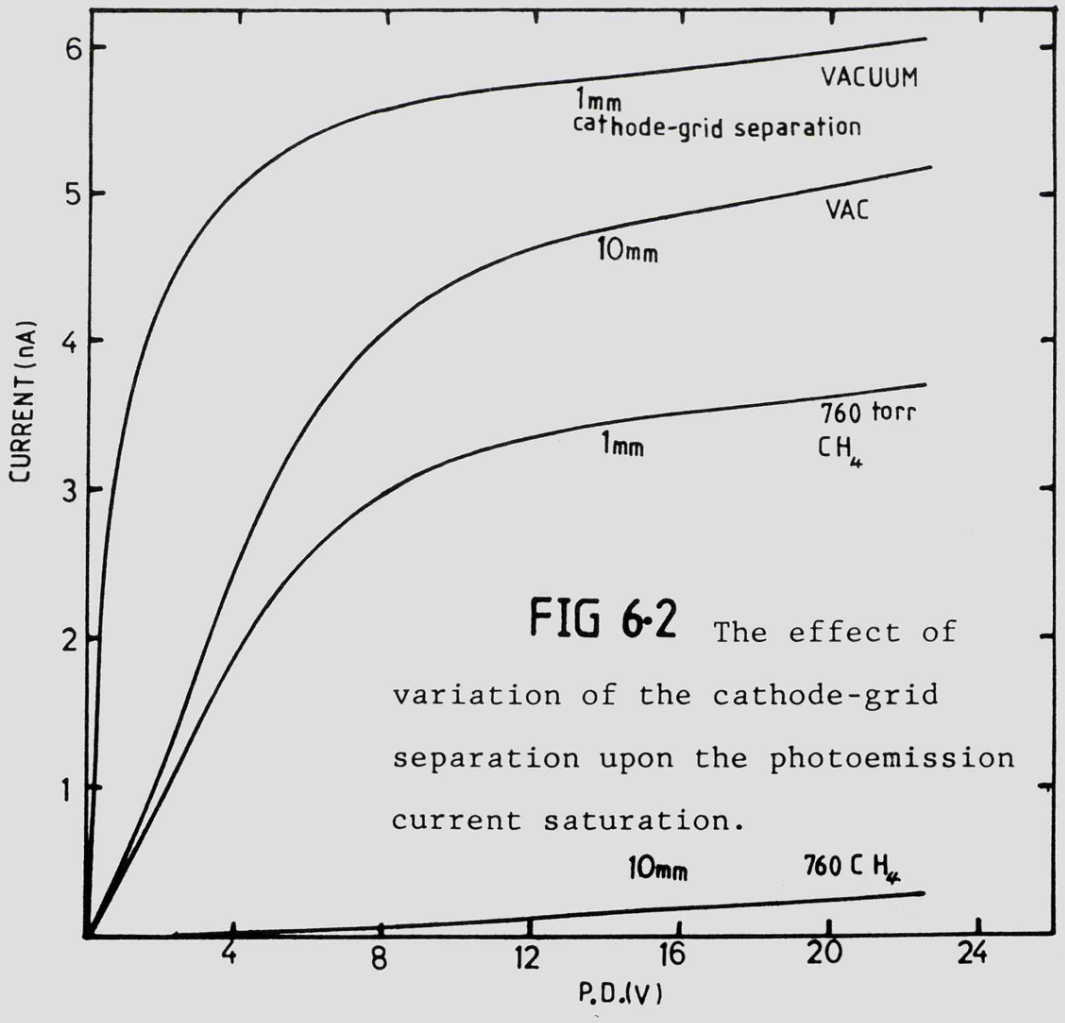

FIG 6.2 The effect of variation of the cathode-grid separation upon the photoemission current saturation.

TABLE 6.1 OPTIMISATION OF GOLD THICKNESS ON TRANSMISSION PHOTOCATHODE.

GOLD THICKNESS (Å)	% TRANSMISSION OF 254 nm UV.	RESISTANCE (Ω) EDGE - CENTRE	RELATIVE PHOTO-EMISSION CURRENT
60	51	2000	0.57
100	37	1500	1.00
200	24	100	0.86
300	10	0	0.60
400	4	0	0.00

wave amplitude of the same order as, or lower than that to set up the same electric field in the head as in the drift region. A 2 mm separation is also large enough for the electron swarm to reach equilibrium in the field before entering the drift region of the chamber.

A mechanical light chopper was constructed and used to discover any current due to UV light transmitted into the chamber through the photocathode, i.e. a current unmodulated by the square wave applied to the photocathode. The chopper was in the form of a rotating aluminium disc with alternate quarters cut away. It was placed between the UV source and the end of the light guide. The remaining quarters of the disc stopped the UV producing a square wave modulated UV light. The chopped light was monitored with a photodiode to provide a reference for the P.S.D. All electrons reaching the collector which were produced by photoemission must be modulated and therefore register on the P.S.D. output. With a reverse bias in the photocathode-grid region any UV dependent current measured by the P.S.D. must originate from photoemission from surfaces in the chamber below the grid. This proved that all the photoemission current infact originated from the photocathode. Although the photocathode transmits 37 % of the incident UV the grid used in this experiment must block almost all of this as it has a central hole with a diameter of only 0.72 mm.

Initial difficulties revealed that the currents to the centre and to the outer parts of the collector could be out of phase by as much as 45^{o} under some circumstances (which would be unusual during a run but appropriate to testing the apparatus). This phase difference was found to be dependent upon the settings of the potentiometers of the

collector amplifiers as used by El-Hakeem (1978) see figure 6.3. Feeding a small amplitude (30 mV) square wave to one of the amplifiers and varying the potentiometer ratio r would be expected to produce an output voltage linearly dependent upon 1/r. However this was not the case, figure 6.4. So $V_o \neq - iR/r$.

Examination of the circuit diagram, figure 6.3 reveals that the amplifier behaves as an integrator when $r = 0$ and an inverter when $r = 1$, introducing a phase difference between the outputs of the two amplifiers for different r settings.

The circuit was changed for all the measurements in this work, the modified circuit is shown in figure 6.5. For this circuit $V_o = - r\, i\, R$.

In the work of El-Hakeem (1978) the effect described here was observed as a dependence of the measured value of D/μ upon the current ratio $i_c/(i_c + i_o)$. The results presented by El-Hakeem were corrected empirically when the current ratio was higher or significantly lower than 0.5. At $r = 0.5$ no correction was necessary as both the potentiometer settings would be the same and so both amplifier outputs in--phase. No correction of the measured D/μ values has been necessary in the present work with the modified amplifier circuits.

Work with different gases revealed that the characteristics of the electron source were complicated by gas dependent effects. Typical photoemission currents and saturation characteristics were obtained by applying a D.C. bias in the photocathode-grid region and measuring the collected currents with a Hewlett-Packard DC Microammeter. For the 2 mm cathode-grid separation the photoemission current reached a

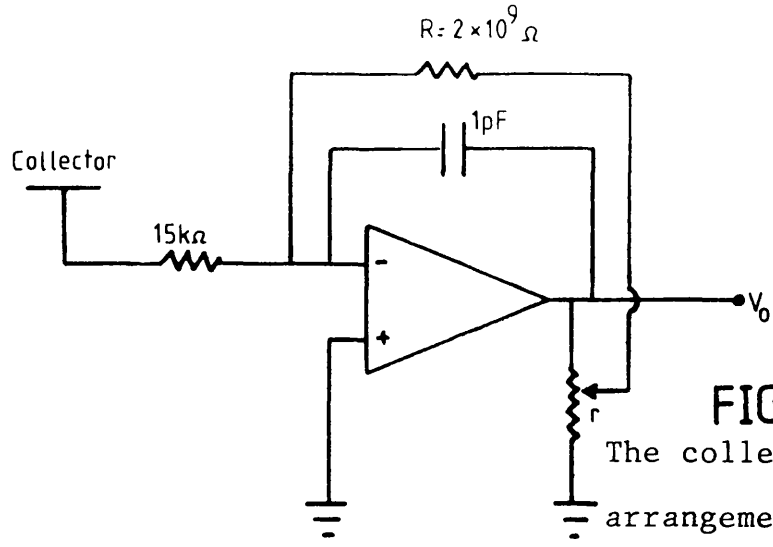

FIG 6·3

The collector amplifier arrangement of El-Hakeem.

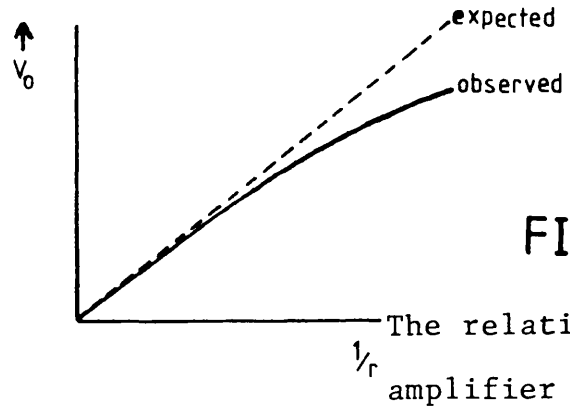

FIG 6·4

The relationship between the amplifier output voltage V_o and the potentiometer setting r for the El-Hakeem arrangement.

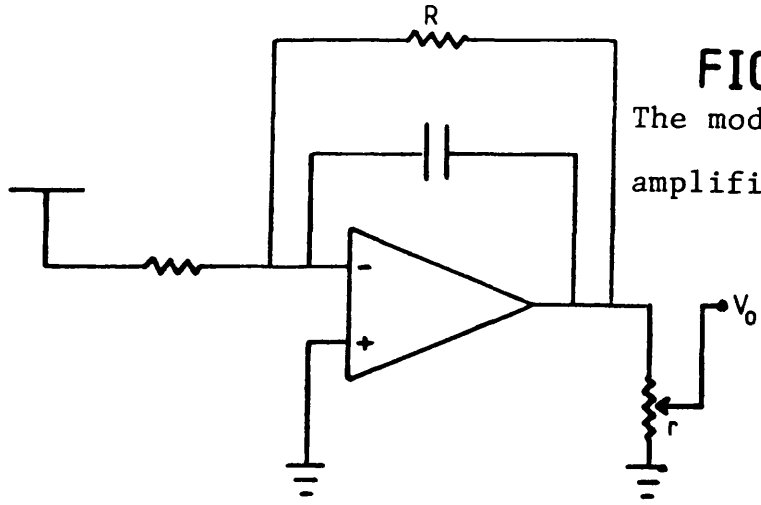

FIG 6·5

The modified collector amplifier arrangement.

saturation current of the order of 1.6×10^{-10} A in vacuum by applying a few volts. In gases such as argon + 10 % methane, argon + 50 % methane and 100 % methane at pressures as high as 400 torr, currents of the same order can be obtained when voltages of 20 - 30 V (100 - 150 V/cm) are applied. So in these gases the photoemission current is at its saturation level, or very close to it for the E/p range of interest. However in gases such as argon and nitrogen this is not so. In argon about 80 V (400 V/cm) and in nitrogen a much higher voltage is needed to reach the saturated photoemission current at a pressure of just 50 torr.

Following the work of Al-Dargazzelli et al (1980) on drift velocities in argon/nitrogen mixtures an attempt was made to measure D/μ in argon + 10.7 % nitrogen.

Typical collected currents in other gases were of the order of 10^{-13} A for a head current of about 10^{-10} A. The photoemission current in argon + 10.7 % nitrogen would not be near to saturation if the field in the head was set at the same value as the field in the drift chamber. Indeed the collected currents under this condition were very low, too low to produce satisfactory data. However increasing the field in the head resulted in a drop in the collected current. The voltage required in argon + 10.7 % nitrogen for a saturated photoemission current was very high, so the increased field strength which resulted in the drop in collected current could not have significantly increased the photoemission current. Useful currents of the order of 5×10^{-14} A could only be collected by reducing the field in the head to very low values, e.g. E/p in the head of 0.03 V/cmtorr for an E/p in the drift chamber of 0.5 V/cmtorr. There was a strong dependence then upon the ratio of the fields above and below the grid, as discussed by

Buneman et al (1949). This effect could also be observed in argon and in nitrogen, but not in the other gases used in this work due to the greater significance of saturation of the emission current.

Reliable results could not be obtained by using the small head fields which allowed transmission of the electron current through the grid with argon, nitrogen and their mixt--ures. A strong drift field dependence was observed. This led to an investigation of equilibrium distance, using Monte-Carlo calculations which are discussed later in this section.

The reason for the high voltage saturation in argon, nitrogen and their mixtures was considered. These gases have very low drift velocities compared with the other gases studied. By plotting the head current against drift velocity a clear dependence was revealed, figures 6.6 and 6.7, for argon, nitrogen, methane and argon + 10 % methane. The effect that the drift velocity would have on the space-charge would not seem to explain this. An estimate of the field produced by space-charge for a particular drift velocity can be made as follows.

Let the current be 10^{-10} A = 10^{-10} coulombs/s. Let this current flow through an area of 1 mm^2, which is an under-estimation for the real situation.

$$\text{Current density } J = 10^{-10} \text{ coulombs/mm}^2\text{s}$$
$$= 10^{-1} \text{ coulombs/m}^2\text{s}$$
$$\text{Let drift velocity } W = 5 \text{ cm/}\mu\text{s (100\% methane, E/p=0.5)}$$
$$\text{Space charge } \rho = J/W = 2.10^{-6} \text{ coulombs/m}^3$$
$$\text{Field produced } E = \frac{\rho}{4\pi\varepsilon_o} = \frac{2.10^{-6}\ 10^{12}}{12\text{x}8.85} \text{ V/m}$$

So for a cathode-grid separation of 2 mm the field produced by the space-charge is 0.4 V/cm, which is not significant.

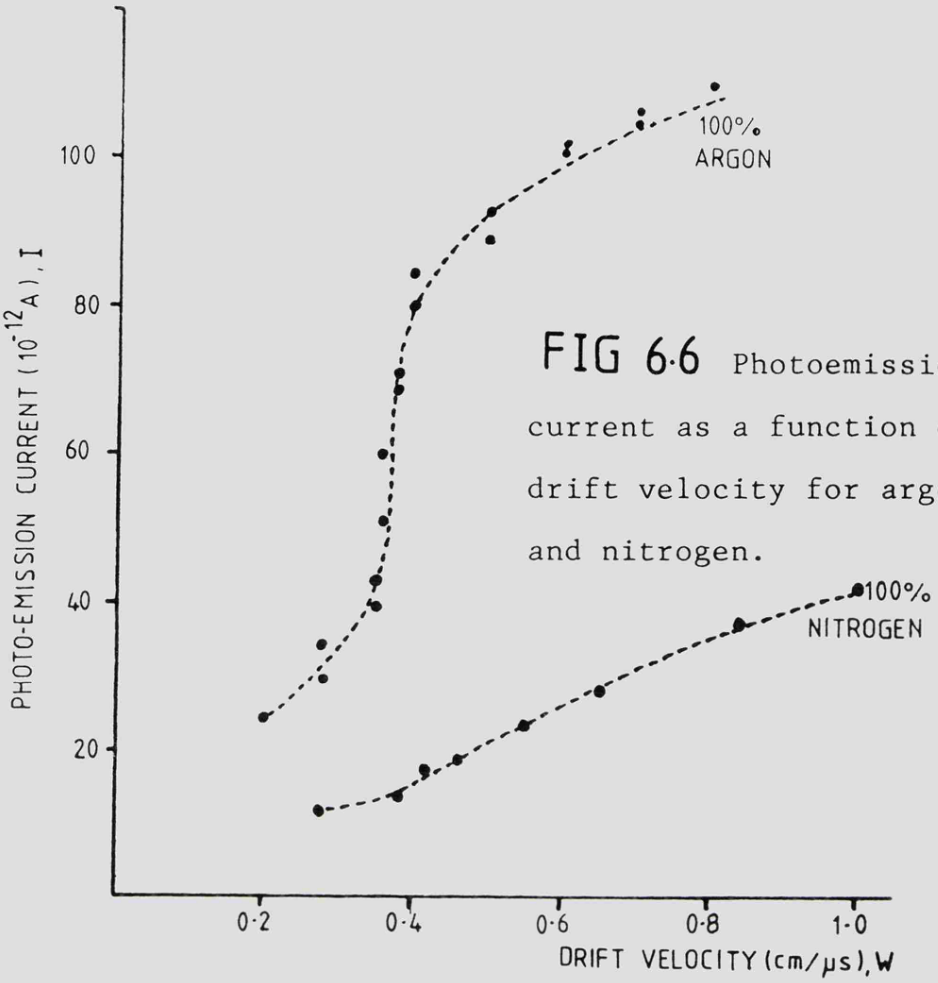

FIG 6·6 Photoemission current as a function of drift velocity for argon and nitrogen.

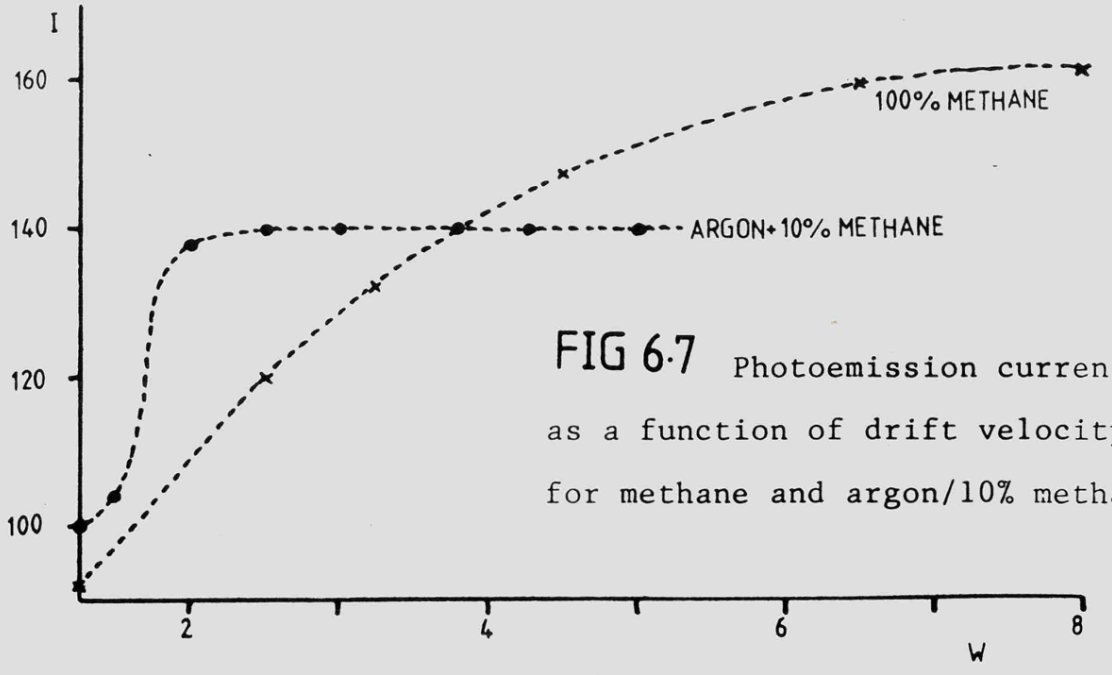

FIG 6·7 Photoemission current as a function of drift velocity for methane and argon/10% methane.

For the space-charge to have a great effect, such as that observed in argon, the drift velocity would need to be at least two orders of magnitude smaller, i.e. 0.05 cm/μs, producing a space-charge field of 40 V/cm opposing a typical applied field of 100 V/cm. Alternatively the space charge would have to be non-uniform.

If the current is space-charge limited the current must, to some extent, be independent of the UV inten--sity. Figure 6.6 for 100 % argon resembles the characteristic of a thermionic diode, so if there is a space-charge limited current this should be observable at W = 0.28 cm/μs (E/p=0.1). At this point however the photoemission current was totally dependent upon the UV intensity, rising and falling in exactly the same ratio as an increase or decrease in the saturation current obtainable in vacuum for a particular intensity.

It seems that the major effect which was observed was back-diffusion of electrons to the photocathode. This is strongly indicated by Monte-Carlo calculations of the fraction of electrons produced which completely escape from the photo--cathode. This fraction increases with E/p and the proportion of methane in argon + methane mixtures, table 6.2.

As the E/p increases the field drawing electrons from the photocathode increases, increasing the fraction which escape. As the amount of diffusion falls with the proportion of methane in the mixture the fraction of the electrons produced which escape increases for a particular E/p.

Tables 6.3 and 6.4 summarise the results of Monte-Carlo simulations carried out to examine the equilibrium distance in argon + 10 % methane and 100 % methane. It would have been useful to carry out similar simulations in argon + 10.7 % nitrogen, but no inelastic cross-sections were available

TABLE 6.2 THE FRACTION OF PHOTOELECTRONS ESCAPING FROM THE PHOTOCATHODE IN ARGON + 10 % METHANE AS A FUNCTION OF E/p.

E/p (V/cm.torr)	Fraction escaping (%)
0.05	24.6
0.10	27.0
0.25	39.7
0.50	37.9
1.00	41.2

TABLE 6.3 RESULTS OF MONTE-CARLO SIMULATIONS IN ARGON + 10 % METHANE TO EXAMINE EQUILIBRIUM DISTANCE.

E/p (V/cm.torr)	d (cm)	F	W (cm/μs)	D/μ (V)	D_L/μ (V)
0.5	0.142	0.286	4.150	0.568	0.370
	0.283	0.286	4.265	0.541	0.164
	0.422	0.286	4.213	0.463	0.321
	0.559	0.286	4.179	0.459	0.545
1.0	0.049	0.357	3.145	0.934	0.395
	0.094	0.357	3.064	1.804	0.330
	0.138	0.357	3.008	1.503	0.289
	0.182	0.357	2.989	1.618	0.152
	0.225	0.357	2.993	1.209	0.307
	0.268	0.357	2.994	0.994	0.363

TABLE 6.4 RESULTS OF MONTE-CARLO SIMULATIONS IN 100 % METHANE.

E/p	d	F	W	D/μ	D_L/μ
1.0	0.223	0.417	8.022	0.125	0.192
	0.445	0.417	7.989	0.128	0.474
	0.667	0.417	8.008	0.184	0.370
2.0	0.143	0.556	8.393	0.261	0.441
	0.287	0.556	8.427	0.250	0.601
	0.431	0.556	8.382	0.336	0.599
	0.575	0.556	8.368	0.266	0.784
	0.791	0.556	8.381	0.207	0.700
	0.863	0.556	8.379	0.245	0.658

In the tables above d = distance travelled by the centroid of the electron group and F = the fraction of electrons escaping from the photocathode.

for nitrogen. These simulations released 10 electrons and produced the data in the tables after every 5000 collisions. In both gases the drift velocity stabilises quickly, but D/μ and D_L/μ require much longer drift lengths to stabilise, in excess of 5 mm in argon + 10 % methane and of 8 mm in 100 % methane.

6.2.2 Electron production by a glow discharge.

All the results given in this work were obtained using a photoemission electron source, but considerable time and effort was used in an investigation of alternative electron sources. An electron source able to produce large electron currents in the source head would have been a great advantage in gases requiring a large bias to produce saturated photoemission currents, such as argon and nitrogen. Also the ultra-violet light sources used in these measurements were generally extremely unreliable, several mercury-xenon arc lamps exploded after only 10 hours operation. This problem alone caused considerable delay in the progress of work.

The use of an alpha-particle source, such as Americium-241 foil used by Milloy and Crompton (1977) or Polonium-210, was ruled out because of the small risk of long term low level contamination of the equipment or the laboratory, where considerable research using and developing detectors is carried out.

Attempts to produce electrons by thermionic emission in various atmospheres were unsuccessful except in pure argon. Attention was quickly moved to the feasibility of using a glow discharge as used by several other workers in the field (Lawson and Lucas, 1965; Cochran and Forester, 1962).

The initial prototype arrangement consisted of a small loop of 10 μm tungsten wire, forming the cathode about 3 mm from a flat metal plate for the anode, figure 6.8. In argon 1 kV across the electrodes produced a very steady electron current of about 2 μA measured on a Hewlett-Packard DC Micro-Volt Ammeter Model 425 A. The immediate aim was to measure lateral diffusion coefficients in methane and argon/methane mixtures. The same arrangement was used to set up a discharge in an atmosphere of pure methane. The voltage required to strike the discharge in methane was 3 kV, the discharge then ran with an unstable current of 25 μA +/- 20 % (2.5 kV now being dropped across the series resistor). The discharge was left running for one hour. During this time a carbon whisker formed to produce finally a short circuit between the cathode and the anode plate. The instability of the electron current can be attributed to the carbon deposition.

By assuming that every molecule of methane colliding with the cathode, the centre of the discharge, dissociates, and taking a typical gas flow rate, the contamin-ation which would be produced in the drift chamber if a glow discharge was used can be estimated from elementary kinetic theory.

The total number of collisions per unit time per unit area $= \frac{1}{4} n \bar{c}$

where n = number of molecules per unit volume.

Cathode area $A = 1.5 \times 10^{-7}$ m^2

Chamber volume $V = 5 \times 10^{-3}$ m^3

Fraction of molecules in the chamber colliding with the cathode per unit time $= \frac{1}{4} \frac{A}{V} \bar{c} = 0.003$

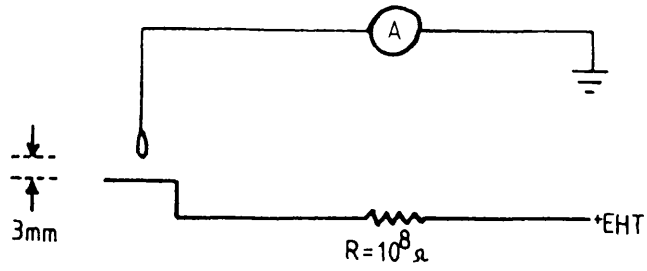

FIG 6·8 The initial prototype arrangement used to produce glow discharges.

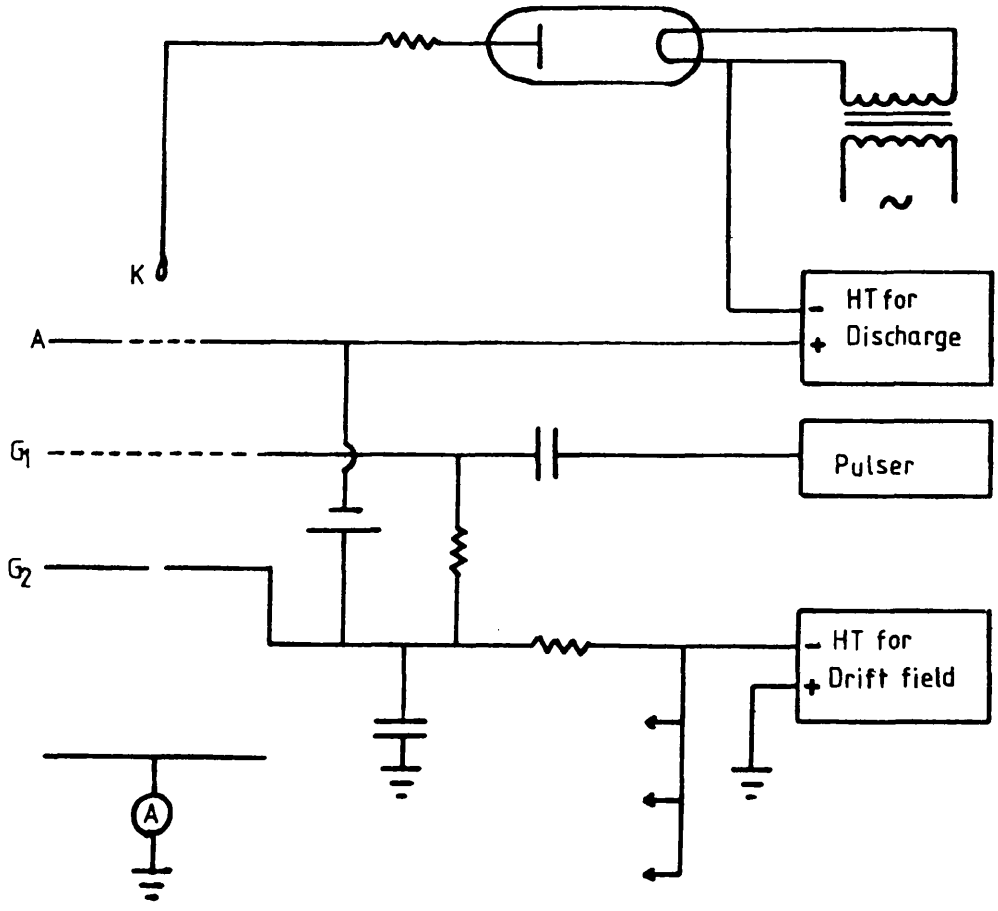

FIG 6·9 The final glow discharge electron source arrangement.

So approximately 0·3 % of the molecules in the chamber would dissociate every second.

The gas flow produces a fixed gas change-over rate. For operation at 50 torr the flow rate into the chamber would be, at most, 640 cm^3/min. The time for a complete change-over of gas being at least 500 s and the maximum change-over rate is 0.2 %/s. Under these conditions the contamination would be at least 0.3 %/s. Clearly if a glow discharge was used arrangements to pump the source head directly would be required to avoid contamination of the gas in the drift region of the chamber.

A directly pumped glow discharge source head was produced and operated in the drift chamber. Unstable and intermittent currents in the chamber led to a number of modifications. The final arrangement illustrated in figure 6.9 incorporated a thermionic diode for current control as used by Huxley and Zaazou (1949), two grids to provide the necessary modulation of the currents. The anode is in the form of a can enclosing the cathode to prevent electrons avoiding modulation, however it proved impossible to achieve 100 % modulation of the chamber current. The circuit was arranged to give a large reverse bias between the grids G_1 and G_2 during half the square wave cycle and a small forward bias during the other half. The level of modulation achieved was less than 15 %.

The discharge is considered to have extended further than the anode, possibly into the drift region of the chamber, this was particularly indicated when it was observed that increasing the field voltage in the chamber increased the mean current down the chamber. It was considered necessary because of shortage of time to terminate this investigation.

6.3 ELECTRON PRODUCTION FOR DRIFT VELOCITY AND LONGITUDINAL DIFFUSION COEFFICIENT MEASUREMENTS.

The electron source head, comprised of a photocathode and a copper micromesh grid separated by a 5 mm space, is described in chapter 5.

Figure 6.10 illustrates the effect of the pulse applied to the cathode and a reverse bias applied to the cathode-grid region. The time T corresponds to the prompt electron peak, and the time τ, to the delayed electron peak. For some experimental conditions these two peaks were overlapping as illustrated here, but in general were fairly well separated.

The delayed electron peak in the time-of-flight spectrum, i.e. the peak corresponding to electrons originating from the photocathode was found to be asymmetrical. The asymmetry can be described as a tail to the peak stretching to greater drift times. This tail has been referred to by Wagner et al (1967). The situation was improved by reverse biassing the cathode-grid region. A likely explanation of the asymmetry is that the drift field is able to act to some significant extent beyond the grid. Further evidence of this is the observation that the electronic cathode pulse width can be less than the time required for an electron to cross from the cathode to the grid, but still there is a significant delayed electron count rate.

A very short duration pulse of electrons was required for this experiment; normally the cathode pulse was approximately equal to the transit time of an electron from the cathode to the grid, for the reason described above. Careful adjustment of this pulse width and reverse bias value

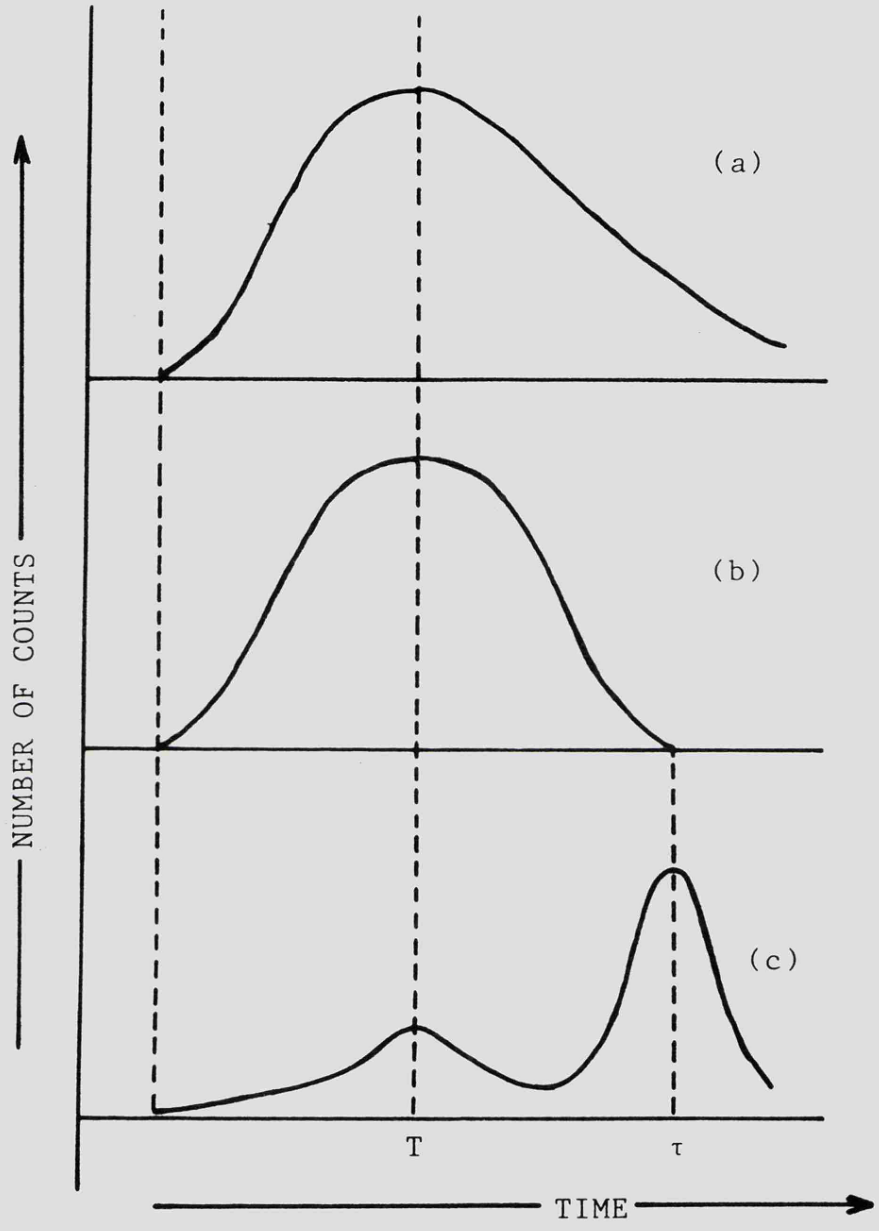

FIG 6·10 Typical time-of-flight spectra obtained under different conditions

(a) no pulse, no reverse bias,

(b) no pulse, reverse bias on,

(c) pulse on, reverse bias on.

produced fairly symmetrical arrival time spectra. However the width was always very large compared with any diffusion contribution.Consequently changes in width for different drift lengths were very small, making the quantification of electron longitudinal diffusion difficult and subject to large errors. This is discussed further in chapter 7.

CHAPTER 7.

EXPERIMENTAL PROCEDURES.

7.1 INTRODUCTION.

Experimental methods of determining lateral and longitudinal diffusion coefficient to mobility ratios and drift velocities of electrons in gases have been reviewed in chapter 2. The actual experimental arrangements used in this work to determine these parameters have been described fully in chapter 5. The procedures followed in each experiment will be discussed here, revealing how the three parameters were determined from measurements made during the experiments.

7.2 LATERAL DIFFUSION EXPERIMENT.

The Townsend method has been reviewed in section 2.1. The ratio of the diffusion coefficient to the drift velocity or the mobility can be obtained from the ratio R, of the current to the central part of the collector to the current collected by the whole collector using the expression

$$R = 1 - \frac{h}{d} \exp(-\lambda(d - h)) \qquad (7.1)$$

where $\lambda = \frac{W}{2D}$ and the dimensions h, d and b are shown in figure 7.1.

This expression can be rearranged as follows,

$$d^2 = h^2 + b^2$$

$$\text{so } R \cong 1 - \frac{h}{d} \exp\left(\frac{-W.b^2}{2D\ 2h} \right) \text{ if } b \ll h$$

$$\cong 1 - \exp\left(\frac{-W.b^2}{2D\ 2h} \right)$$

$$\text{Now } R = \frac{i_c}{i_c + i_o}$$

$$\text{so } \frac{1}{\ln\left(\frac{1}{1 - R} \right)} = \frac{4\ D\ h}{W\ b^2}$$

Drift velocity $W = \mu E$, where μ is the electron mobility and E is the electric field strength,

$$\text{so } \frac{1}{\ln\left(\frac{1}{1 - R} \right)} = \frac{4\ D\ h}{E\ \mu\ b^2} \qquad (7.2)$$

In the present work the ratio R is determined at several drift lengths h for the same gas, E/p and pressure. The ratio D/μ is then found from the relationship between $\frac{1}{\ln\left(\frac{1}{1 - R} \right)}$ and h, this can be plotted and D/μ obtained from the slope of the straight line, knowing E and b^2.

The current ratio R was determined from readings

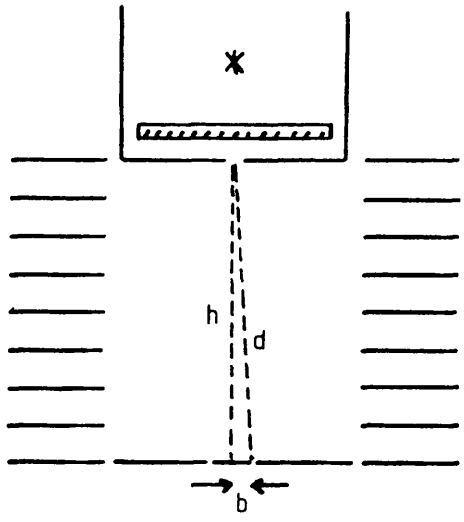

FIG 7·1 Dimensions of the Townsend lateral diffusion apparatus.

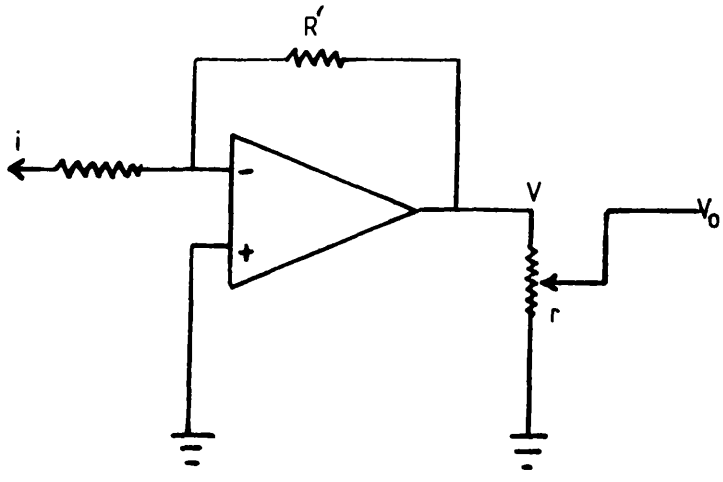

FIG 7·2 The collector amplifier circuit.

on potentiometers in the amplifiers connected to the two parts of the collector, see figure 7.2.

In figure 7.2 r is a fraction of the full potentiometer resistance, read from a vernier scale, this will also be the output V_0 as a fraction of the full output of the operational amplifier V.

For a collected current i,

$$V = -i R'$$

and $$V_0 = -r i R'.$$

Both the amplifiers have the same arrangement. The outputs are connected to the A and B inputs of a phase-sensitive detector which gives an output proportional to the difference between the two inputs.

Let the two potentiometer readings be r_c and r_o for the amplifier on the central part of the collector receiving current i_c and the amplifier on the outer part of the collector receiving current i_o respectively. r_c and r_o are then adjusted until the phase sensitive detector gives a zero output, this indicates that the two amplifiers have equal outputs V_0. Because of random fluctuations in the output this was monitored by a plotter so a judgement that the output was zero was based on many minutes of observation. Then

$$-r_c i_c R' = -r_o i_o R' = V_0$$

$$\text{and so } \frac{1}{1 - R} = \frac{r_c + r_o}{r_c} \qquad (7.3)$$

The term $\dfrac{1}{\ln\left(\dfrac{r_c + r_o}{r_c}\right)}$ is plotted against h and the gradient yields D/μ.

The gradient was found using a least squares best fit program on a PDP-11 computer. This also produced a figure for the error due to scatter of the points about

the best line, this is a measure of the random errors affecting reproducibility.

The axial alignment of the source hole and the collector is an important factor in reducing errors (Crompton and Jory, 1962). If they are not aligned the current ratio falls producing a high value for D/μ at a particular drift length. When diffusion is large in a certain gas, e.g. argon + 10 % methane, or at a long drift length the effect of the misalignment upon R is less. In the present system misalignment is readily observed from the graph of the 1/ln term against h, the line develops a positive intercept on the ordinate instead of passing through the origin, and the slope would indicate a value of D/μ lower than the actual value.

In order to ensure good alignment, which is particularly important in gases producing a small amount of diffusion, the micrometer arrangement for moving the collector was employed (see section 5.5). By observing the current to the central collector only alignment was achieved by moving the collector to maximise this current. Adjustments could be made to within 40 μm, but this precision was never required, as the current exhibited a relatively wide steady maximum value against collector position, typically the maximum extended over 0.5 mm, but varied with gas and drift length.

7.3 TIME-OF-FLIGHT EXPERIMENT.

The experimental arrangement is described in chapter 5, a block diagram of it is given in section 5.8.2 (figure 5.15).

Electrons released from the electron source are timed as they drift to the detector over the drift length. A pulse is produced for each detected electron by a time-to-amplitude converter, the amplitude of this pulse is related to the drift time of the electron. Because of longitudinal diffusion a variation in drift time is produced for a particular drift length.

Electrons were detected at a rate of between 5 and 10 per second, the photocathode was pulsed at 100 Hz, consequently no 'Poisson' statistical distortion of the distribution of arrival times should occur, see section 2.3.

Pulses from the time-to-amplitude converter were collected for periods of 1 to 3 hours by a pulse-height analyser, resulting in a time-of-arrival spectrum made up from up to 100 000 counts displayed as the number of counts in each of 256 channels of time.

The T.A.C. and P.H.A. are calibrated to find the time per channel, having established a sensitivity which allows the whole spectrum to be displayed by the 256 channels available. The calibration was carried out using a generator of start and stop pulses for the T.A.C. with a variable but accurately known delay between them. By using the zero offset facility of the analyser up to 10 reference points could be established, and the average time per channel found for a particular conversion gain and fixed settings of the T.A.C. Typical channel widths used in this work are 6.6 ns and 3.3 ns,

which were used for argon + 10 % methane and argon + 50 % methane respectively.

The photocathode pulse and the UV flash were triggered by a master pulser operating at 100 Hz. In order to place the arrival time spectrum centrally in the display of 256 channels of the P.H.A., and so maximise the time sensitivity of the system, a delay was introduced between the cathode pulse and the start pulse to the T.A.C., this time T_a was measured by a digital counter.

If the peak of the arrival time distribution is at channel c_p, then the arrival time of the peak, for a channel width of t is given by

$$t_m = T_a + c_p t - T_b$$

where T_b is the counter avalanche to T.A.C. stop delay.

then $t_m = T_a + T - T_b$.

t_m is never known in this experiment, only $t_{exp} = T_a + T$.

The drift velocity W is given by

$$W \cong \frac{h}{t_m}(1 - \beta) \text{ where } \beta = D_L/Wh = \frac{D_L/\mu}{V} \ll 1.$$

As t_m is not known the drift velocity is found by computing the best fit to t_{exp} and drift length points, the slope gives the drift velocity and the scatter will yield a figure for the reproducibility. This will be returned to later.

The review of the experiments for the deter-mination of the longitudinal diffusion coefficient, section 2.3 gives the equation

$$D_L = \frac{h^2 (\delta t)^2 (1 - 2\beta)}{4\, t_m^3}$$

where $\delta t = t_1 - t_m$ is the time difference between the peak and 1/e of peak value. This can be rewritten as

$$D_L = \frac{W^2 (\delta t)^2}{4\, t_m} \frac{(1 - 2\beta)}{(1 - \beta)^2} \cong \frac{W^2 (\delta t)^2}{4\, t_m} \quad \text{since } \beta \ll 1.$$

The observed distribution is approximately gaussian and it is convenient to consider the standard deviation of the distribution.

For a gaussian distribution $\delta t = \sigma\sqrt{2}$ where δt is the time difference between 1/e value and peak value. Diffusion is only one contribution to this time difference. As far as the diffusion contribution σ_D is concerned we can write the very approximate relationship

$$\sigma_D^2 = \frac{2 D_L t_m}{W^2} \qquad (7.4)$$

The observed standard deviation σ is the quad--ratic resultant of σ_D and the other instrumental contributions σ_e. That is $\sigma^2 = \sigma_D^2 + \sigma_e^2 = \frac{2 D_L t_m}{W^2} + \sigma_e^2$

For a particular gas and fixed values for E and p, (σ^2, t_{exp}) points can be obtained by varying the drift length h. These points should then fall on a straight line with a slope given by $2D_L/W^2$.

At each E/p and drift length a print-out of the number of counts in each channel of the P.H.A. was obtained. A Commodore PET microcomputer and a simple program was used to calculate the probability of an electron arriving in each channel, a print-out was obtained listing the integrated probability, which ranged from 0 % for a number of channels from channel 1 to 100 % for a number of channels up to channel 256. This information was then plotted on graph paper with a normal distribution scale and a linear scale. These graphs were produced for each drift length at each E/p. They were found to be linear over an appreciable range, at least from a probability of 20 % to 70 %. Using those points which fell on the straight line, the line was drawn and used to find the

variance σ^2 of the distribution, and the peak channel from the 50 % probability level.

It can be shown that the number of channels between 25 % and 75 % probability is equal to 1.349σ for a gaussian distribution. Both $1 \cdot 349\,\sigma$ and the peak channel could be found to within 0.25 channels (about 1.5 ns) from the graphs. σ^2 and t_{exp} were obtained, expressed in units of time.

Several (σ^2, t_{exp}) points were obtained for each E/p value by varying the drift length. Typically 5 or 6 points were used to obtain the best straight line, the slope of which is given by $2D_L/W^2$. Having calculated the drift velocity D_L/μ was calculated.

This method of analysis produced a self-consistent set of results for W and D_L/μ in argon + 10 % methane over an E/p range of 0.1 to 1.0 V/cm.torr and for W in methane. Considerable variation was evident in the D_L/μ data for argon + 50 % methane. A considerable amount of time was spent developing a computer program to fit the arrival time spectra data directly to a gaussian curve (M. Burrage, 1982).

Computer analysis has the advantage of reducing the time required to transfer data from a print-out to the micro-computer, as the Cyber-73 computer was able to accept punched tape delivered by the P.H.A. The time-of-flight spectra of argon + 50 % methane contained a background count level and were not symmetrical. In the final version of the fitting program, the data was compared with a gaussian curve superimposed upon a straight line and a best fit obtained. Without the straight line function all background was ignored and so values of σ obtained were too large. The effect of the asymm-etry was checked by fitting the curve and the line to different parts of the data, so that the distortion on the

long arrival time side of the spectrum was avoided. This distortion was attributed to a partial cut-off of the electron pulse due to chamber field leakage into the cathode-grid region of the electron source. However the asymmetry did not have a great effect upon the results. Figures 7.3, 7.4 and 7.5 show examples of the curves produced to fit the data provided, which is represented by the asterisks.

A great improvement in the consistency of the results was produced, but they are still subject to fairly large errors. The amount of diffusion which the experiment attempts to quantify is very small and inevitably its value cannot be measured with much degree of accuracy. The drift velocity results however are reproducible to within small limits.

In a typical set of data for argon + 50 % methane, E/p = 1.0 V/cm.torr, at h = 6 cm; σ^2= 0.0033 μs^2 and at h = 15 cm σ^2 = 0.0053 μs^2, or for a 4 ns channel width σ increases from 17.3 to 22.0 channels over the full range of drift lengths used. So the maximum variation of σ which can be expected due to diffusion is about 25 %, the other contributions to the width of the arrival-time spectrum are very significant in comparison, these are discussed in section 5.8.2.

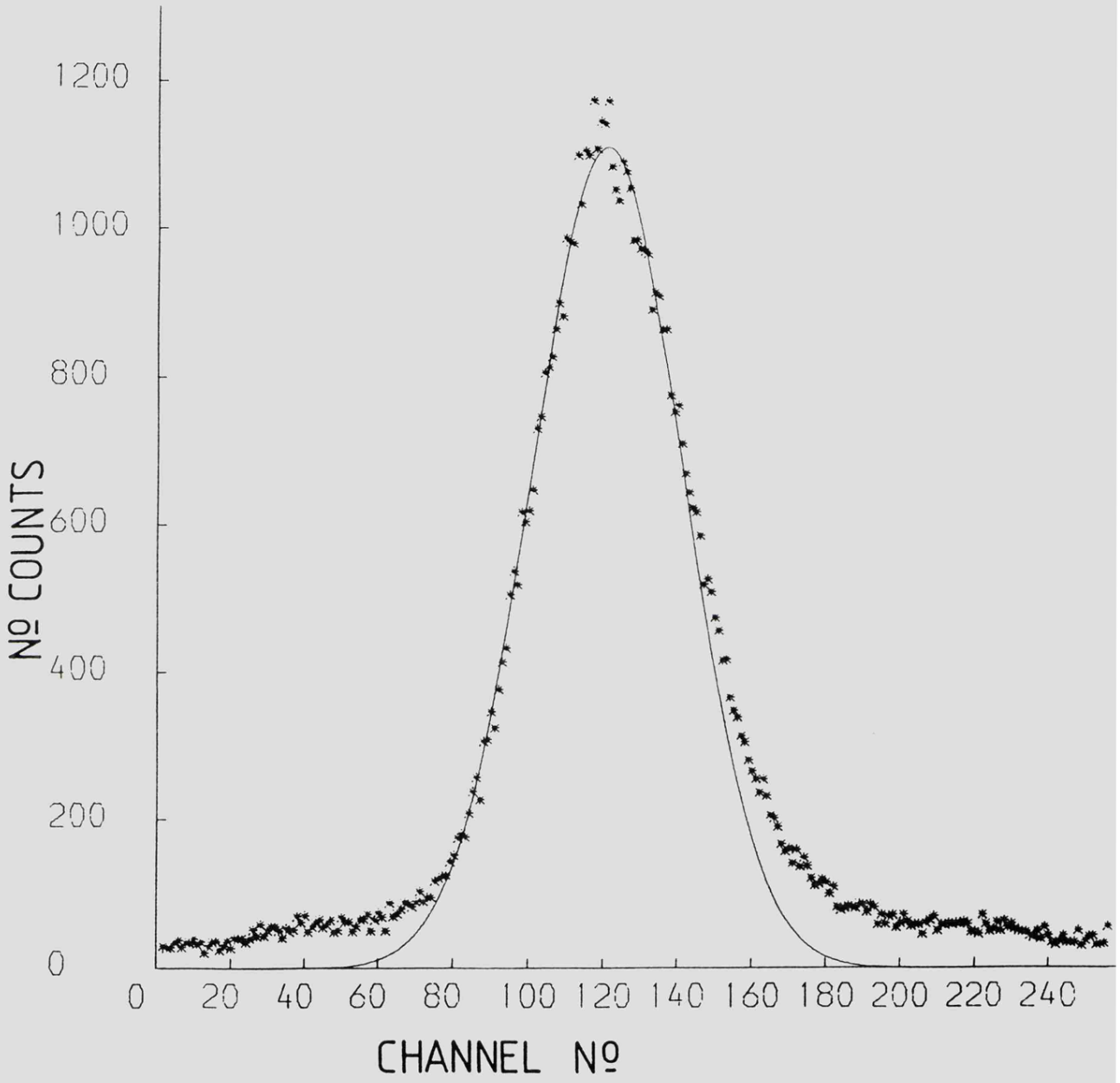

FIG 7·3 Result of computer curve fitting to an arrival time spectrum obtained in argon/50% methane, E/p = 1.2 V/cm.torr, h = 15 cm.

Fit to gaussian only.

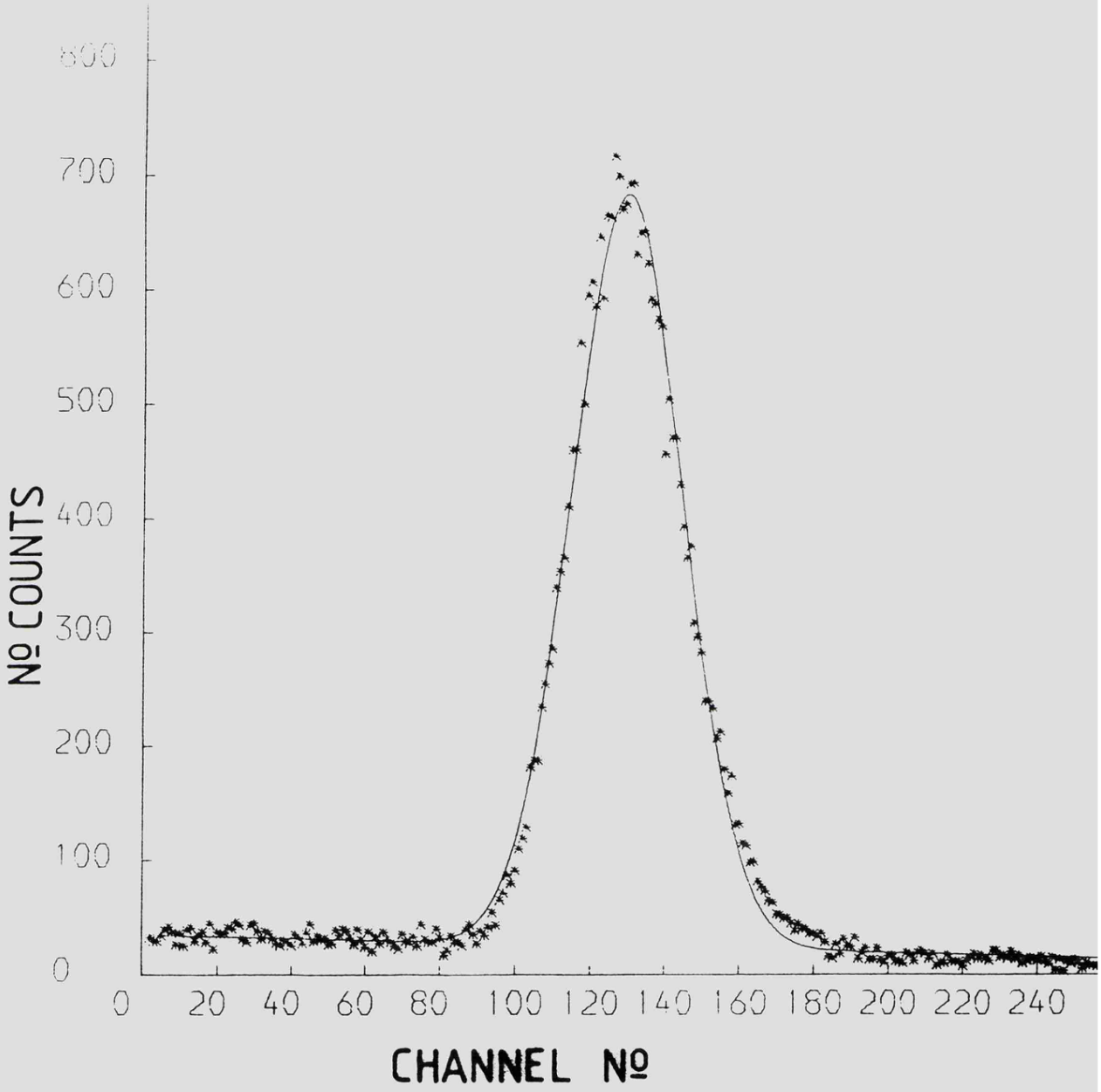

FIG 7·4 Result of computer curve fitting to an arrival time spectrum obtained in argon/50 % methane, E/p = 0.6 V/cm.torr, h = 5 cm.
Fit to **gaussian + straight line.**

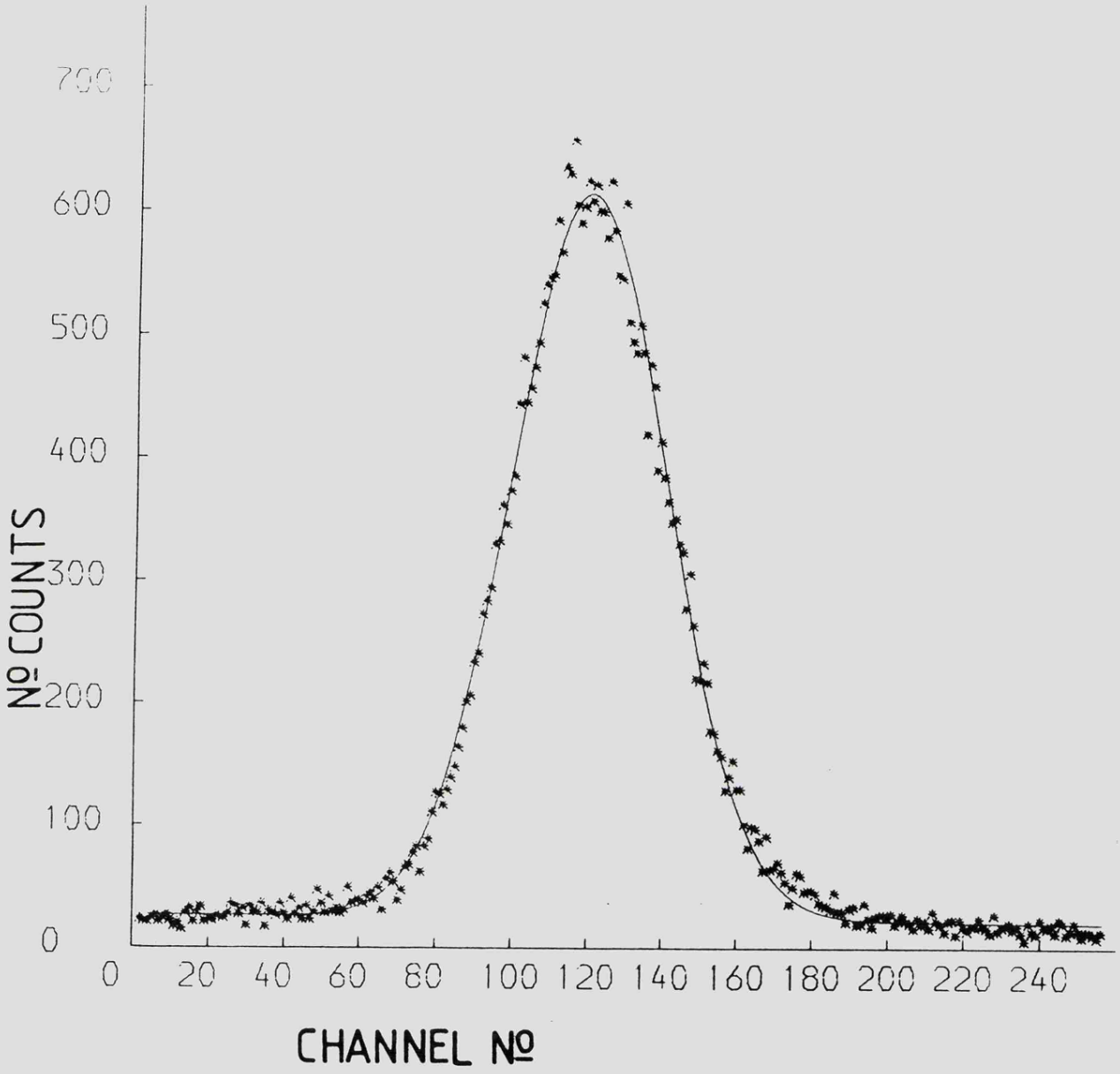

FIG 7·5 Result of computer curve fitting to an arrival time spectrum obtained in argon/50% methane, E/p = 0.4 V/cm.torr, h = 12 cm.
Fit to gaussian + straight line.

CHAPTER 8.

RESULTS.

The two experimental arrangements described in chapter 5 were used to obtain measurements of D/μ in a large selection of gases and measurements of D_L/μ and W in a limited number of gases. The experimental results are compared here with predictions calculated using the Boltzmann equation and by Monte-Carlo simulation, see chapters 3 and 4.

8.1 LATERAL DIFFUSION COEFFICIENT TO MOBILITY RATIOS.

The experimental results presented in this section were obtained with the experimental arrangement described in chapter 5 and the procedure discussed in section 7.2.

Argon/methane and argon/carbon dioxide mixtures in a range of proportions were examined, and also a few other common counter gases. In some cases comparison with results obtained by other workers has been possible, but for most gases no other work was published for comparison.

8.1.1 100 % Methane.

Pure methane has been examined in the work of Duncan and Walker (1972), the theoretical predictions given here use collision cross-sections obtained by Walker and her co-workers.

The gas used in this work was C.P. grade methane supplied by B.O.C. Special Gases. The typical analysis given by B.O.C. is 99.2 % methane with the major impurities, 0.7 %

being argon and nitrogen.

The experiment was run several times to check for reproducibility and also to compare the results for different cylinders of C.P. grade methane. Overall the results obtained with different cylinders agreed to within a few percent.

Figure 8.1 compares the experimental results obtained in this work with those of Duncan and Walker. Above E/p = 1.0 V/cm/torr the present results are higher than those of Duncan and Walker. Although they are very close if the errors in Duncan and Walker's results (+/-5%) and the present results are taken into account, but a definite tendency does exist. Duncan and Walker's results are in excellent agreement with Boltzmann predictions. A possible explanation is the presence of impurities in the gas used in this work as Duncan and Walker used elaborate purification techniques.

A study was made of the variation of D/μ in methane with a range of levels of nitrogen contamination (0 - 5 %) at E/p = 2.0 V/cm/torr. This study was made without a gas flow through the chamber. This revealed that D/μ falls with nitrogen contamination by 1.1 % per % contamination, this effect was confirmed by Boltzmann calculations.

Figure 8.2 compares the present experimental results with Boltzmann calculations and Monte-Carlo simulations.

8.1.2 Argon / Methane Mixtures.

Figures 8.3, 8.4 and 8.5 show the experimental values of D/μ for argon + 75 % methane, argon + 50 % methane and argon + 10 % methane as functions of E/p, compared with both Boltzmann and Monte-Carlo predictions.

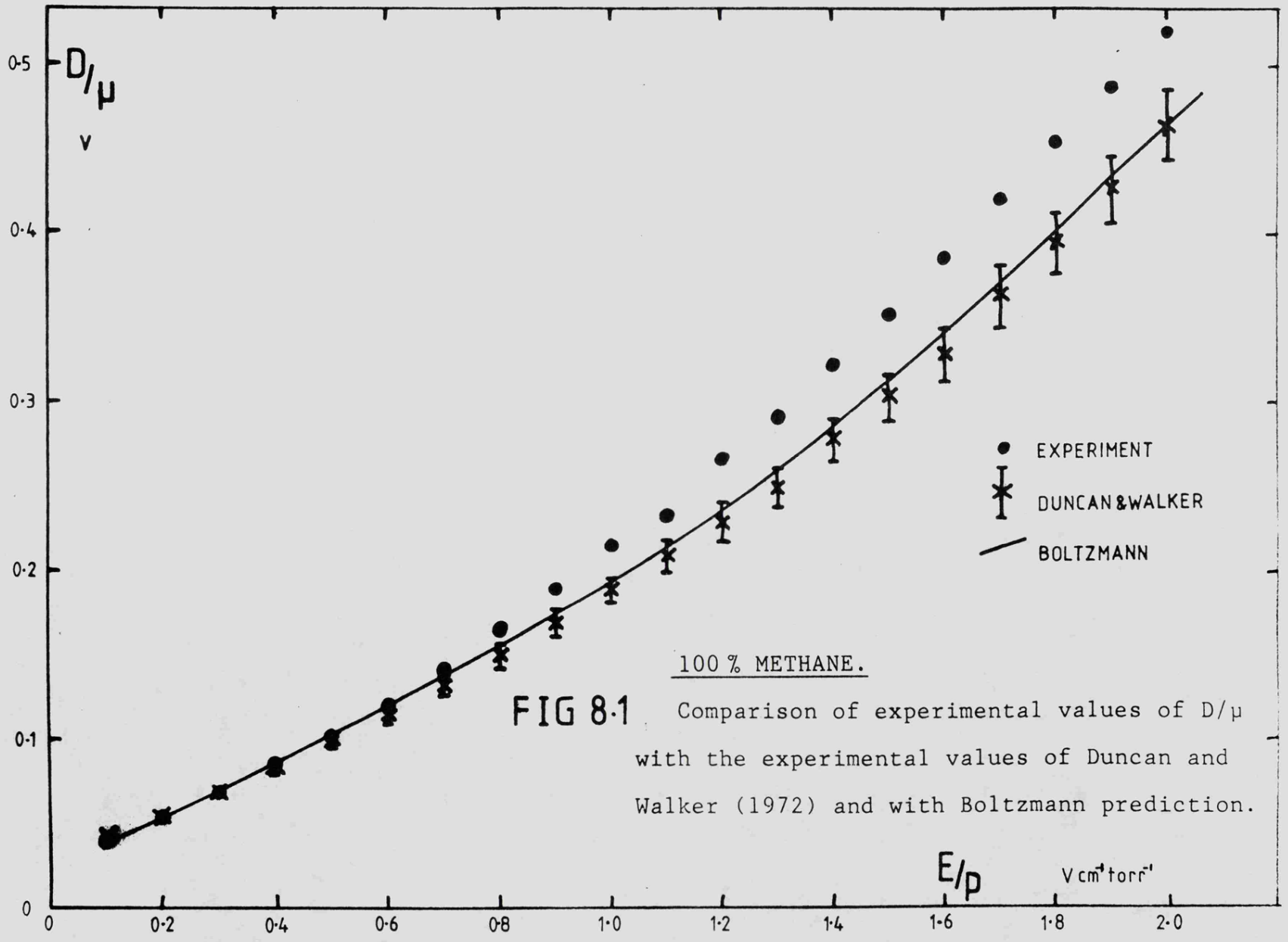

100 % METHANE.

FIG 8·1 Comparison of experimental values of D/μ with the experimental values of Duncan and Walker (1972) and with Boltzmann prediction.

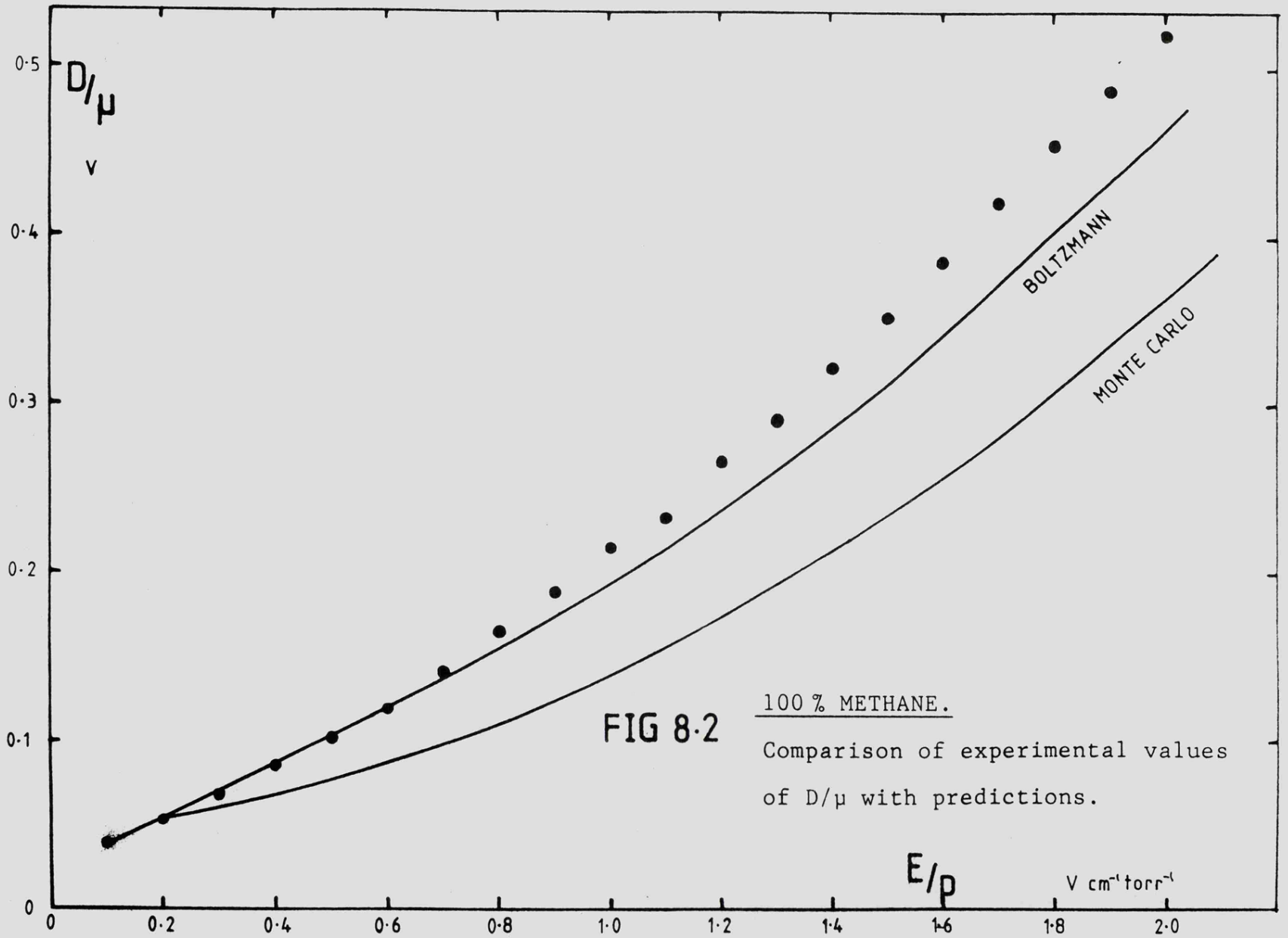

FIG 8·2

100 % METHANE.

Comparison of experimental values of D/μ with predictions.

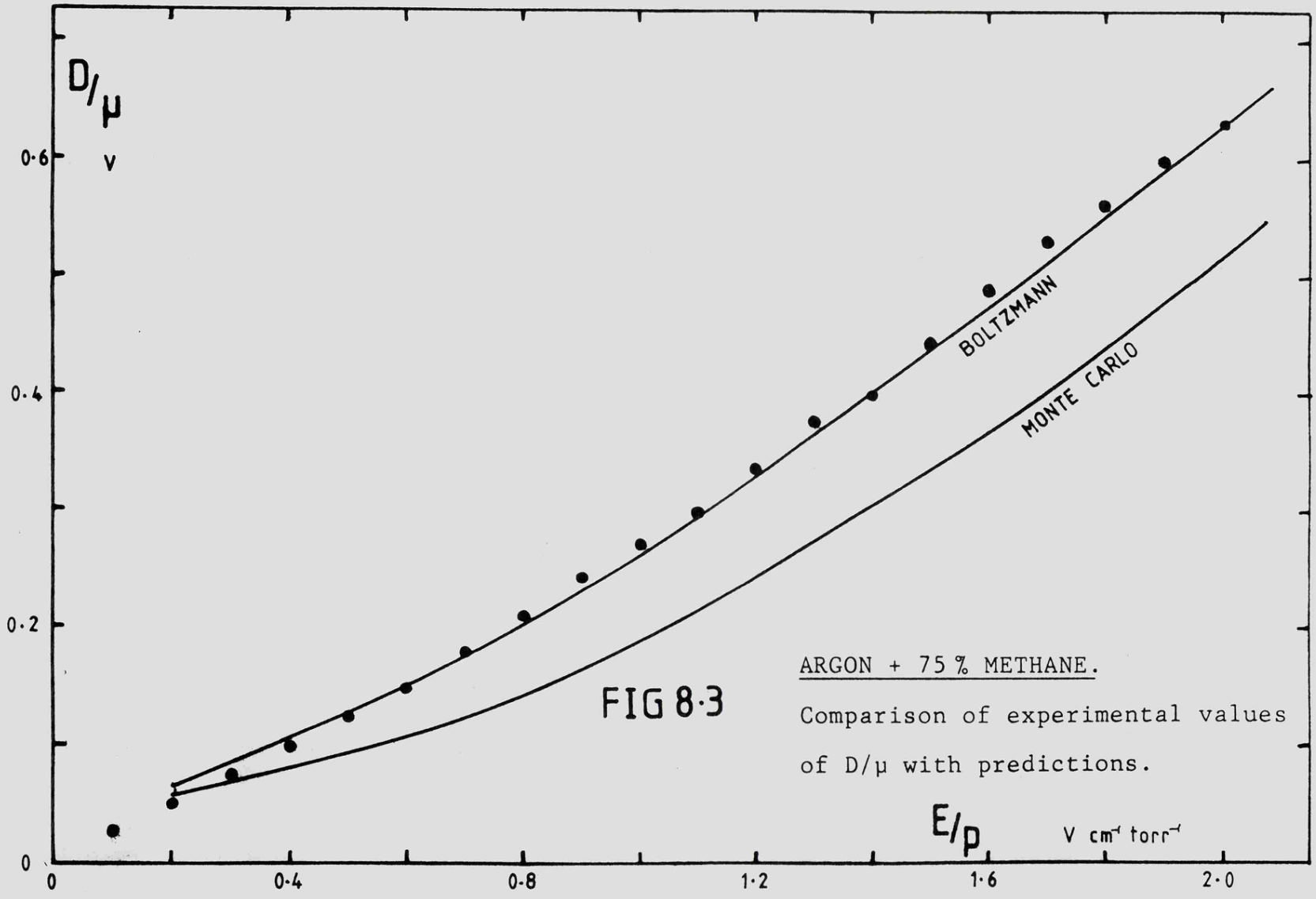

FIG 8·3

ARGON + 75 % METHANE.

Comparison of experimental values of D/μ with predictions.

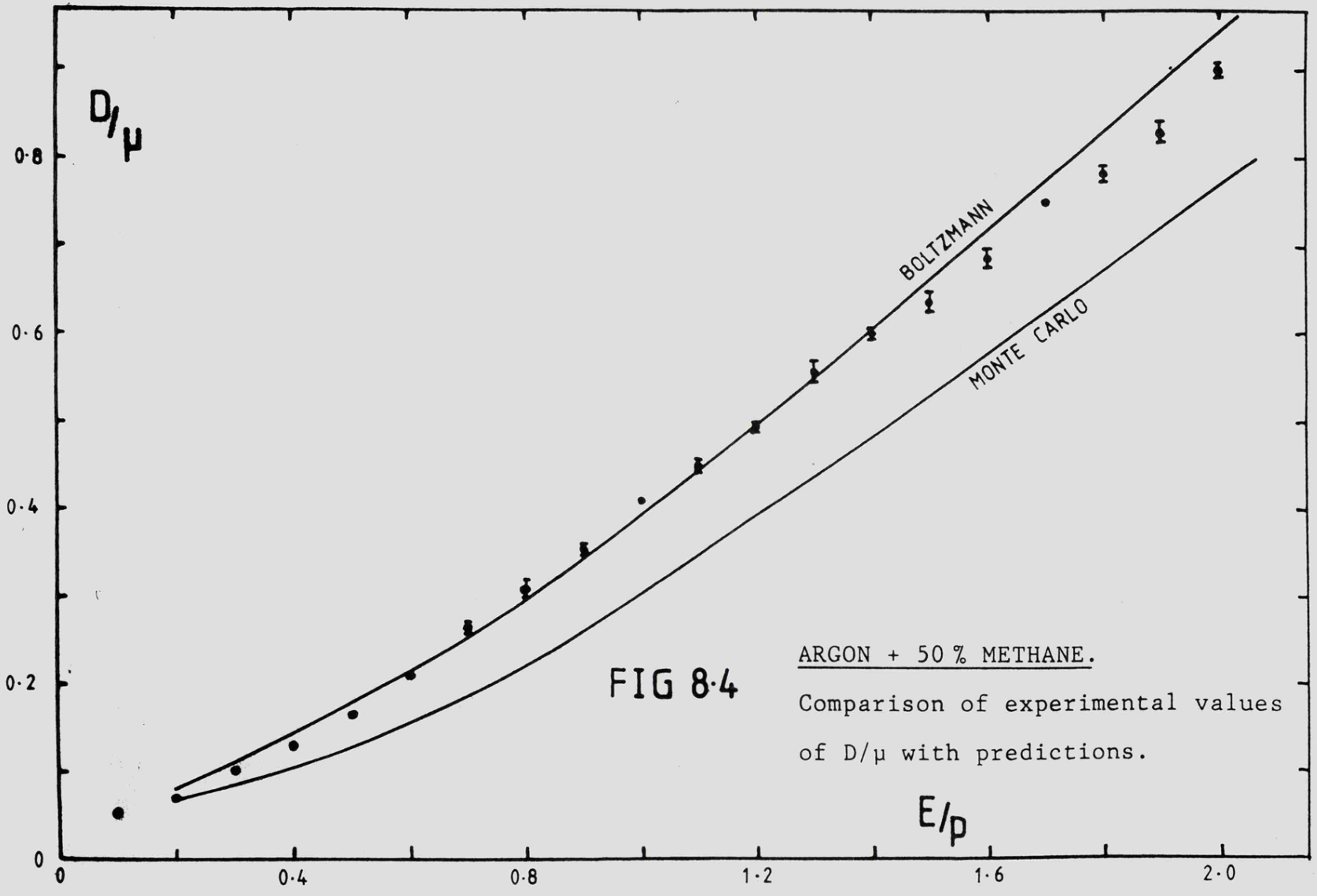

FIG 8·4

ARGON + 50 % METHANE.

Comparison of experimental values of D/μ with predictions.

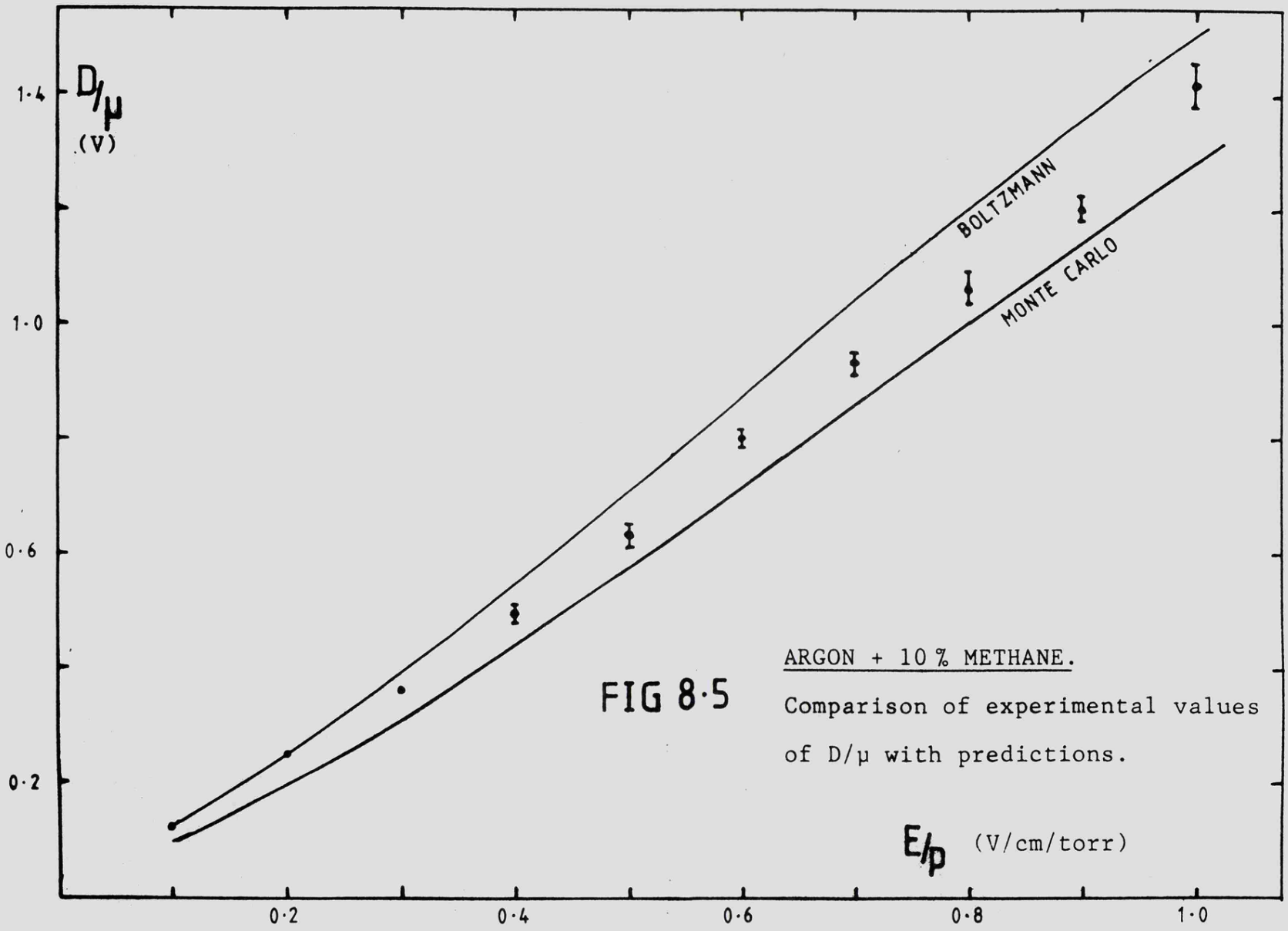

FIG 8·5

ARGON + 10 % METHANE.

Comparison of experimental values of D/μ with predictions.

The experimental values show good agreement with Boltzmann predictions for argon + 75 % methane and argon + 50 % methane. For all three mixtures and 100 % methane the Monte-Carlo values are lower than the Boltzmann values, as the proportion of methane falls the experimental points fall relative to the predictions, in argon + 10 % methane there is closer agreement with the Monte-Carlo prediction. Unfortunately no other experimental values are available for these mixtures for comparison.

Figure 8.6 shows D/μ as a function of the proportion of methane in an argon/methane mixture for a range of E/p values. This figure was compiled from the experimentally determined values of D/μ for the mixtures discussed here and 100 % methane from section 8.1.1.

All three mixtures were C.P. grade and supplied by B.O.C. Special Gases. The argon in the mixtures is Zero grade with a specification of 99.998 % argon, C.P. grade methane is referred to in section 8.1.1. The gas components are mixed volumetrically by B.O.C. with the following tolerance specifications for two different mixtures; 10 % ± 0.7 % and 50 % ± 2.75 %, typically it is ± 5 % of the component.

Reproducibility between cylinders was examined for argon + 10 % methane. It was found to be very good, better than ± 5 %.

8.1.3 100 % Carbon Dioxide.

Figure 8.7 compares experimental values of D/μ obtained in this work with those of Warren and Parker (1962) and with Boltzmann and Monte-Carlo predictions. The value of D/μ at low E/p in carbon dioxide is very small, close to the

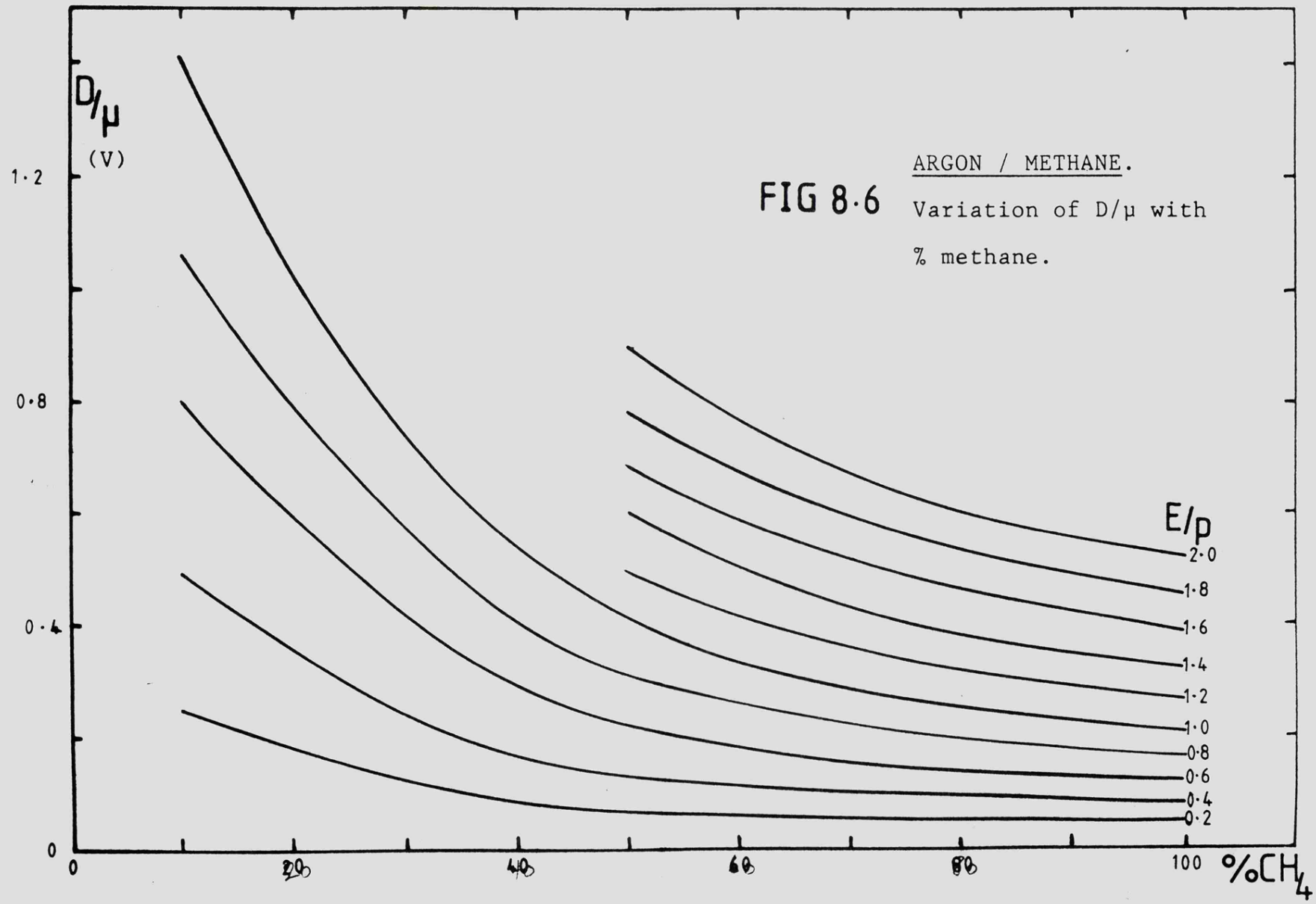

FIG 8·6 ARGON / METHANE.
Variation of D/μ with % methane.

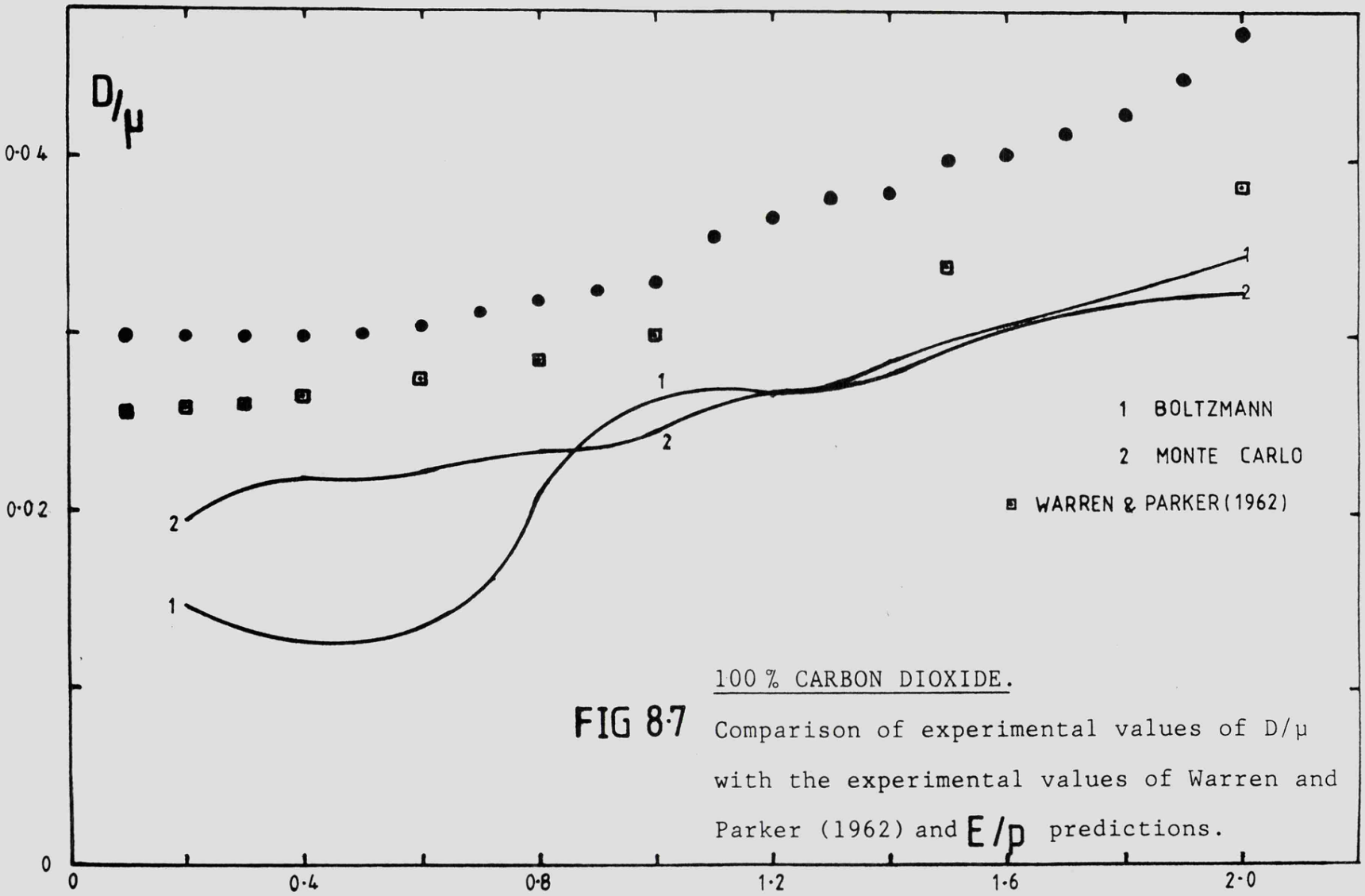

FIG 8·7 100 % CARBON DIOXIDE.

Comparison of experimental values of D/μ with the experimental values of Warren and Parker (1962) and E/p predictions.

thermal value, 0.026 V. The results of Warren and Parker show this. The experimental values obtained in this work are presumably effected by impurities in the gas as they show slightly higher values. The theoretical predictions were made assuming zero molecular velocity, i.e. at a temperature of 0 K, and so agreement cannot be expected at low E/p values. C.P. grade carbon dioxide, which is also in the mixtures below is 99.995% pure

8.1.4 Argon / Carbon Dioxide Mixtures.

Figures 8.8, 8.9 and 8.10 show the experimental values of D/μ for argon + 50 % carbon dioxide, argon + 25 % carbon dioxide and argon + 10 % carbon dioxide as functions of E/p, these are compared with predictions. Argon + 50 % carbon dioxide shows the best agreement between prediction and experiment. In each case the predictions were obtained for a temperature of 0 K, whereas the experiments were carried out at approximately 300 K.

Figure 8.11 shows the variation of D/μ with the proportion of carbon dioxide in the mixture.

8.1.5 Other counter gases.

Several other gases were examined using the same arrangement, however the results were not obtained with as much thoroughness as those above because of limited availability of the gases, the complications of in-laboratory mixing and certain other problems, they are presented here for completeness.

(i) Argon + 5 % Carbon Dioxide + 3 % Acetylene.

This is a C.P. grade gas mixture supplied by

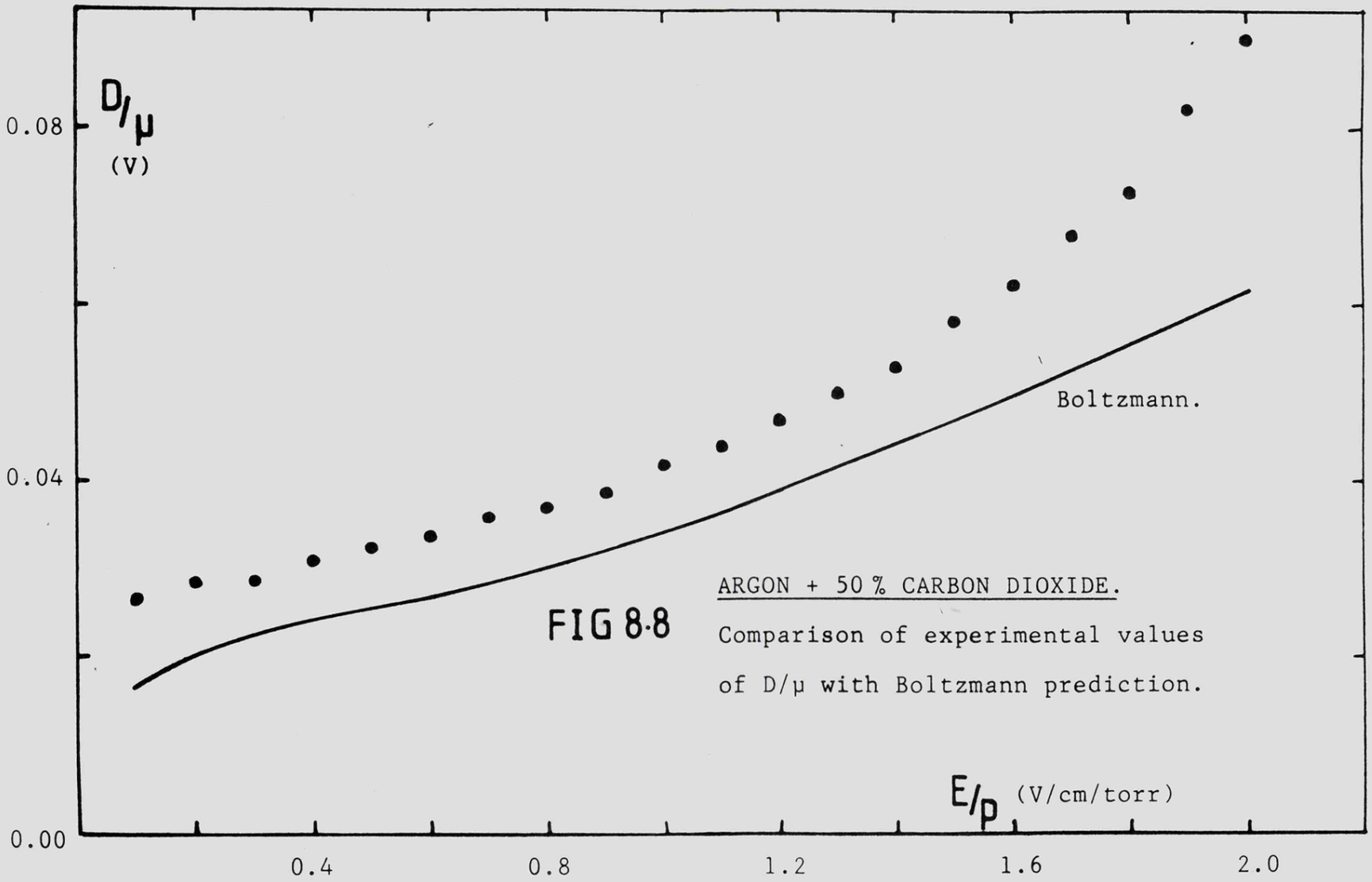

FIG 8·8

ARGON + 50 % CARBON DIOXIDE.

Comparison of experimental values of D/μ with Boltzmann prediction.

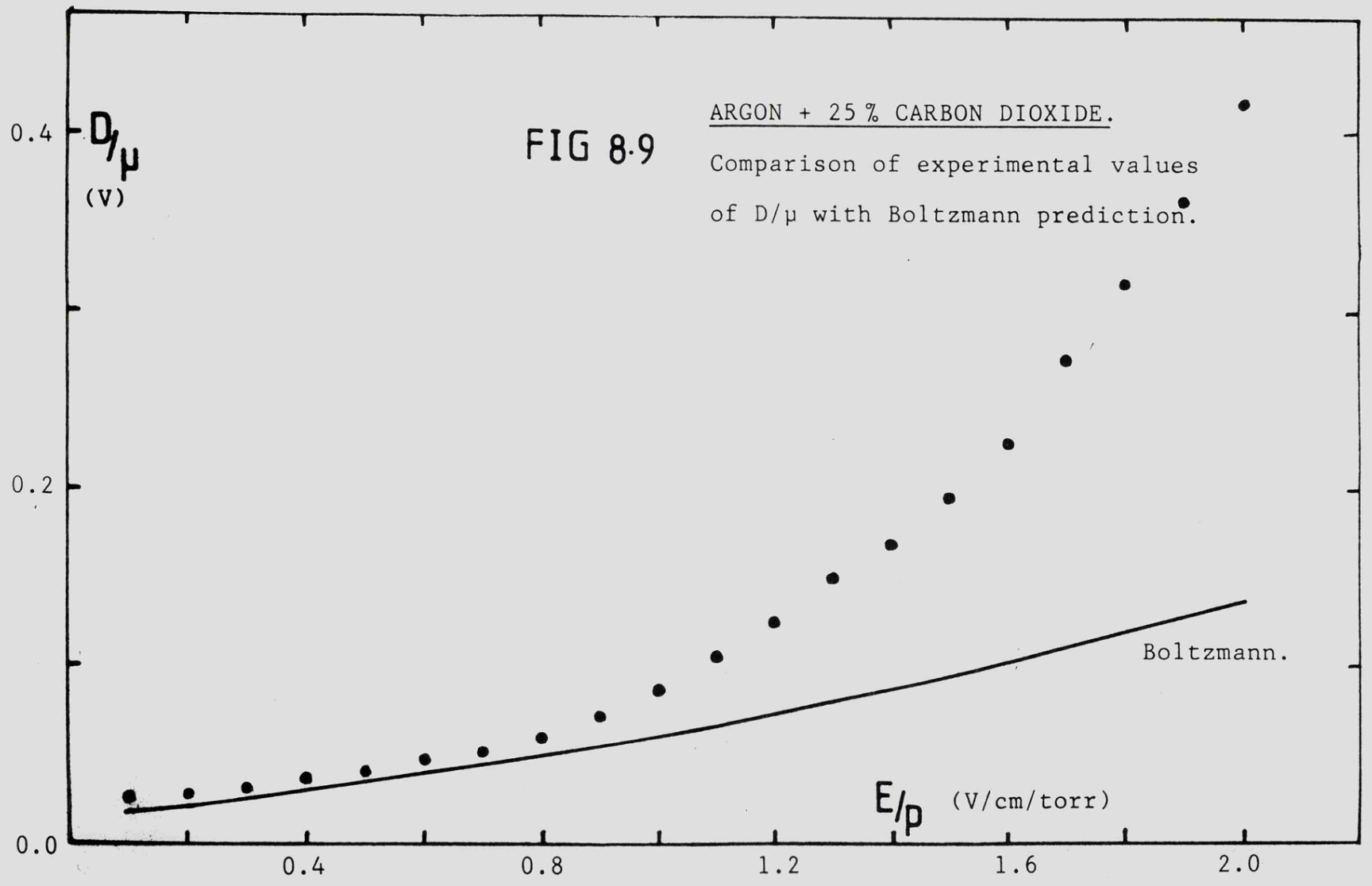

FIG 8.9

ARGON + 25 % CARBON DIOXIDE.

Comparison of experimental values of D/μ with Boltzmann prediction.

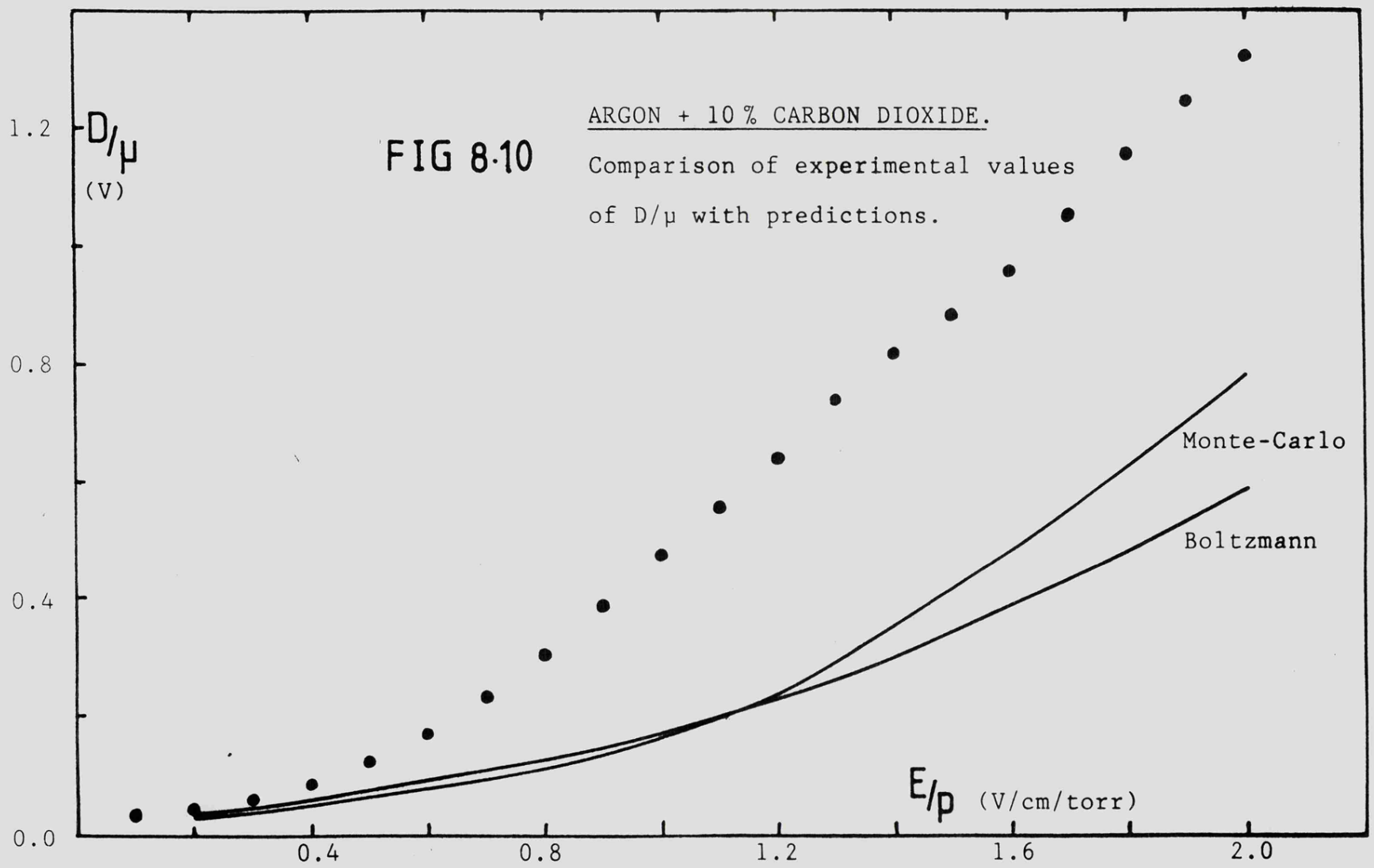
FIG 8·10
ARGON + 10 % CARBON DIOXIDE.
Comparison of experimental values of D/μ with predictions.
D/μ (V)
1.2
0.8
0.4
0.0
0.4
0.8
1.2
1.6
2.0
E/p (V/cm/torr)
Monte-Carlo
Boltzmann

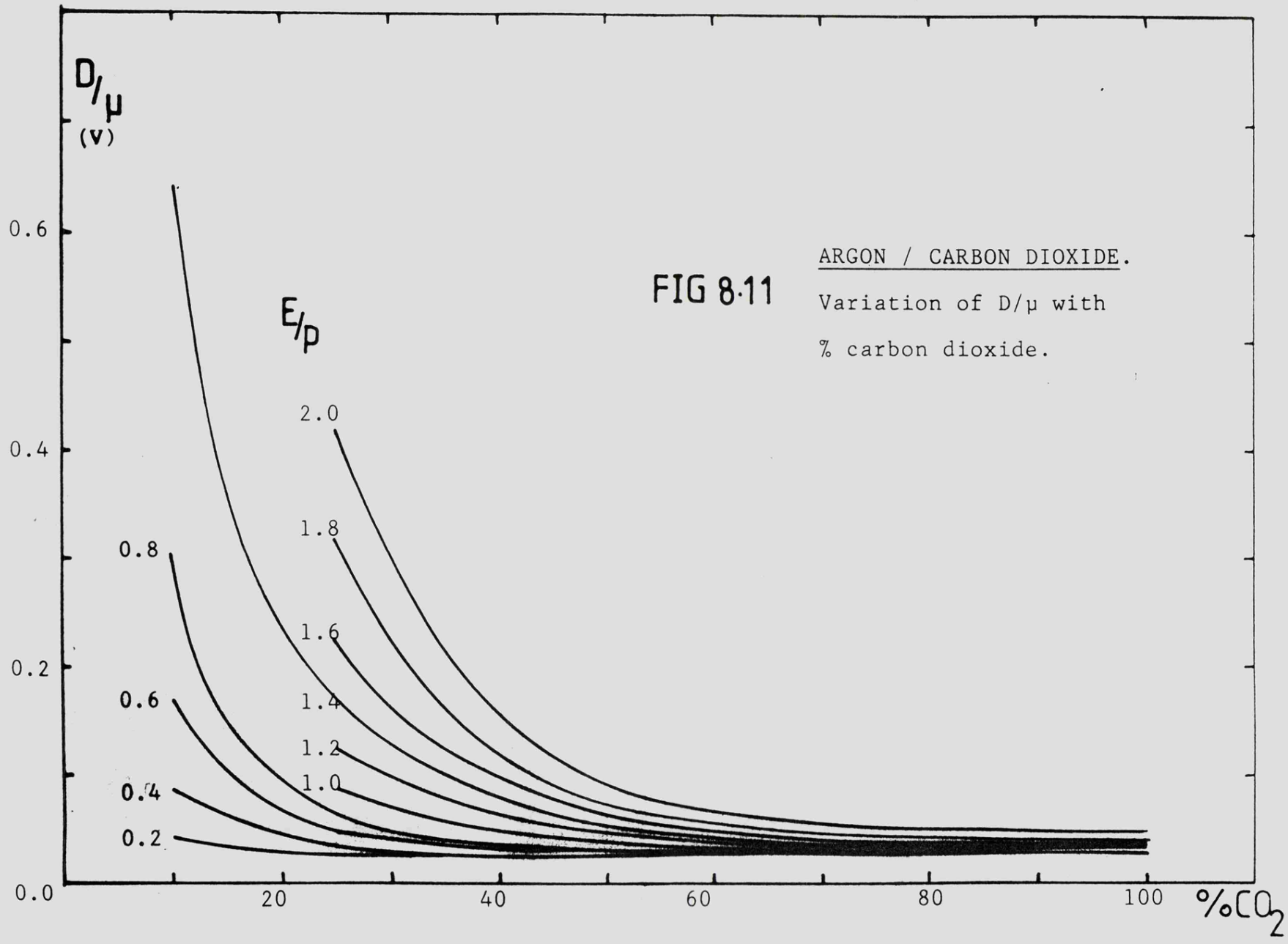

FIG 8·11

ARGON / CARBON DIOXIDE.

Variation of D/μ with % carbon dioxide.

B.O.C. D/μ as a function of E/p is presented in figure 8.12.

(ii) Argon + 25 % Isobutane.

This gas mixture has been used quite extensively by workers at C.E.R.N.,(Palladino and Sadoulet, 1975; Charpak et al, 1973), in a range of proportions as well as this particular one.

This mixture proved to be a problem for the pumping arrangement, also after completing part of the work on the gas under increasing difficulties it was found that the gas had permanently damaged the light guide, which then had to be replaced. It was not known initially that the light guide could by damaged so easily by certain organic vapours.

Figure 8.13 illustrates the results obtained while the apparatus was functioning.

(iii) Argon + 10.7 % Nitrogen.

The drift velocity of electrons in this mixture was examined by Al-Dargazelli et al (1980), but D/μ has not been measured previously. The original intention was to investigate this particular mixture, and to produce a set of data showing the variation of D/μ with the proportion of nitrogen in the mixture, to complement the similar layout of the work of Al-Dargazelli et al on drift velocity.

The mixture was produced as a chamber fill from B.O.C. Zero grade argon (99.998 % argon) and C.P. grade nitrogen (99.95 % nitrogen).

D/μ values could not be produced successfully with any accuracy. D/μ apparently increased with drift length. Attempts were made to identify the process causing this effect. A discussion of this work is given in section 6.2.1.

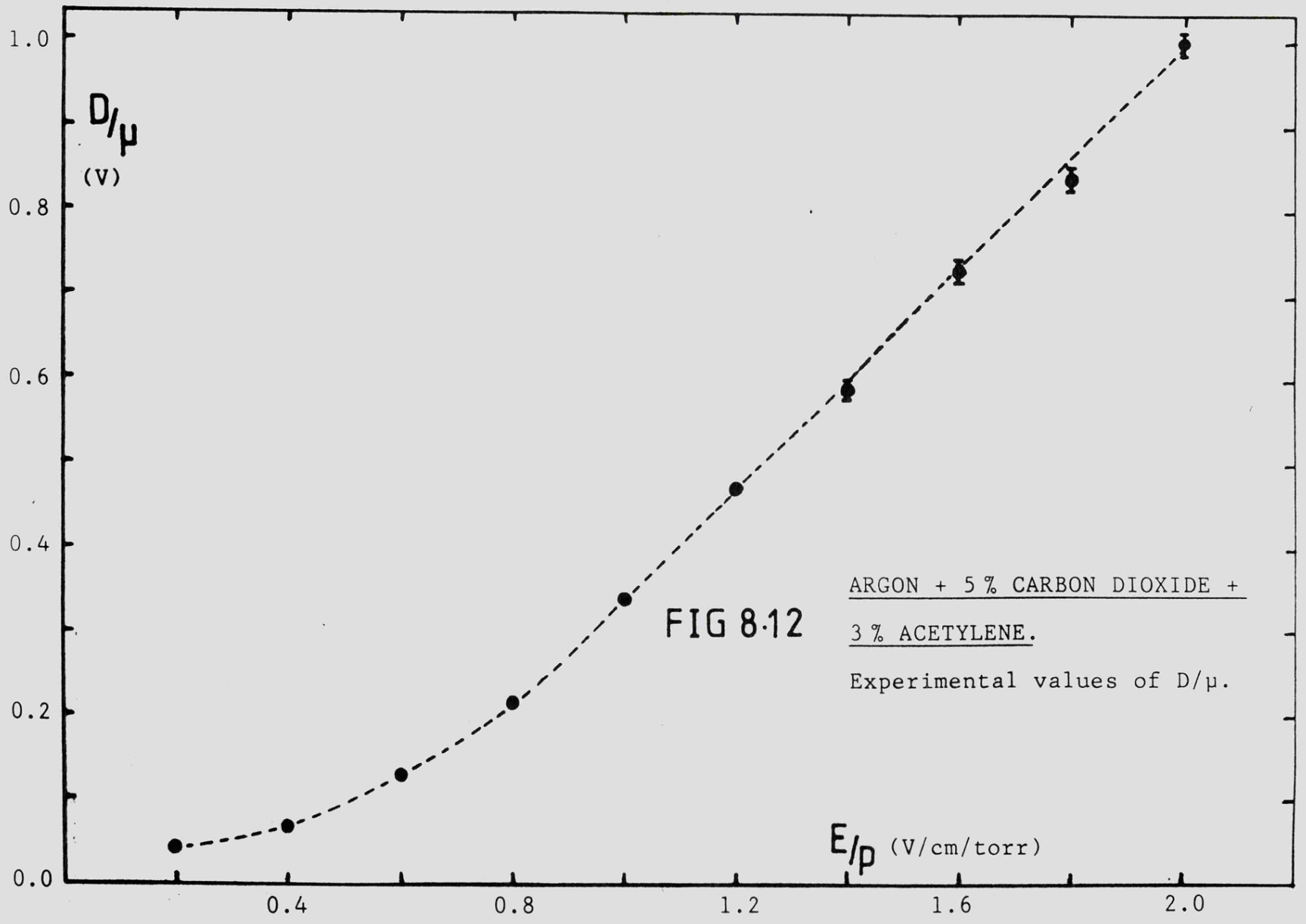

FIG 8·12

ARGON + 5 % CARBON DIOXIDE + 3 % ACETYLENE.

Experimental values of D/μ.

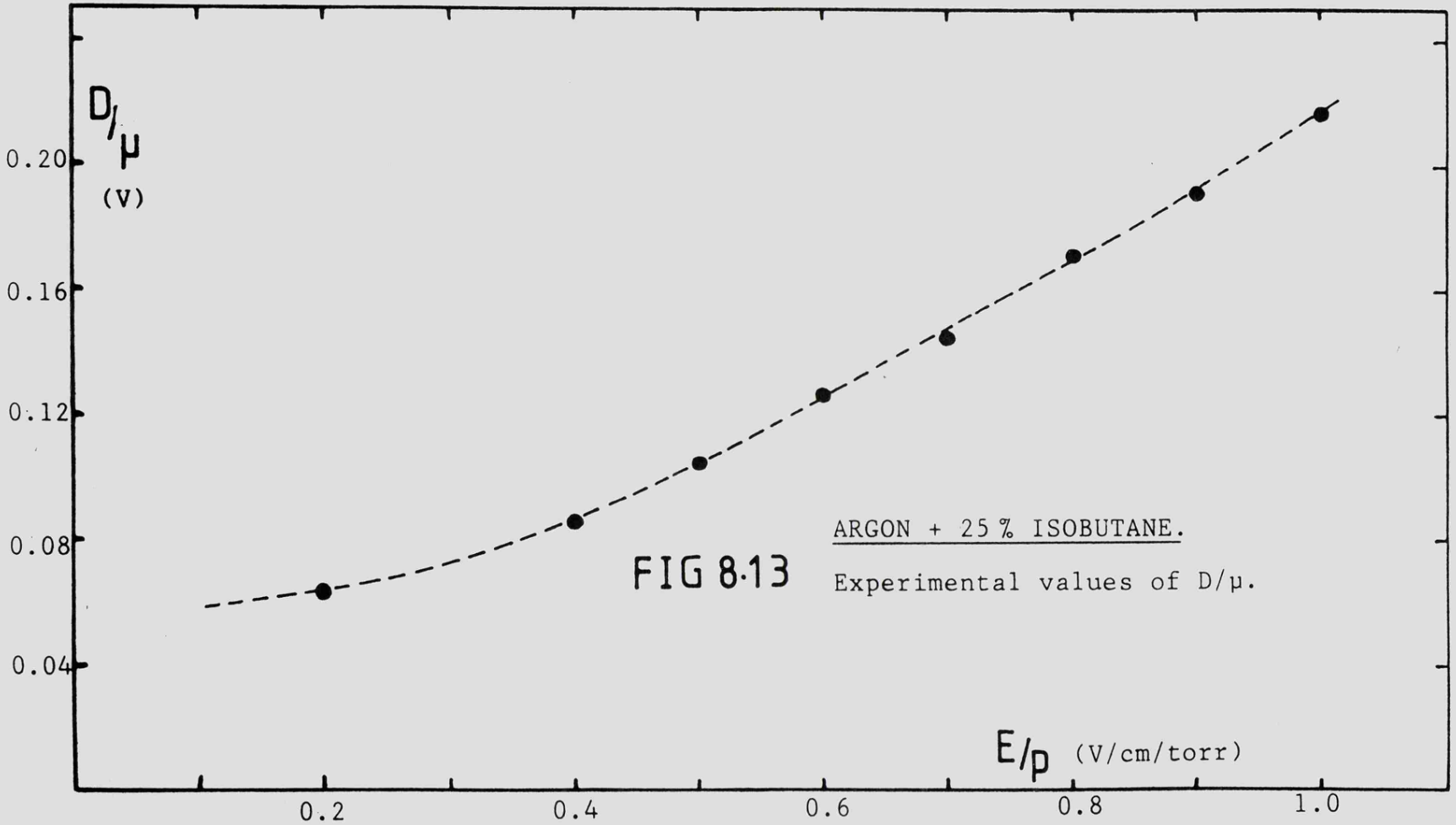

FIG 8.13 ARGON + 25 % ISOBUTANE.

Experimental values of D/μ.

However D/μ seemed to be very large, of the order of 1.0 V over the E/p range 0.4 - 1.0 V/cm/torr, rising rapidly between E/p = 0 and 0.4.

(iv) Neon + 10 % Methane.

Figure 8.14 shows the experimental values of D/μ compared with the Boltzmann prediction, they are in excellent agreement. These results are also in agreement with the experimental values of El-Hakeem (1978), but greater accuracy has been achieved. The gas mixture was B.O.C. C.P. grade (C.P. grade neon is 99.995 % pure).

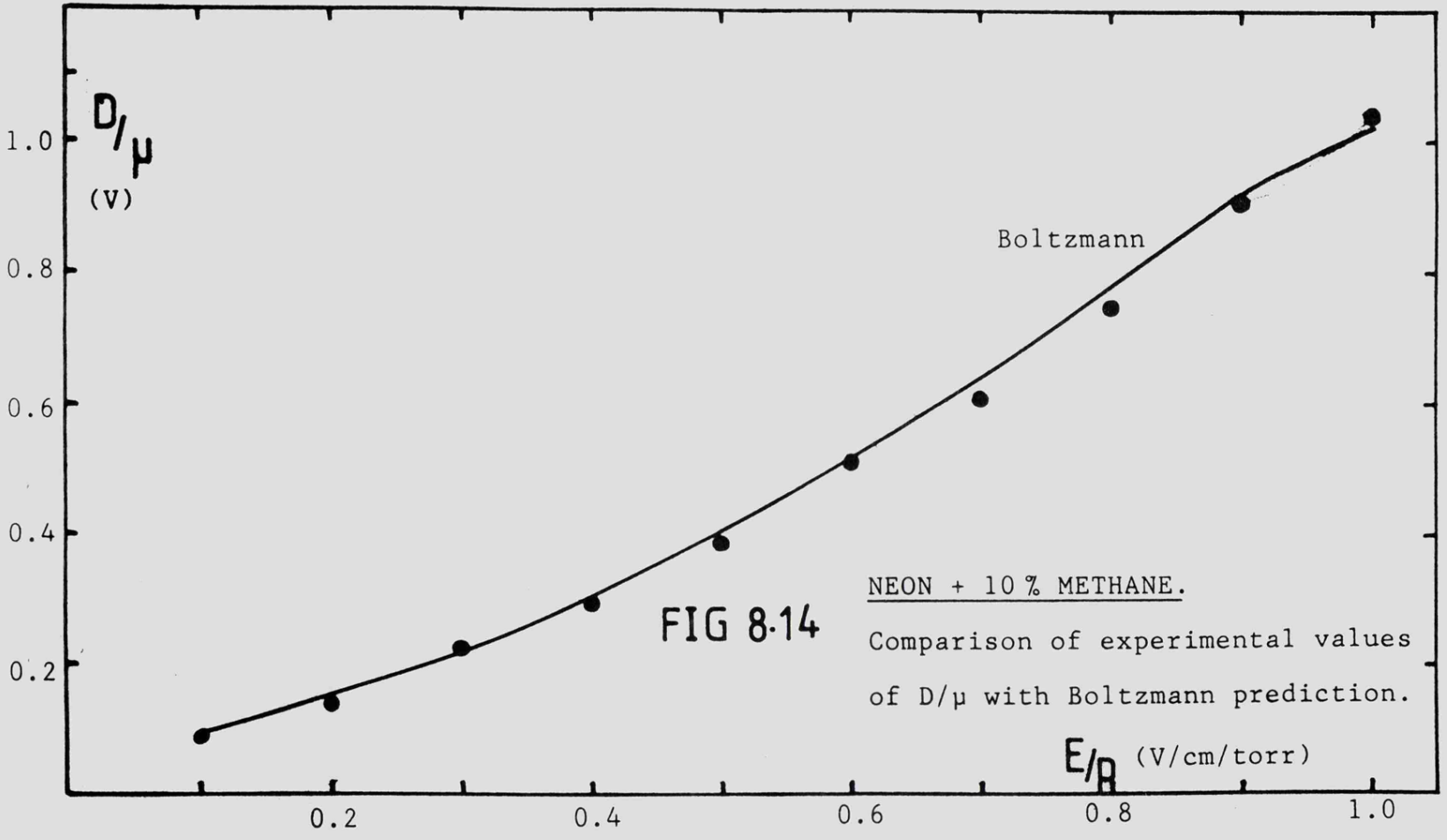

FIG 8.14

NEON + 10 % METHANE.

Comparison of experimental values of D/μ with Boltzmann prediction.

8.2 DRIFT VELOCITY.

The experimental arrangement used to find the electron drift velocity in the gases below is discussed in section 5.8.2 and the experimental procedure in 7.3.

The gases investigated were 100 % methane, argon + 50 % methane and argon + 10 % methane. Figure 8.15 illustrates the experimental values of W in methane as a function of E/p and compared with Boltzmann and Monte-Carlo predictions. There is excellent agreement between the experimental values and the Boltzmann prediction, the Monte-Carlo prediction agrees to within 10 %. The experimental results of Cottrell and Walker (1965) also agree fairly closely with the present results.

The results for argon + 50 % methane, figure 8.16 also show excellent agreement. In argon + 10 % methane the agreement between the Boltzmann and Monte-Carlo predict--ions is improved, but at low E/p values the experimental results are not in agreement, figure 8.17. The values obtained by El-Hakeem (1978) showed the same trend, for comparison some experimental values obtained by English and Hanna (1953) are also shown, these are in good agreement with the predicted values.

The drift velocities determined in this work were found with very small errors and good reproducibility, on average the error is around 2 %.

Although there were no problems finding drift velocities with good precision, these were found simultaneously with D_L/μ, see section 8.3, this part of the experiment required a long running time and so limited the range of gases studied with regard to drift velocity as well.

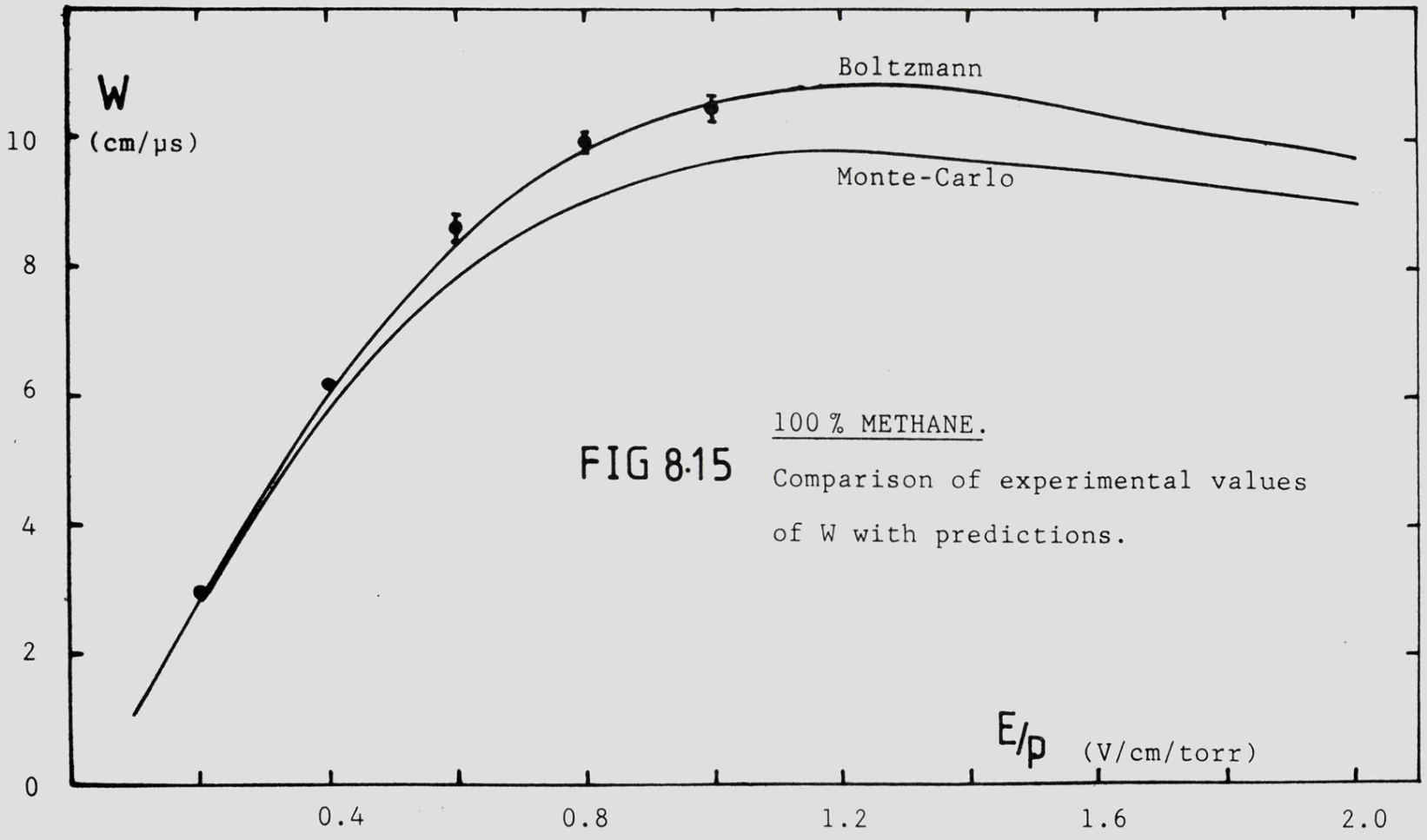

FIG 8.15

100 % METHANE.

Comparison of experimental values of W with predictions.

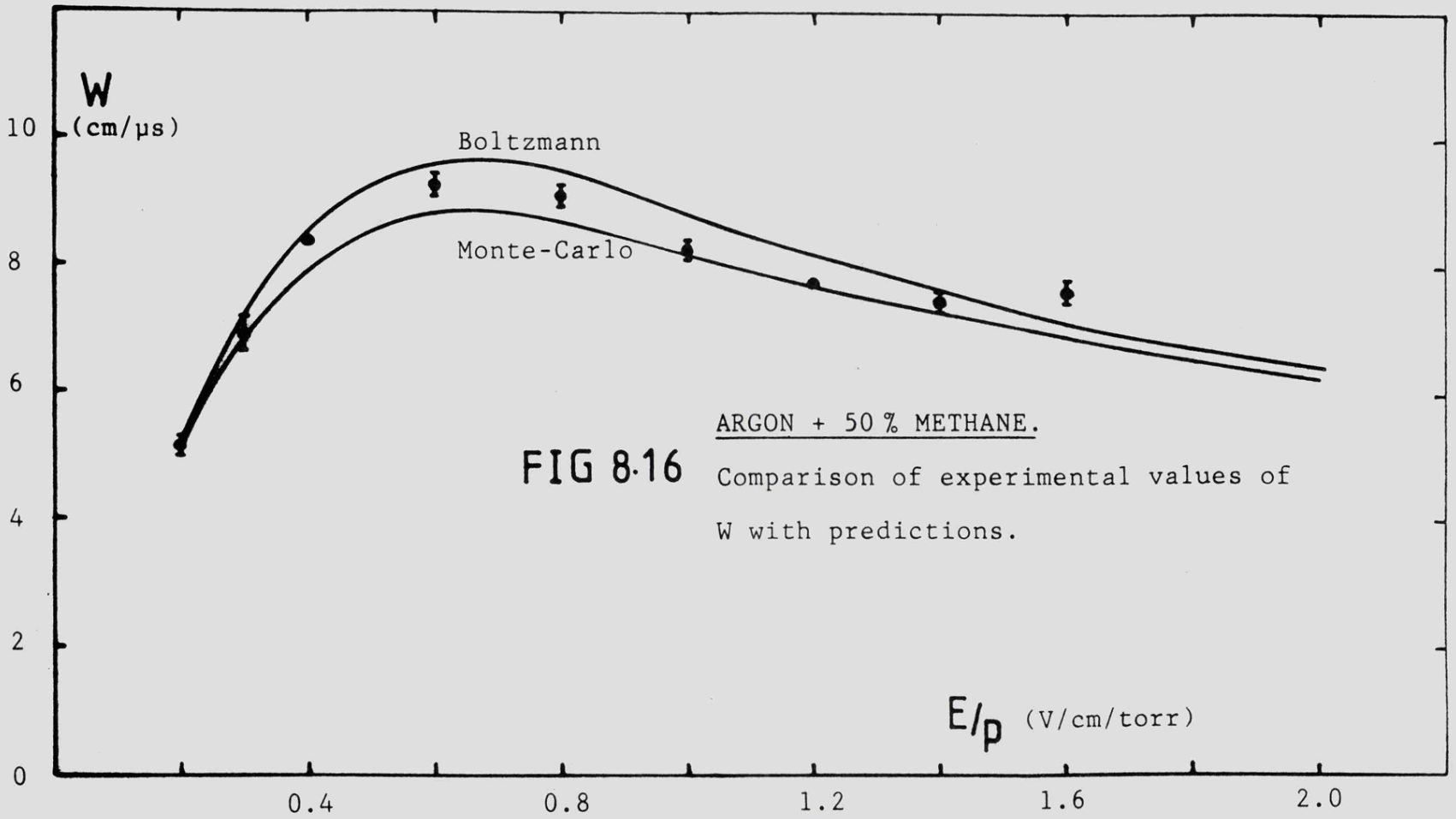

FIG 8.16 ARGON + 50 % METHANE.

Comparison of experimental values of W with predictions.

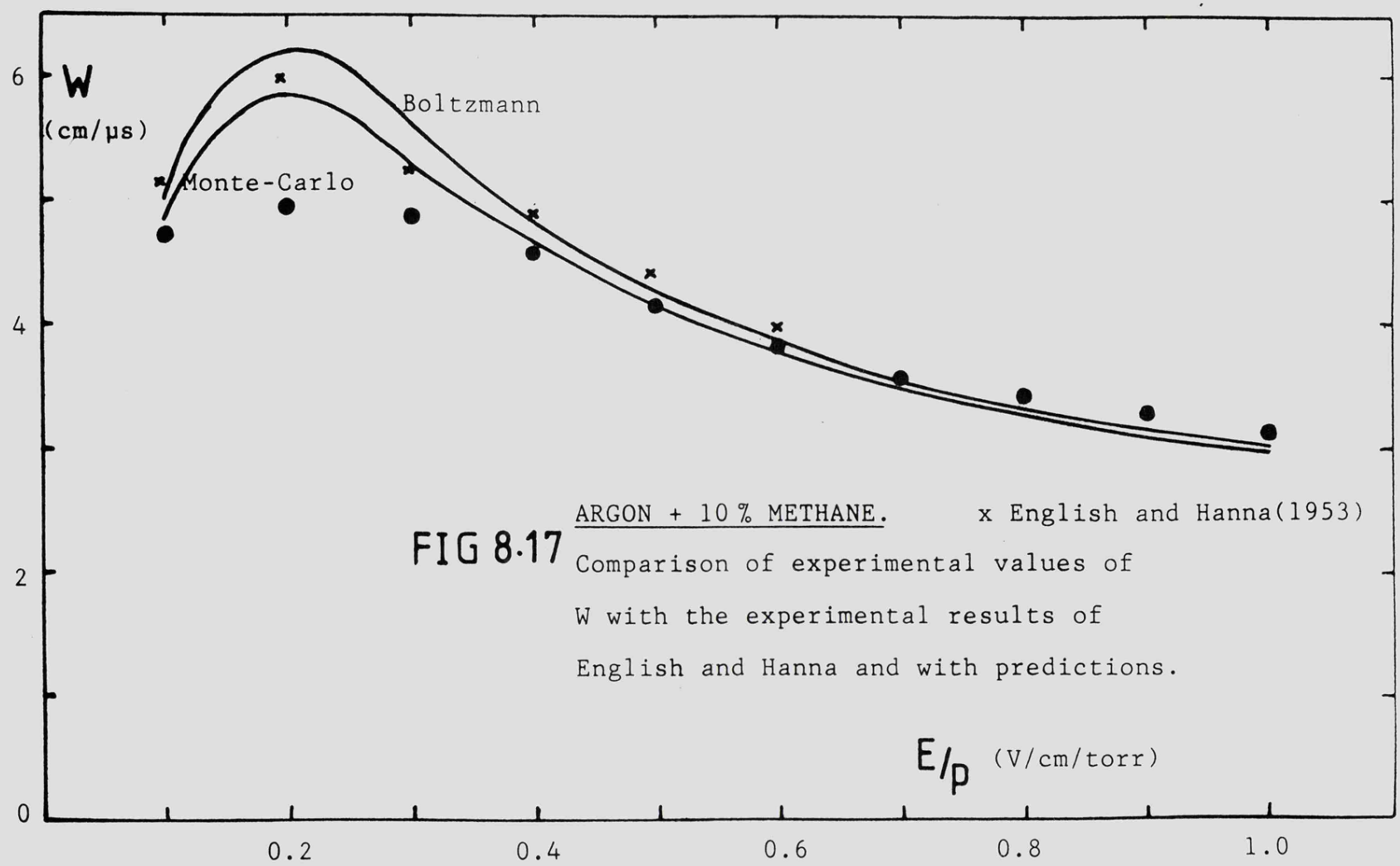

FIG 8.17 ARGON + 10 % METHANE. x English and Hanna(1953)

Comparison of experimental values of W with the experimental results of English and Hanna and with predictions.

8.3 LONGITUDINAL DIFFUSION COEFFICIENT TO MOBILITY RATIOS.

The experimental arrangement employed to find drift velocities should, in principle, as discussed in chapters 3 and 7, also yield D_L/μ.

The results of this experiment for argon + 10 % methane and 100 % methane were obtained by a manual graph-plotting method of analysing the electron time-of-flight spectra data, and those for argon + 50 % methane by computer analysis of the data, see section 7.3.

A great deal of time was spent obtaining the argon + 10 % methane results (Figure 8.18) and the argon + 50 % methane results (Figure 8.19). Relatively little time could be spent on 100 % methane (Figure 8.20). The experimental results are compared in the figures with Monte-Carlo predict--ions. The results of calculation and experiment are not in agreement in any of the gases. The predicted values are, in some cases, as much as four times greater than the experiment--ally determined values.

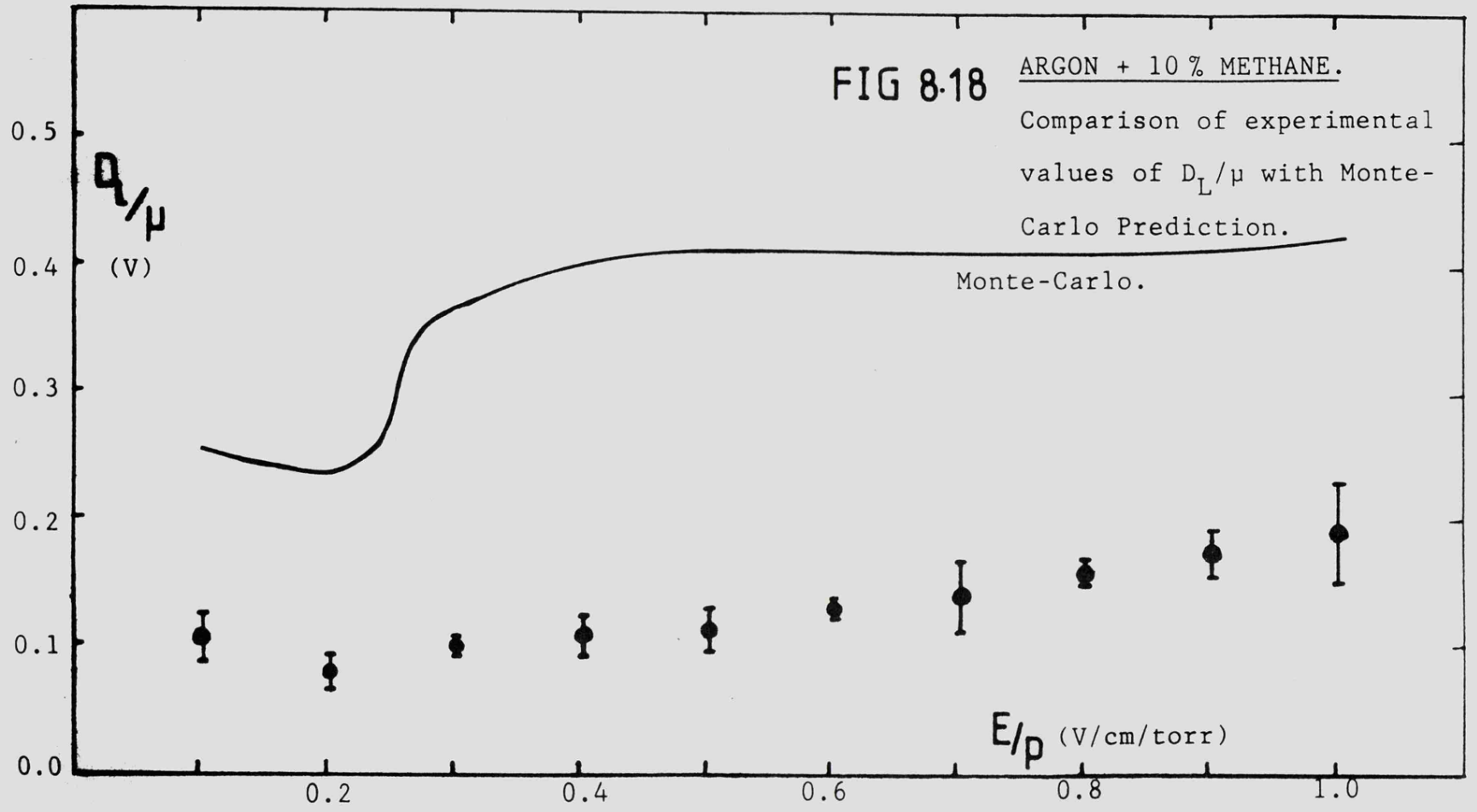

FIG 8.18 ARGON + 10 % METHANE.

Comparison of experimental values of D_L/μ with Monte-Carlo Prediction.

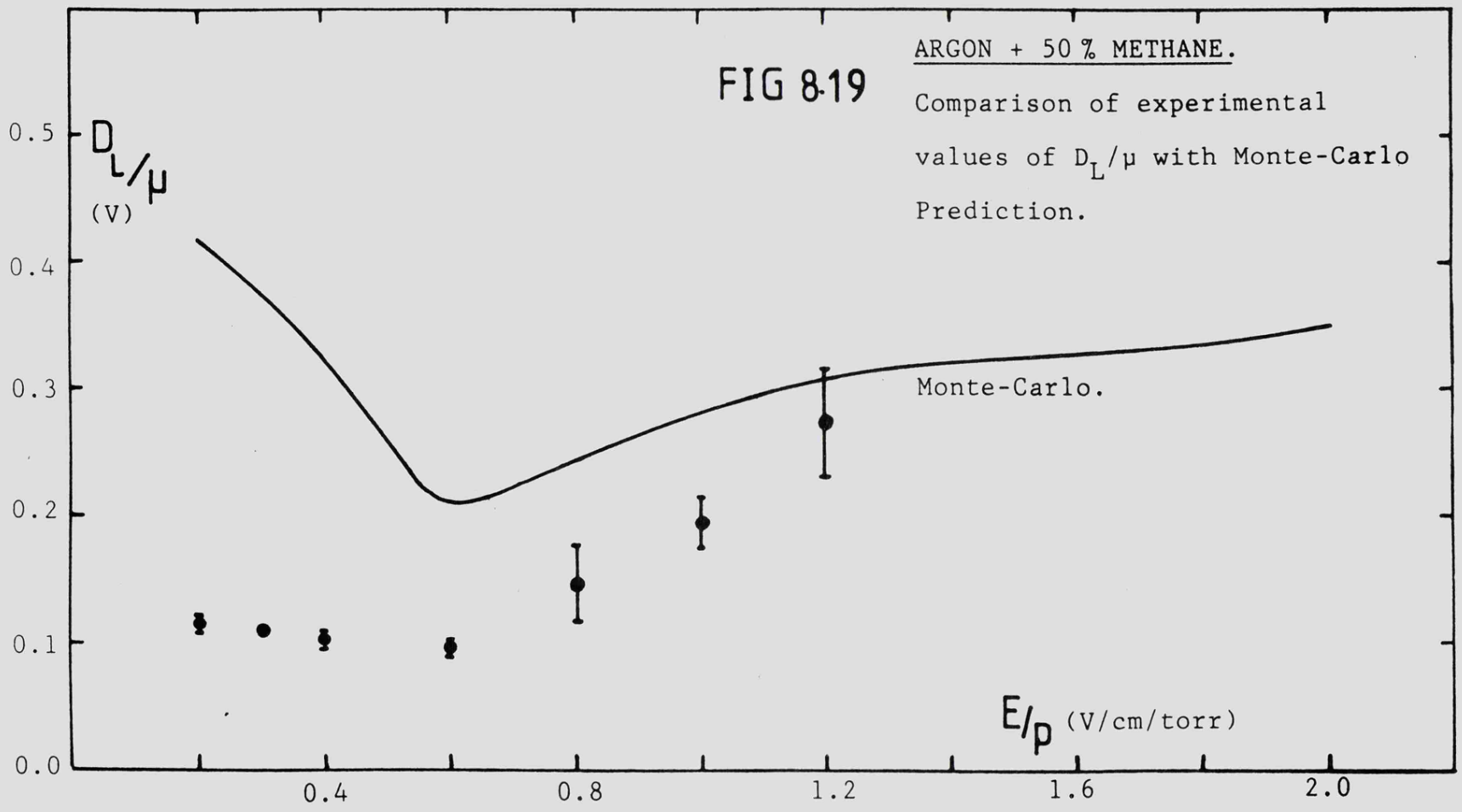
FIG 8.19
ARGON + 50 % METHANE.
Comparison of experimental values of D_L/μ with Monte-Carlo Prediction.
D_L/μ (V)
Monte-Carlo.
E/p (V/cm/torr)
0.0
0.1
0.2
0.3
0.4
0.5
0.4
0.8
1.2
1.6
2.0

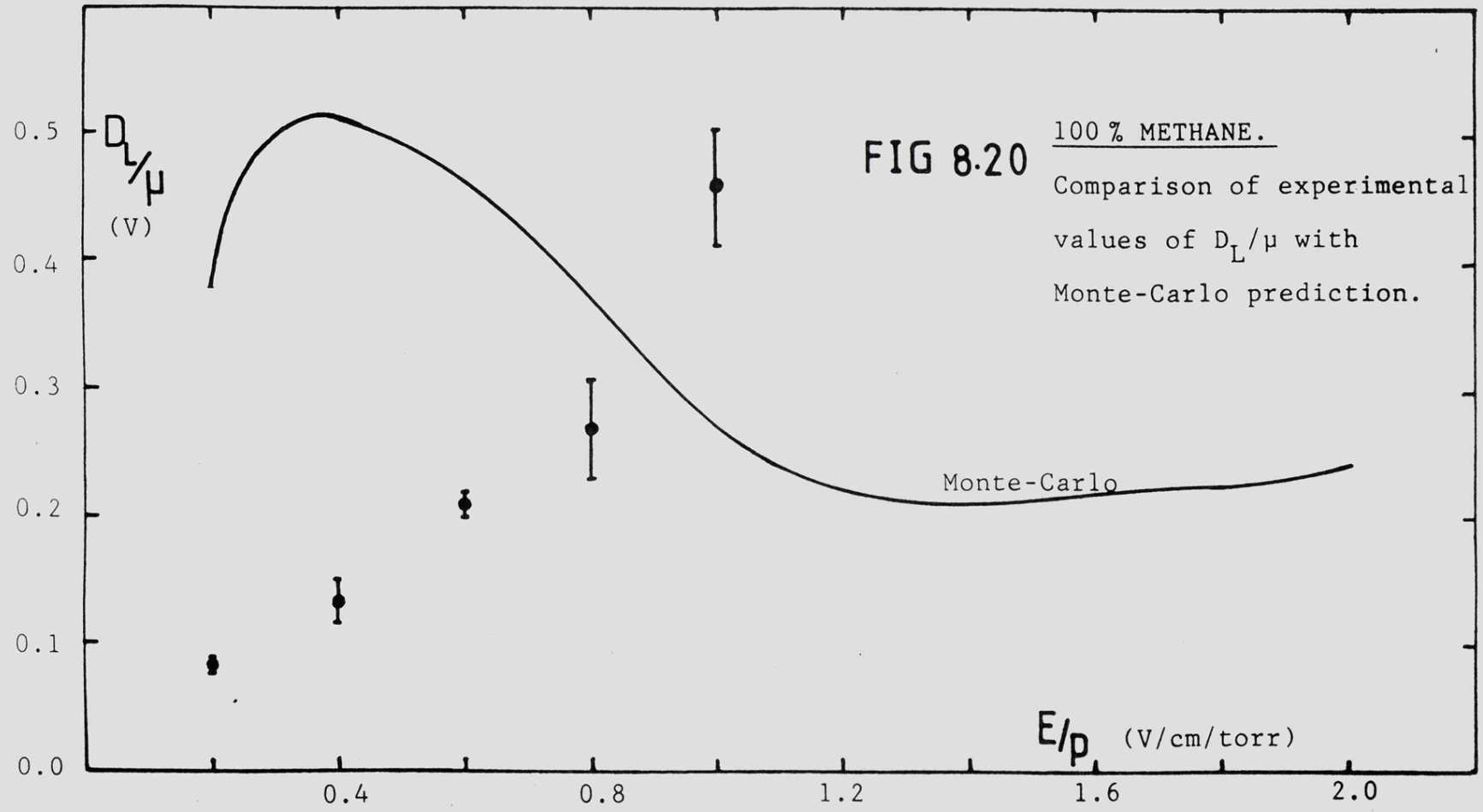

FIG 8.20 100 % METHANE.

Comparison of experimental values of D_L/μ with Monte-Carlo prediction.

CHAPTER 9.

CONCLUSION.

A large proportion of the time spent on this work was invested in the development and assembly of the system, particularly the drift chamber. Initial studies using the system of El-Hakeem (1978) were followed by the design of a similar chamber. The new chamber featured a much longer drift length (15 cm instead of just 5 cm) and a very effective gas pressure and flow control arrangement. In order to achieve greater accuracy in the determination of the lateral diffusion coefficient to mobility ratio D/μ, the results of the preliminary studies were used to decide the dimensions of the Townsend collector. An arrangement to ensure the precise alignment of the collector was included in the design. Different methods of electron production were considered, finally an improved photoemission source with an optimised photocathode and a robust construction was developed.

Mixtures of argon and methane are particularly useful as filling gases for proportional counters and multi-wire proportional chambers. However few detailed measurements have been made of electron diffusion in these mixtures. The pure gases have received considerable attention and accurate experimental results are available for D/μ (Milloy and Crompton, 1977; Duncan and Walker, 1972) and the drift velocity W (Robertson, 1977; Pollock, 1968; Mathieson and El-Hakeem, 1979) for both gases. The need for experimental data on drift and diffusion in counter gases to determine the errors in

position determination of multi-wire gas detectors and drift chambers is clear (Sauli, 1978).

Reproducible values of D/μ have been obtained in this work for ranges of proportions in mixtures of argon and methane and of argon and carbon dioxide, and also pure methane, pure carbon dioxide and several other counter gases which are commonly used. One of these gases (argon + 25% isobutane) contains isobutane in a similar proportion to that in the 'magic' gas used by the group at C.E.R.N. (argon + 30.3% isobutane + 2.5% methylal) in their drift chambers. This gas component damaged part of the chamber used in this work and can be dangerous to work with in drift chambers; an argon + carbon dioxide mixture has been suggested as a replacement (Ezban and Morganti, 1974). The experimental values obtained in this work have in most cases been compared with theoretically determined values. Some discrepancy appears between the experimental and the theoretical values, but the gases used were only of counter purity, which contain finite levels of impurities. Further contamination of the gases was avoided carefully by pumping the chamber for long periods of time between gas changes, maintaining a continuous flow of gas etc. The agreement between experimental and theoretical values is close enough to show that, in principle, D/p can be determined approximately, and close enough for most practical purposes, by means of either the Boltzmann equation or Monte-Carlo simulation for an arbitrary mixture of gases at any reduced field strength E/p, using available collision cross-section data for each component

gas.

The electron currents used in the experiment to determine D/μ needed to be small ($< 10^{-12}$ A) to avoid space-charge effects, in practice the currents were much less than this ($\sim 5.10^{-14}$A). The system was workable with this magnitude of electron current, but larger currents would have simplified and accelerated the experimental work. Some time was spent optimising the photoemission method and investigating alternative means of electron production. Further work in this area would be useful.

The development of the experiment to measure the drift velocity and the longitudinal diffusion coefficient proved to be problematical and lengthy. The final arrangement made observation of longitudinal diffusion possible, as a drift length dependent increase in the width of an electron time of arrival spectrum, obtained from the detection in a Geiger counter of single electrons, each electron originating from separate pulses of electrons released by the photoemission source. However there were several other more significant contributions to the widths of these spectra, particularly the initial electron pulse width. Because of this it was necessary to run these experiments for very long periods of time to obtain sufficient counts in the spectra for the statistics to be acceptable. Time only allowed three gases to be studied, methane and two argon / methane mixtures. The analysis of the experimental data to obtain the diffusion coefficient was complicated. Computer facilities were used to extract background from the spectra and to fit the remaining

spectra to gaussian distributions; the peak and the variance of the distributions were then obtained. However asymmetry of the spectra required rather arbitrary judgements to be made. The position of the peak was immune to the judgement but the variance did vary somewhat. A consistent procedure was applied but the results for the longitudinal diffusion coefficient lack reliability. The diffusion information obtained by this long process does not show an acceptable degree of reproducibility. It suggests a level of diffusion rather less than the theoretical predictions indicate in all three gases. The contribution of diffusion to the widths of the spectra was very small and further work aimed at increasing the relative contribution is essential to be able confidently to determine the longitudinal diffusion coefficient. The pulsed cathode method of producing electron pulses is not satisfactory. In principle infinitesimal pulse widths can be obtained in this way, but penetration of the drift field through the electron source grid prevented this from being the case. A very narrow UV light flash (< 5 ns) is the ideal solution, in which no grid is required, but commercially available flash-tubes are very far from this specification.

After the completion of this work, and after the writer had left the Leicester department, Piuz (1983) reported on his work at C.E.R.N., employing a time-of-flight system for velocity and diffusion measurement in various counter gases. Unfortunately only methane was common to both experiments; for this gas drift velocity measurements are in very close agreement over the full E/p range.

Piuz was also able to obtain some longitudinal diffusion measurements. This success was mainly due to the

availability of a flash UV source with FWHM duration less than about 7 ns (produced by the Racah Institute, Jerusalem). In fact the largest error contribution in the arrival time spectrum was estimated at about 5 ns R.M.S. due to the variable transit times in the multi-wire detector. Arrival time spectra widths down to about 10 ns could be measured. Apart from argon + 20 % carbon dioxide, only for very low fields ($E/p \leq 0.2$ V/cmtorr) did the arrival time width exceed 20 ns R.M.S. This figure would correspond to about 50 ns for the maximum drift length in the Leicester apparatus and represents roughly the width uncertainty due to source effects.

An analysis of Piuz's results for methane, argon + 20 % methane and argon + 20 % carbon dioxide shows that, over the field range studied and within the understandably limited accuracy of the measurements, longitudinal diffusion and theoretically predicted lateral diffusion are approximately equal; there appears to be isotropic behaviour. The relatively large spread in arrival times in argon + 20 % carbon dioxide is solely due to the extremely slow velocity in this gas at low field values ($\mu \cong 3.8 \times 10^{-3}$ cm^2/Vμs); paradoxically the diffusion is actually at the thermal limit at these field values, with $eD/\mu \cong kT$. In the present work all effort was given to argon/methane mixtures since these have been employed in so many previous investigations in the department. In hindsight it appears that longitudinal diffusion in argon/carbon dioxide mixtures could have been just measurable (as distinct from detectable) with the Leicester apparatus.

The present work has produced new and reliable data on the lateral diffusion and drift velocities of electrons in counter gas mixtures at low values of the reduced field

E/p. The experimental system is sufficiently reliable to be able to produce sets of this data through a routine procedure for most counter gases. Considerable reproducibility was found and also close agreement for drift velocity in particular with theoretical predictions. However, unfortunately, longitudinal diffusion has not been measured successfully despite qualitative demonstration of its presence.

Further attempts are to be made in the department to obtain data on longitudinal diffusion. Probably a different approach will be used; the present work has shown the severe practical limits which are encountered in the conventional time-of-flight method using a gas counter. A programme of theoretical work is also to be started to evaluate longitudinal diffusion coefficients in gas mixtures. Both these enterprises represent major work and are still only in their very early stages.

BIBLIOGRAPHY.

BIBLIOGRAPHY.

Bortner, T.E. et al, 1957
Rev. Sci. Inst. 28 (2), 103.

Bowe, J.C., 1960
Phys. Rev. 117 (6), 1411.

Bradbury, N.E., 1933
Phys. Rev. 44, 883.

Bradbury, N.E. and Nielsen, R.A., 1936
Phys. Rev. 49, 388.

Braglia, G.L., 1977
Physica 92C, 91.

Braglia, G.L. and Baiocchi, A., 1978
Physica 95C, 227.

Breare, J.M. and Von Engel, A., 1964
Proc. Roy. Soc. A282, 390.

Buneman, O. et al, 1949
Can. J. Research 27, 191.

Burrage, M.D., 1982
M.Sc. Project Report, Physics Department, Leicester University.

Charpak, G. et al, 1973
Nucl. Inst. and Meth. 108, 613.

Cochran, L.W. and Forester, D.W., 1962
Phys. Rev. 126, 1785.

Cottrell, T.L. and Walker, I.C., 1965
Trans. Faraday Soc. 61, 1585.

Cottrell, T.L. and Walker, I.C., 1967
Trans. Faraday Soc. 63, 549.

Cravath, A.M., 1929
Phys. Rev. 33, 605.

Crompton, R.W. and Jory, R.L., 1962
Aust. J. Phys. 15, 451.

Crompton, R.W., Elford, M.T. and Gascoigne, J., 1965
Aust. J. Phys. 18, 409.

Crompton, R.W. et al, 1970
Aust. J. Phys. 23, 667.

Dargazelli-Al, S.S. et al, 1980
Nucl. Inst. and Meth. 176, 523.

Daum, H. et al, 1978
Nucl. Inst. and Meth. 152, 541.

Duncan, C.W. and Walker, I.C., 1972
Trans. Faraday Soc. 68, 1514.

Elford, M.T. and Robertson, A.G., 1973
Aust. J. Phys. 26, 685.

English, W.N. and Hanna, G.C., 1953
Can. J. Phys. 31, 768.

Ezban, R. and Morganti, M., 1974
C.E.R.N. Report NP/OM666, 4 November 1974.

Ferrari, L., 1978
Physica 93A, 531.

Francey, J.L.A. and Stewart, P.K., 1972
J. Phys. B 5, 2025.

Frost, L.S. and Phelps, A.V., 1962
Phys. Rev. 127, 1621.

Gilardini, A., 1972
" Low energy electron collisions in gases." Published by
John Wiley, New York and London, 1972.

Hakeem-El, N.S. and Mathieson, E., 1978
3rd. International Meeting on Drift and Proportional Chambers,
Dubna, 1978.

Hakeem-El, N.S., 1978
" Electron Drift and Diffusion in Counting Gas Mixtures."
Ph.D. Thesis, University of Leicester, 1978.

Hakeem-El, N.S. and Mathieson, E., 1979
Nucl. Inst. and Meth. 166, 447.

Harris, T.J., 1972
M.Sc. Thesis, University of Leicester, 1972.

Hornbeck, J.A., 1951
Phys. Rev. 83, 374.

Hurst, G.S. et al, 1963
J. Chem. Phys. 39 (1), 1341.

Hurst, G.S. and Parks, J.E., 1966
J. Chem. Phys. 45 (1), 282.

Huxley, L.G.H., 1940
Phil. Mag. 30, 396.

Huxley, L.G.H. and Zaazou, A.A., 1949
Proc. Roy. Soc. A 196, 402.

Huxley, L.G.H. and Crompton, R.W., 1955
Proc. Phys. Soc. B 68, 381.

Huxley, L.G.H. and Crompton, R.W., 1974
" Diffusion and Drift of Electrons in Gases." Published by
John Wiley, New York, 1974.

Itoh, T. and Musha, T., 1960
J. Phys. Soc. Japan 15, 1675.

Jacob, J.H. et al, 1979
J. Appl. Phys. 50, 3185.

Jean-Marie, B. et al, 1979
Nucl. Inst. and Meth. 159, 213.

Kleban, P. and Davis, H.E., 1977
Phys. Rev. Lett. 39, 456.

Klema, E.D. and Allen, J.S., 1950
Phys. Rev. 77, 661.

Lawson, P.A. and Lucas, J., 1965
Proc. Phys. Soc. 85, 177.

Lin, S.L. et al, 1979
J. Chem. Phys. 71, 3483.

Lowke, J.J., 1962
Aust. J. Phys. 15, 39.

Lowke, J.J., 1963
Aust. J. Phys. 16, 115.

Lowke, J.J., 1973
Aust. J. Phys. 26, 469.

Lowke, J.J. et al, 1977
Phys. Rev. A 15, 1237.

Lucas, J. and Saelee, H.T., 1975
J. Phys. D 8, 640.

Mathieson, E. and El-Hakeem, N.S., 1979
Nucl. Inst. and Meth. 159, 489.

Mc.Intosh, A.I., 1974
Aust. J. Phys. 27, 59.

Milloy, H.B. and Crompton, R.W., 1977
Aust. J. Phys. 30, 51.

Milloy, H.B. and Watts, R.O., 1977
Aust. J. Phys. 30, 73.

Milloy, H.B. et al, 1977
Aust. J. Phys. 30, 61.

Moruzzi, J.L., 1967
Rev. Sci. Inst. 38, 1284.

Pack, J.L. and Phelps, A.V., 1961
Phys. Rev. 121, 798.

Palladino, V. and Sadoulet, B., 1975
Nucl. Inst. and Meth. 128, 323.

Parker, J.H. and Warren, R.W., 1962
Rev. Sci. Inst. 33, 948.

Parker, J.H. and Lowke, J.J., 1969
Phys. Rev. 181, 290.

Parker, J.H. and Lowke, J.J., 1969
Phys. Rev. 181, 302.

Phelps, A.V. et al, 1960
Phys. Rev. 117, 470.

Piuz, F., 1983
Nucl. Inst. and Meth. 205, 425.

Pollock, W.J., 1968
Trans. Faraday Soc. 64, 2919.

Reid, I.D., 1979
Aust. J. Phys. 32, 231.

Robertson, A.G., 1977
Aust. J. Phys. 30, 39.

Sauli, F., 1978
C.E.R.N. Reprint of Invited Paper at the Wire Chamber Conference Vienna, February 1978.

Skullerud, H.R., 1969
J. Phys. B 2, 696.

Townsend, J.S., 1899
Phil. Mag. 47, 109.

Townsend, J.S., 1908
Proc. Roy. Soc. A 81, 464.

Townsend, J.S. and Tizard, H.T., 1912
Proc. Roy. Soc. A 87, 357.

Townsend, J.S. and Tizard, H.T., 1913
Proc. Roy. Soc. A 88, 336.

Townsend, J.S., 1915
"Electricity in Gases." Published by Oxford University, Clarendon Press, 1915. Chapter 5.

Townsend, J.S. and Bailey, M.A., 1921
Phil. Mag. 42, 873.

Townsend, J.S., 1937
Phil. Mag. 23, 880.

Townsend, J.S., 1947
"Electrons in Gases." Published by Hutchinson, London, New York, Melbourne, Sydney and Cape Town, 1947.

Tyndall, A.M. et al, 1928
Proc. Roy. Soc. A 121, 172.

Van de Graaf, R.J., 1928
Phil. Mag. 6, 210.

Wagner, E.B. et al, 1967
J. Chem. Phys. 47, 3138.

Warren, R.W. and Parker, J.H., 1962
Phys. Rev. 128, 2661.

Zeleny, J., 1900
Phil. Trans. A 195, 193.